Electric Motors Using High Temperature Superconducting Materials Applied to Power Generating Station Equipment

TR-101127-V2
3149

Final Report, January 1997

Prepared by
Reliance Electric Company
Rockwell Automation
Cleveland, Ohio

Principal Investigators
R. F. Schiferl
D. I. Driscoll

Prepared for
Electric Power Research Institute
3412 Hillview Avenue
Palo Alto, California 94304

EPRI Project Manager
J. Stein

Fossil Power Plants
Generation Group

DISCLAIMER OF WARRANTIES AND LIMITATION OF LIABILITIES

ORGANIZATION THAT PREPARED THIS REPORT:

RELIANCE ELECTRIC COMPANY
ROCKWELL AUTOMATION

ORDERING INFORMATION

Requests for copies of this report should be directed to EPRI Distribution Center, 207 Coggins Drive, P.O. Box 23205, Pleasant Hill, CA 94523, (510) 934-4212.

REPORT SUMMARY

Large high-temperature superconducting (HTS) electric motors have the potential to operate with much greater efficiencies than conventional iron core induction motors of the same rating. This study describes the design and successful testing in the superconducting state of two synchronous motors, a 2 horsepower motor with stationary HTS field coils and a 5 horsepower motor with rotating HTS field coils.

Background

The first volume of this report, published in 1992, concluded that large AC motors driving fluid handling devices such as pumps and fans would be prime targets for commercialization of HTS technology. Large HTS motors would have approximately half the losses of conventional induction motors in such applications. For a 10,000 HP motor, the energy savings for one year of operation would be nearly one million kWh, an energy savings with a present value of $500,000 over the lifetime of the motor. Synchronous motors with rotating, superconducting field windings and copper armature windings were chosen as the best candidate for commercial HTS motors. The motors will be driven by an adjustable speed drive (ASD).

Objectives

To develop analysis methods for air core synchronous motors; to design, build, and test demonstration motors of increasingly higher rating using state-of-the-art HTS coils.

Approach

To verify the accuracy of air core synchronous motor electromagnetic design methods, the project team constructed and tested a 3600 rpm air core motor with a liquid nitrogen cooled copper field windings and a peak output power of 3.5 HP. The team then constructed a 2 horsepower motor with stationary HTS field coils and a 5 horsepower motor with rotating HTS field coils. Both motors were tested with inverter power to investigate the effects of time harmonic currents on the performance of the HTS field windings.

Results

Tests and analysis with a nonsuperconducting 3600 rpm air core motor with a liquid nitrogen cooled copper field winding showed that the two -dimensional magnetic field modeling used for air core motor design is adequate to predict motor power capability.

Because of limitations in the current carrying capability of HTS wire in a magnetic field, the first superconducting synchronous motor constructed was a 2 horsepower iron core motor with HTS field coils. This motor was demonstrated in March of 1993. Subsequently, a five horsepower motor with rotating HTS field coils was demonstrated in December 1993. The synchronous motors had robust, reliable superconducting coils with hundreds of meters of HTS wire. They were tested with inverter power to investigate the effects of time harmonic currents on HTS field winding performance. Tests showed no degradation in HTS coil performance, an important finding since the first commercial HTS motors are expected to be coupled with an adjustable speed inverter for pump and fan duty.

EPRI Perspective

This report ends current EPRI work on electric motors with liquid nitrogen cooled HTS coils. The future prospects for HTS motor development depend largely upon overcoming the performance limitations of high temperature superconducting coils at 77° Kelvin. The decreased loss and size reduction needed for an economically viable HTS motor requires superconducting coils that can operate in high magnetic fields. At an operating temperature of 20° to 40° Kelvin, however, short sample HTS wire is already available with the required performance in a high magnetic field. Work continues to construct commercially viable electric motors to operate in this temperature range.

TR-101127-V2

Interest Categories

Fossil power plants O&M cost reduction
Strategic innovations

Key Words

High temperature superconductivity
Electric motors
Adjustable speed drives

ABSTRACT

The design and test results of a nonsuperconducting air core test motor and two high temperature superconducting (HTS) synchronous motor demonstrations is presented. The largest of the HTS synchronous motors utilized a rotating HTS field winding and demonstrated an output power of 5 horsepower while operating in the superconducting state. The synchronous HTS motors, using liquid nitrogen to cool the superconducting windings, were tested with inverter power to investigate the effects of the time harmonic currents on the HTS field winding performance. The HTS coils were comprised of hundreds of meters of HTS wire, and proved to be robust and reliable. The data from the nonsuperconducting air core motor tests were used to validate motor design techniques for commercial air core HTS motors of the future.

ACKNOWLEDGMENTS

American Superconductor Corporation provided the HTS wire and coil technology which made the 2 and 5 horsepower HTS synchronous motor demonstrations possible. The Department of Commerce Advanced Technology Program provided funding for the development of the coils used in the 2 and 5 horsepower HTS synchronous motor demonstrations. Argonne National Laboratory and Intermagnetics General Corporation provided HTS coils for testing and demonstrations. Oak Ridge National Laboratory provided consultation in such areas as cryostat design, AC loss and quench issues.

CONTENTS

Section **Page**

LIST OF ILLUSTRATIONS

Figure **Page**

Figure **Page**

Figure **Page**

LIST OF TABLES

1

INTRODUCTION

Benefits of HTS Motors

The Reliance Electric Company, in the early stages of this Electric Power Research Institute project [EPRI (RP3149-01)], conducted an extensive investigation into the potential applications of high temperature superconductors in electric motors and concluded that large AC motors driving fluid handling devices such as pumps and fans would be prime commercialization targets [A]. Synchronous motors with rotating, superconducting field windings and copper armature windings were chosen as the best candidate for commercial HTS motors. The motors will be driven by an adjustable speed drive (ASD). These large motor drives, ranging in size from a few thousand horsepower (hp) up to 20,000 horsepower (14.9 MW), are widely used in electric power generating plants, refineries, pipelines and many other industrial applications. Electric power generating station applications include boiler feed pumps, and induced and forced draft fans with motors that have rated speeds from 600 to 3600 rpm. These applications generally require continuous operation of the motor so that the energy savings of an HTS motor will be fully realized.

The major motivation for users to purchase a superconducting motor is the energy savings potential. An economic analysis, performed by Reliance Electric, showed that large HTS motors will have approximately half the losses of conventional energy efficient iron core induction motors of the same rating. For a 10,000 hp (7.5 MW) motor the energy savings for one year of operation is nearly one million kWh. Translating this into dollars, a present value for this energy savings over the lifetime of the motor is in excess of $500,000. Therefore, the total sell price of the motor, approximately $400,000, is returned to the user in terms of energy savings. Furthermore, the HTS motor will also be smaller in size than its conventional motor counterpart.

The fluid handling pump and fan markets are undergoing significant change. Energy savings considerations are fostering a transition from the use of constant speed AC motors to adjustable speed drives which are comprised of an electronic control and an AC motor. The reason for this transition is the energy savings that are realizable with adjustable speed control when compared to the same flow control using throttling. In many applications the dollar savings are sufficient to pay back the cost of the electronic

control within 1 to 3 years. As energy costs increase this payback period will become so attractive that, in the future, we anticipate that virtually all new installations of large horsepower pumps and fans will utilize adjustable speed drives. Therefore, the HTS motor work at Reliance for future products, as well as for present day prototype designs, has focused on motors which can be operated efficiently from electronic controls used to achieve adjustable speed. The HTS demonstration synchronous motors described in this report were all tested with PWM inverters.

The U. S. Department of Energy studies have established that approximately 58% of the electrical energy generated in the United States is utilized by electric motors. Nearly half of this is utilized by motors in the size ranges that are potential candidates for conversion to superconducting motors. Based on Frost and Sullivan and the U. S. Department of Commerce data, the U. S. market for motors in the size range of interest is between $50-100 million per year and is growing 5% per year. The world wide market is 3 times this size.

In conclusion, superconducting motors can have a potentially large impact on electrical energy utilization through reduced losses and size when compared to conventional energy efficient iron core motors. This reduced loss and smaller size will be the driving force for their commercial introduction in industrial applications. Preliminary first cost analyses predict that large HTS motors (larger than 1000 hp or 746 kW) will be an economically viable commercial product. The quantity of superconducting motors will be large and the energy savings potential as a result of their application will be substantial both in the U. S. and world wide.

HTS Wire Development

Superconductors are used in electric motors to create a magnetic field in the air gap that is about twice the value as that found in a conventional, nonsuperconducting motor. The increased magnetic field results in a smaller motor size and reduced motor loss for the same motor output power compared to a conventional motor. Commercially viable HTS motors will require high performance HTS wire. The HTS field winding in the superconducting motor must carry a current density in the superconducting material on the order of 100,000 amps/cm^2 (645,000 amps/in^2) in a magnetic field of 5 Tesla [I].

The success of HTS motor development, is therefore, strongly linked to the successful development of long length HTS wire that can carry 10^5 amps/cm^2 (645,000 amps/in^2) current density in a magnetic field of 5 Tesla. In 1987, Reliance Electric (under EPRI contract RP 7898-12, "Superconducting Wire Investigation for Motors") evaluated proposals from potential wire vendors for HTS wire development for motor applications. This was intended to lead to an EPRI funded contract with a wire vendor in support of the Reliance Electric motor program. This contract was never awarded and, instead, Reliance Electric entered into agreements, on a purchase order basis, to

purchase state-of-the-art HTS coils for motor development thereby relying on U. S. Department of Energy, U. S. Department of Commerce and private company funded research in wire development to support the motor program. Since 1990, when the first HTS motor coil was tested at Reliance, HTS coils have been received and tested from Argonne National Labs and two U. S. HTS wire manufacturers. The close working relationship between HTS wire vendors and Reliance Electric has been a key contributor to the success of the motor demonstration portion of this HTS motor program. From 1990 through 1993 HTS wire technology progressed from small, extruded ceramic coils to rugged racetrack coils with flexible long length HTS wire. Further improvements in HTS wire current density in a magnetic field is needed to make commercially viable HTS motors realizable.

Commercial HTS Motor Topology

Figure 1-1 presents the salient features of the HTS synchronous motor topology. Its geometry is similar to that of superconducting synchronous generators developed in the past. The motor has an air core (i.e. nonmagnetic) construction so that the air gap field can be increased without the core loss and saturation problems imposed by a laminated stator and rotor iron core. Only the outer layer, the laminated frame and flux shield, is made of magnetic material which acts as a flux shunt to confine the high magnetic fields within the motor. A nonmagnetic and nonconducting support structure for the copper armature winding is located inside the frame.

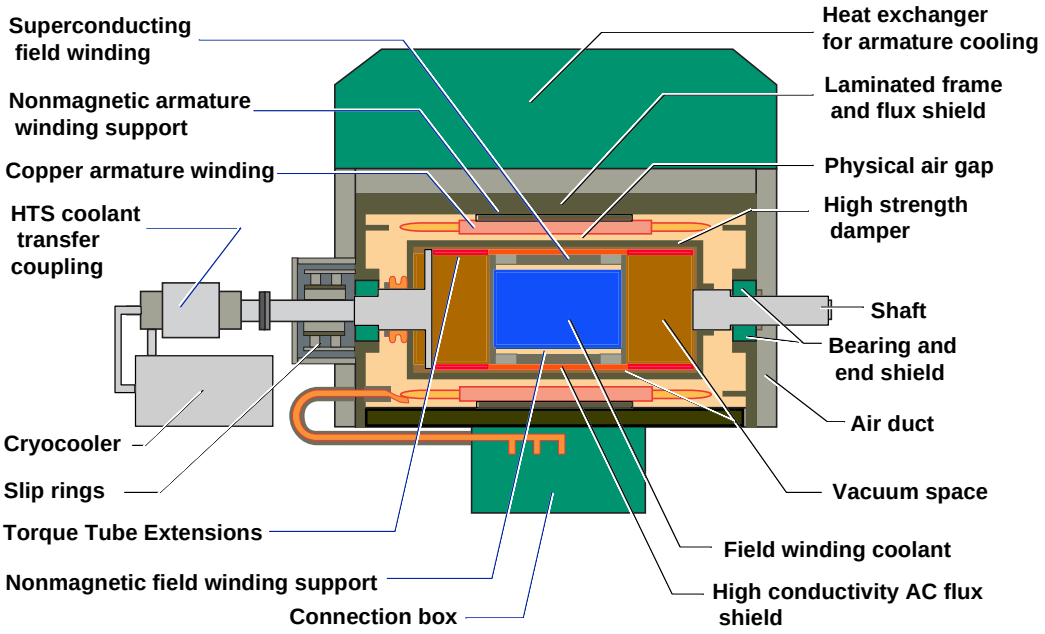

Figure 1-1
Cross-section of a large horsepower synchronous motor with HTS field windings.

The normal conducting (copper) armature winding lies just outside of the air gap. It must be constructed from transposed filaments to reduce eddy current losses. The armature conductors will experience field levels that are about an order of magnitude above those experienced in a conventional motor. Conventional motor conductors lie in high permeability teeth which redirect the flux away from the conductors so that only the slot leakage flux actually penetrates the copper. In the superconducting motor, since the armature conductors see the entire air gap flux density, the armature winding must be carefully designed to minimize eddy current losses.

Under steady state operation the motor rotor rotates in synchronism with the rotating field created by the three phase armature currents and the superconducting field winding experiences only DC magnetic fields. Under load or source transients, however, the rotor will move with respect to the armature created rotating field and it will experience AC fields. In a conventional synchronous motor these AC fields induce currents in damper windings or bars that create restoring torques to bring the rotor back into synchronism after a disturbance. These damper windings also serve as the rotor cage winding for across-the-line starting.

The superconducting motor will be started by ramping the output frequency of the armature inverter, therefore a starting cage will not be necessary. Damping will be provided by concentric conducting shells located outside of and rotating with the field winding. These are designated as the AC flux shield and high strength damper in Figure 1-1. The shells must also act to shield the field winding from all AC fields created during transients to prevent AC losses from occurring in the superconductors. It is expected that a two layer shielding structure will be utilized to accomplish the damping and shielding effectively. The outer layer (the high strength damper in Figure 1-1) will be a high strength material at room temperature (a warm shield) which will act as the damper winding and provide some AC flux shielding.

Inside of the outer warm shield will be a thermal insulation space (vacuum) that surrounds the rotor cryostat. The inner layer of the rotor damper/shield structure will be a high conductivity shell that is near the operating temperature of the superconducting coils. This inner shield (the high conductivity AC flux shield in Figure 1-1) will provide some damping and, most importantly, acts to shield the superconducting field winding from any AC fields that pass through the outer warm shield. Inside the inner shield is the superconducting field winding on a nonmagnetic support structure. The superconducting field coils will be immersed in some cryogenic coolant. The coolant will leave the cold space of the rotor through heat exchangers which will minimize the conduction of heat into the cold space through the torque tubes. The coolant will be transferred into and out of the rotor through a rotating transfer coupling and be refrigerated by some means outside the motor.

Program Goals

The joint Reliance Electric Company and EPRI research program described herein has been in place since 1987. This effort has concentrated entirely on the technical and economic aspects of large synchronous motors with HTS field coils *cooled by liquid nitrogen* at 77 Kelvin. The goals of this program are:

1. Investigate feasibility of large horsepower motors with HTS coils.

2. Develop design concepts for large horsepower, air core synchronous motors with HTS field windings.

3. Develop analysis methods for air core synchronous motors with HTS field windings to predict performance.

4. Design, build and test demonstration motors, of increasingly higher rating, using state-of-the-art HTS coils.

Results against these goals are summarized below with more details given in the listed references or later in this report.

Results Against Goals

1. Investigate feasibility of large horsepower *motors with HTS coils.*

A survey of motor types that are candidates for HTS materials was conducted in 1987 and the synchronous motor with HTS field winding was chosen as the best motor type for utility and industrial applications [A]. Large pump and fan drives were selected as the best application for HTS technology with the HTS motor powered by an adjustable speed drive. In 1989 Reliance Electric developed a concept design for a 10,000 hp (7.5 MW), 3600 rpm synchronous motor for a boiler feed pump application. The motor topology, similar to that given in Figure 1-1, was first described in [B] along with a list of design considerations for commercial HTS motor development. At the same time, a cost study comparing actual manufacturing cost of a 10,000 hp (7.5 MW), 3600 rpm Reliance Electric induction motor with an estimated cost of the 10,000 hp (7.5 MW) synchronous motor with liquid nitrogen cooled HTS field coils was conducted. Operating cost comparisons of these two motors were also completed for a boiler feed pump application. Results (described in [B]) showed installation and operating cost savings with the HTS motor, compared to the present day induction motor, of 1 to 2 times the HTS motor first cost would be realizable over a 30 year lifetime. This 1989 design and cost study indicated the potential economic viability of large horsepower HTS motors at the early stages of the Reliance/EPRI HTS motor program.

2. Develop design concepts for large horsepower, air core synchronous motors with HTS field windings.

The first design concepts for large horsepower HTS motors were the result of the economic feasibility study described under Goal 1 above. This 1989 work established motor dimensions and electromagnetic requirements for a 10,000 (7.5 MW) HTS motor. A key design decision concerned the method of cooling the HTS coils on the rotor. Two possibilities were considered: 1) pool boil cooling in which the HTS coils are immersed in a pool of liquid nitrogen and 2) flow boil cooling in which the HTS coils are cooled by liquid nitrogen that flows through axial channels in the HTS coil space in close proximity to the HTS conductors.

The pool boiling cooling option results in a pool of liquid nitrogen that has a large radial pressure gradient that may result in elevated temperature liquid nitrogen at the outer edge of the rotor cold space. Since the ability of HTS wire to carry current in a magnetic field degrades rapidly with increasing temperature, a higher temperature region at the outer edge of the cold space would reduce the current carrying capability of the HTS conductor. There was also a concern about wave action causing dynamic balance problems with the rotating liquid nitrogen pool.

The flow boil cooling option consists of axial cooling channels running between liquid nitrogen pools (headers) at each end of the rotor. This option presents a modeling challenge since cooling channel flow is dictated by the difference in radial pressure gradient in the two headers.

Both of the cooling options were investigated. Two 5000 hp (3.7 MW) motor concept designs were developed, one for each cooling option. Preliminary cooling system analysis and HTS coil specifications were generated for each design. The HTS wire specification resulting from these concepts was a wire critical current density (in the HTS part of the conductor) of 100,000 amp/cm ^{2} (645,000 amps/in^2) in a 5 Tesla magnetic field. The pool boil cooling option was further investigated by building and testing a rotor/cryostat containing mock HTS coils and a simulated motor armature. The rotor/cryostat was then eventually used as the rotor for the five horsepower (3.7 kW) motor described in this report (see Figure 1-4). The flow boiling option was further investigated by computer modeling of the flow boil rotor system for the 5000 hp (3.7 MW) motor design. This modeling was begun in 1991 by Sandia National Laboratory.

Results of the pool boil testing are reported in Chapter 4. Flow boiling cooling analysis results from Sandia have been presented in technical papers [G,5]. Reported results showed that the liquid nitrogen temperature at the outer radius of the field winding exceeded 80 Kelvin (44 R) for this 3600 rpm motor. A lower temperature rise in the nitrogen could be realized by higher flow rates in the rotor.

The flow boiling cooling system requires liquid nitrogen input and output through the transfer coupling which may complicate the transfer coupling design and refrigerant handling requirements. The pool boiling cooling system requires liquid input and gas output for the transfer coupling at much lower liquid nitrogen flow rates. Based upon the successful test of the five horsepower (3.7 kW) motor described in Chapter 4, the pool cooling method has the most merit for future liquid nitrogen cooled motor development.

3. Develop analysis methods for air core synchronous motors with HTS field windings to predict performance.

Conventional electric motors have cross sections that are largely magnetic steel. Air core synchronous motors with HTS field windings have cross sections that are largely nonmagnetic materials. Consequently, different electromagnetic analysis methods must be used to design HTS motors compared to established methods for conventional motors (see Chapter 2 for more details). Electromagnetic modeling of air core motors was based upon methods established for low temperature superconducting generators in the 1970's [1]. To verify this analysis, a 3600 rpm air core motor (with peak output power of 3.5 hp or 2.6 kW) with a liquid nitrogen cooled copper field winding was constructed and tested. Analysis and test results for this air core motor are given in Chapter 2. Results showed that two dimensional magnetic field modeling used for the air core motor design are adequate to predict motor power capability. See Chapter 2 for further discussion.

4. Design, build and test demonstration motors, of increasingly higher rating, using state-of-the-art HTS coils.

Technical milestones of this HTS motor research program were highlighted by a series of motor demonstrations using state-of-the-art HTS coils. The first demonstration was in 1990 using one of the world's first HTS coils. Motor demonstrations were a key part of the Reliance HTS motor program. Although early DC motors (described below) were primitive, at best, they did serve as an important means to establish dialogue between Reliance Electric and HTS wire and coil developers. Coil performance specifications were established for each successive motor design so that motor development could proceed in parallel with HTS motor coil development. In the end, this strategy has been successful as HTS wire and coil developers began to incrementally address HTS wire requirements for the motor application. This strategy continued throughout the project leading to the demonstration of a five horsepower (3.7 kW) synchronous motor described in Chapter 4.

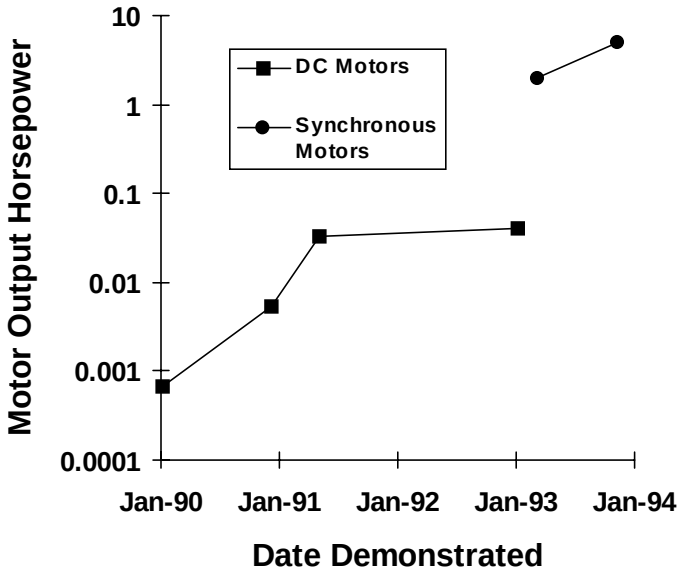

Figure 1-2
High temperature superconducting motor demonstrations as part of the Reliance Electric/EPRI project.

The first four motor demonstrations were DC motors with HTS field windings. A motor demonstration timeline is given in Figure 1-2. Table 1-1 lists specifications and test results for the four DC motors. The DC motor demonstrations were meant to show the state-of-the-art in HTS coil technology. There never was an intent to scale these up to commercial applications, however, the DC motor demonstrations served two important purposes: 1) Generate near term goals for HTS coil development for motors and 2) Provide experience in handling, assembling and testing of HTS coils in motors. More information on these motors is given in the references listed in the table.

The final two motor demonstrations for this project were synchronous motors. A two horsepower (1.5 kW) motor with stationary HTS field coils was demonstrated in March of 1993 and a five horsepower (3.7 kW) motor with rotating HTS field coils was demonstrated in December of 1993. Developments leading up to these motor demonstrations are described in the next section and details of motor design and test results are given in Chapters 3 and 4 of this report.

Reliance Electric completed the design of an iron core, four pole, synchronous motor with rotating HTS field coils in 1991. Iron core construction means a motor with magnetic steel in the field and a full, laminated steel magnetic core for the armature. The magnetic steel in the field and armature result in more air gap flux for a given magnetic field level in the HTS coils than would be obtained with an air core structure. Due to limitations of HTS wire current carrying capability in a magnetic field, it was decided to first demonstrate an iron core motor in order to achieve the highest possible

horsepower rating for the first synchronous motor demonstration. The target rating for this motor was one horsepower (0.7 kW) with a nominal HTS wire specification of 500 amps/cm^2 (3200 amps/in^2) HTS critical current density in a 0.04 Tesla peak magnetic field. The rotor/cryostat for this motor was constructed first (with mock HTS coils) in order to perform pool boiling cooling tests as mentioned above under the results of Goal 2.

Table 1-1
DC motor demonstrations with HTS field windings.

All motors had:

- HTS field coil(s) in a foam insulated liquid nitrogen tank
- Copper wire armature located above a liquid nitrogen pool
- Solenoid HTS field coil(s).

Date Demon-strated	Motor Description	Coil Supplier and Type	Motor Output Power	Jc (in peak mag. field with motor running)*	Refs
1990	• Solid steel field structure. • Single HTS field coil.	• Argonne National Labs • Five layer, extruded yttrium barium copper oxide (YBCO). • 8 meters (26 ft) of wire in 75 turns.	• Shaft rotates without any external load.	29 amps/cm^2 (187 amps/in^2) in 0.0025 Tesla	[H], [B], [F]
1991	• Laminated steel field structure • Single HTS field coil.	• Argonne National Labs • Six layer, extruded, YBCO • 16.4 meters (53.8 ft) of wire in 120 turns	• 4 watts to a fan load	63 amps/cm^2 (406 amps/in^2) in 0.0085 Tesla	[H], [K]
1991	• Laminated steel field structure (same core as 4 watt motor above) • Two HTS field coils.	• American Superconductor Corporation • Multilayer, react and wind, powder in tube, bismuth compound (BSCCO) • 97 meters (320 ft) of silver sheathed wire in 664 turns in two coils	• 25 watts to a fan load	97 amps/cm^2 (626 amps/in^2) in 0.014 Tesla	[H], [J], [E], [K]
1993	• Laminated steel field structure (same core as 4 watt motor above) • Single HTS field coil.	• Intermagnetics General Corporation • Multilayer, wind and react, powder in tube, bismuth compound (BSCCO) • 9.4 meters (31 ft) of silver sheathed wire in 65 turns.	• 30 watts to a fan load	4300 amps/cm^2 (27.7 kA/in^2) in 0.028 Tesla	[K]

* Jc is the critical current density in the superconducting part of the HTS wire.

In April of 1991 HTS coil specifications for the four HTS racetrack shaped coils for the four pole motor were distributed to potential wire vendors. In October of 1992 five racetrack coils were delivered to Reliance Electric by American Superconductor Corporation. One of these coils was purchased as part of this EPRI contract. The other four coils were supplied through a Department of Commerce Advanced Technology Program grant to American Superconductor Corporation. At the time the HTS coils were delivered, modifications to the rotor/cryostat (which were determined necessary after initial testing was completed) had not yet been completed, so two of the five HTS coils were used for a two horsepower (1.5 kW) motor demonstration (in March of 1993) with stationary HTS coils using currently available hardware (see Figure 1-3). After the two horsepower (1.5 kW) motor tests were completed these two coils plus the two best of the remaining three were installed in the rotor/cryostat and this rotor was installed in the stationary armature originally designed for the one horsepower (0.7 kW), four pole, rotating field motor (see Figure 1-4). The HTS coils exceeded their design specifications so that this motor became the five horsepower (3.7 kW) motor (demonstrated in December 1993) that is the subject of Chapter 4.

The remaining chapters of this report describe design, analysis and test results for the two iron core HTS synchronous motors described above (two and five horsepower) plus an air core, nonsuperconducting, synchronous motor that was used to verify design calculations. The air core motor described in Chapter 2 and the two horsepower (1.5 kW) HTS motor described in Chapter 3 shared common hardware as shown in Figure 1-3. This hardware was first used as the electromagnetic test rig which was an iron core, nonsuperconducting motor with air gap AC flux shields, stationary field and rotating armature. It was used to verify electromagnetic design calculations for iron core motors with large air gaps (as in the first HTS synchronous motor demonstration). Test results from this rig are given in [H]. This rig was originally designed with the capability of replacing the iron core field and armature with air core components (stainless steel field and G-10 laminated armature as described in Chapter 2). Once iron core testing was completed the air core motor of Chapter 2 was constructed by replacing the field and armature cores with air core versions (see Figure 1-3). Upon completion of testing of the air core motor the iron core two horsepower (1.5 kW) HTS motor was assembled by reinstalling the iron core armature and fabricating an iron core field to support the two HTS racetrack coils. Motor tests with this first HTS synchronous motor are described in Chapter 3.

Figure 1-4 shows the evolution of the five horsepower (3.7 kW) motor discussed in Chapter 4. First tests, as mentioned above, were conducted on a liquid nitrogen cooled rotor (the rotor/cryostat) with mock HTS coils. Results of these tests are reported in Chapter 4. After completion of these rotor tests, the mock HTS coils were replaced with four racetrack HTS coils and the motor was tested to five horsepower (3.7 kW). Details of design, construction, test and analysis of the five horsepower (3.7 kW) motor are the subject of Chapter 4.

Common to All Hardware Tested:
•Vertical shaft and bearing system
•Armature base, test stand and enclosure
•Cantilevered armature and bearing assembly
•Copper and stainless steel air gap AC flux shields

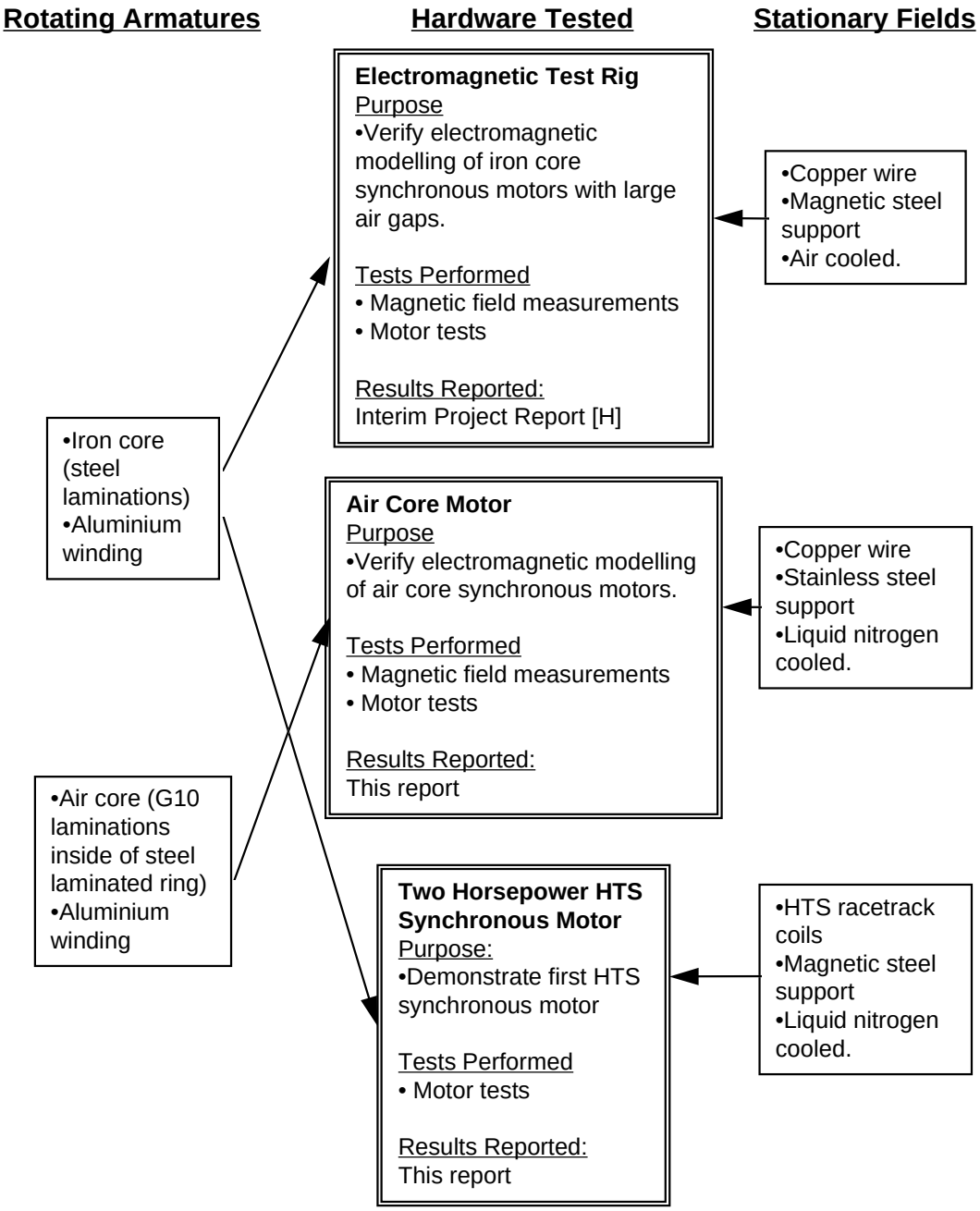

Figure 1-3
Hardware combinations for two pole, 3600 rpm motor tests.

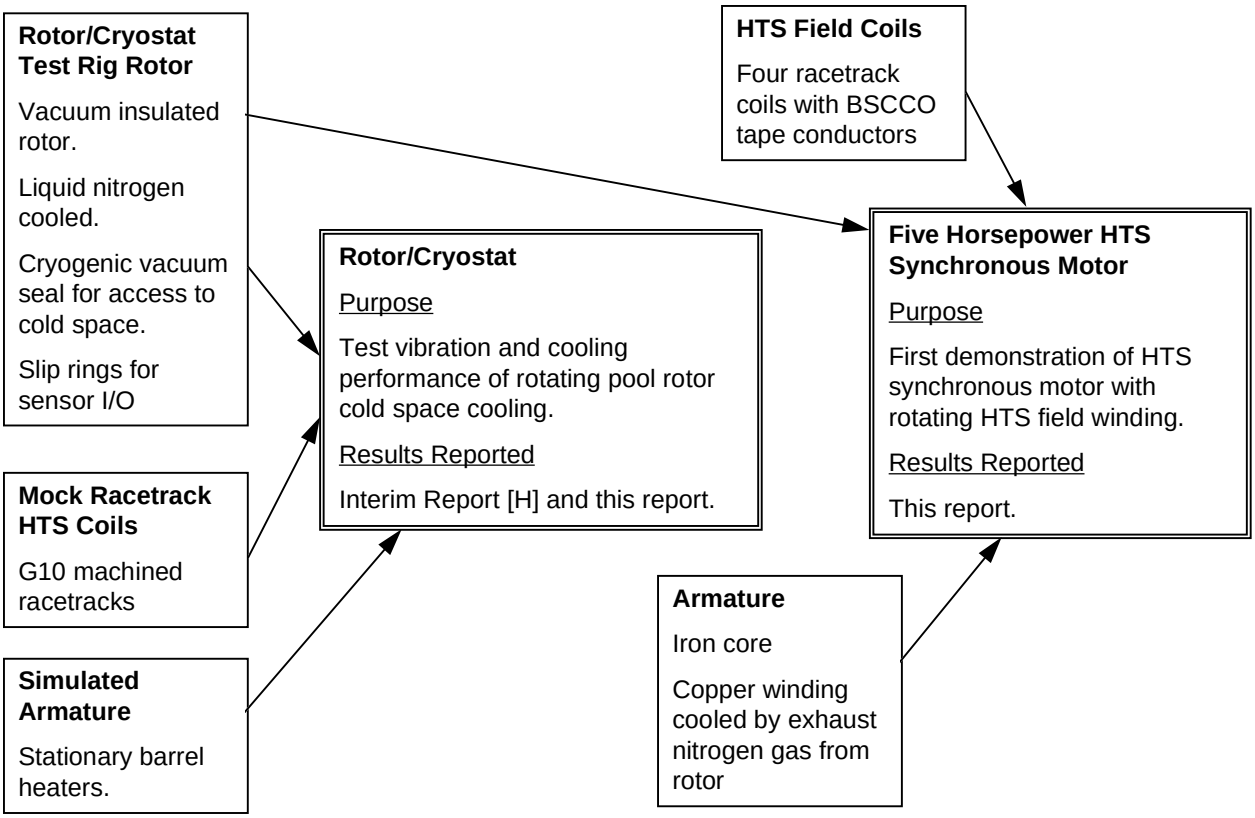

Figure 1-4
Evolution of five horsepower (3.7 kW), four pole, HTS synchronous motor.

2

NONSUPERCONDUCTING AIR CORE MOTOR

Goals

The nonsuperconducting air core synchronous motor was built to meet the following goals:

1. Demonstrate a synchronous motor with an air core geometry that had all of the field components of future HTS motors with the capability to measure magnetic fields in the active motor region. Motor rating goal was two horsepower (1.5 kW) or above developed power.
2. Measure three dimensional magnetic field distribution in the motor and use this data to develop simple models to predict synchronous motor circuit parameters.
3. Verify accuracy of air core synchronous motor electromagnetic design methods.
4. Utilize existing hardware as much as possible.

The air core motor was built exclusively for electromagnetic design verification purposes. At the time this motor was built, high temperature superconducting (HTS) coils were not available, so this air core motor utilized a copper field winding to mimic the superconducting coils.

Commercial, HTS synchronous motors will use the HTS material to create very high magnetic fields in the motor (5 Tesla in the superconducting winding itself). With these high fields most of the magnetic material in the motor will be removed since it will be heavily saturated and (in the armature) will have very high core loss. These types of motors are referred to as "air core" motors since, throughout most of the motor cross section, the magnetic field in the motor is distributed as if it was in air. Chapter 1 described the components of commercial air core HTS motors.

A conventional, iron core, motor has a cross section that is largely made up of magnetic material; usually steel laminations. Electromagnetic analysis of conventional motors is based largely on the effect the small air gap has on the amount of magnetic flux created by the motor windings. The air gap magnetic field is often calculated by ignoring the influence of the MMF drops in the laminated steel portion of the magnetic circuit

altogether. In this case the magnetic field analysis for conventional motors can be classified as a one dimensional analysis. In an air core HTS motor, all of the region inside of the outer laminated frame and flux shield is, essentially, an air gap. At a minimum, two dimensional magnetic field analysis is required for air core motors and three dimensional field modeling may be required. New analysis and design techniques must be used. In order to verify the accuracy of these new techniques a nonsuperconducting air core motor was designed, constructed and tested. This motor was fabricated using many of the parts of the iron core test motor [H] by replacing the field core and most of the armature core with nonmagnetic materials (see Figure 1-3). The resulting synchronous motor had a maximum power capability of 3.5 horsepower (2.6 kW).

Fortunately, with most of the motor iron removed, the two dimensional magnetic field analysis for air core motors can be linear so that closed form solutions exist to obtain the field distribution in a motor cross section. Air core motor field equations were developed for low temperature superconducting generator projects in the 1970's [1]. These same methods were used to determine the performance of the air core motor described in this chapter.

Design

The following paragraphs describe the design aspects of the air core motor. The electrical design is presented first, followed by descriptions of the motor topology and test stand topology. The design was driven by the goals listed in the previous section above.

Electrical

Two dimensional, closed form, magnetic field equations [1] were solved to determine circuit parameters for an air core motor using the bearing and test stand structure of the electromagnetic test rig motor described in [H]. The air core motor is a two pole motor with a rotating armature and a stationary field winding. The copper field winding was cooled in a pool of liquid nitrogen so that the current density could be pushed high enough to obtain integral horsepower capability. The design goal was to obtain at least two horsepower (1.5 kW) developed power. Key motor design parameters are listed in Table 2-1. The motor has a laminated, magnetic steel ring at the outer radius and a G-10 (epoxy/fiberglass) slotted core as shown in Figure 2-1. The initial estimate of motor peak power capability at 3600 rpm, rated voltage conditions was 2.5 horsepower (1.9 kW).

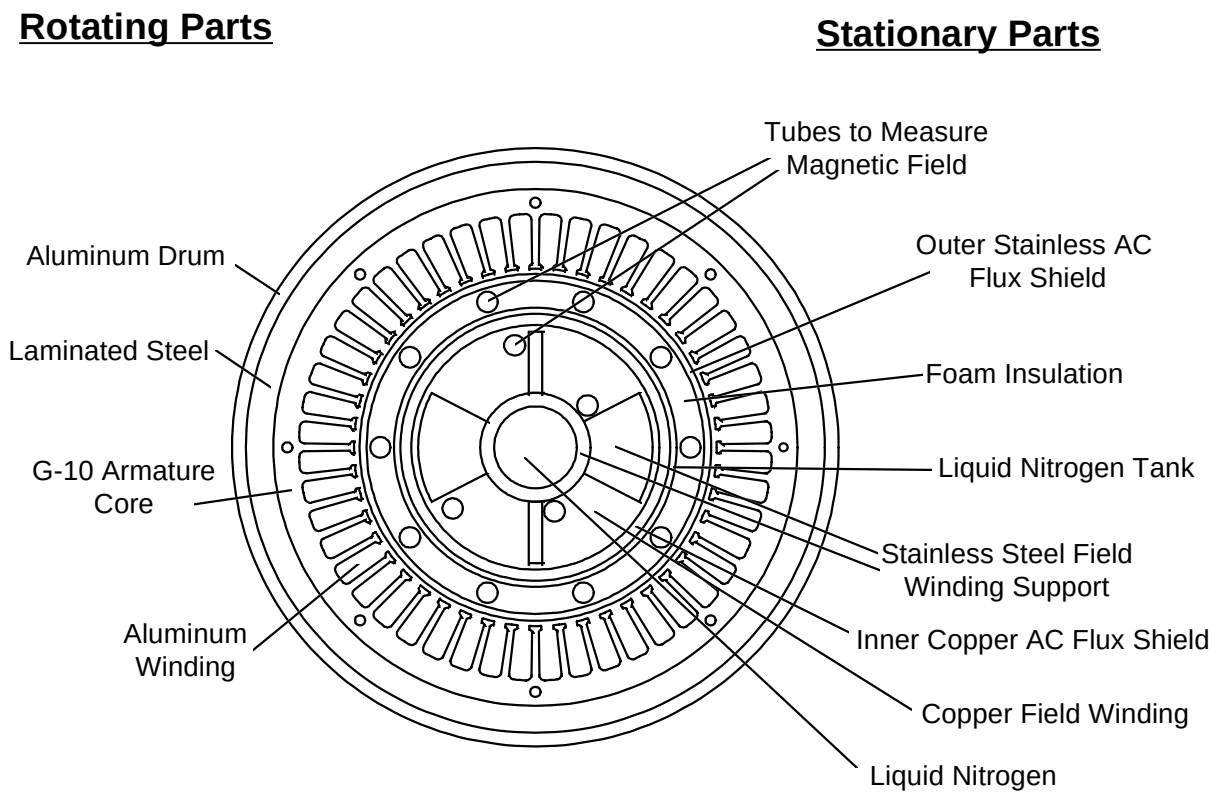

Figure 2-1
Cross-section of the nonsuperconducting air core motor.

The copper AC flux shield (that is liquid nitrogen cooled) acts as a starting cage for the motor. This cold copper shield will result in a low slip (about 1%) steady state induction motor speed at no load so that when field current is applied the motor will pull into synchronism. This was not possible with the old iron core test rig motor [H] which was always operated with a room temperature AC flux shield and had to be synchronized by bringing it up to speed with a pilot motor.

The goals for the air core motor were met by using an unconventional AC synchronous motor design. The field winding was designed to be stationary for ease of access–allowing direct probing of the field while operating the motor–and for ease of modification to the core structure. A majority of the hardware for this construction was available from the iron core test rig that was fabricated and tested earlier in the program [H]. A stationary field winding required that the armature winding be rotating. Rotating the massive armature winding structure resulted in a less efficient motor design, due to higher friction and windage losses, but allowed the experimental design goals to be met.

Table 2-1
Electrical design parameters for the air core motor. Rated conditions are 2 hp (1.5 kW) developed power at 230 V, 60 Hz armature excitation.

Parameter	Value
Armature OD over steel laminations	10.5 in (26.7 cm)
Armature ID of steel laminations	9.5 in (24 cm)
Outer diameter of armature winding	8.5 in (22 cm)
Inner diameter of armature winding	6.8 in (17 cm)
Armature G-10 core length	8.0 in (20 cm)
Straight section of armature end winding extension	0.75 in (1.9 cm)
Total armature end winding extension (per side)	2.75 in (7 cm)
Laminated steel core length	12.0 in (30.5 cm)
Outer diameter of field winding	4.38 in (11.1 cm)
Inner diameter of field winding	2.5 in (6.4 cm)
Total length of straight section of field winding	9.25 in (23.5 cm)
Number of stator slots	36
Number of poles	2
Armature Winding	
Line to line voltage	230 V rms
Number of turns per coil	24
Conductor strands	5
Coil throw	1 to 9
Number of circuits	1
Wire material	Aluminum
Armature bore peak radial field at rated conditions (predicted)	0.06 Tesla
Field Winding	
Number of turns (all poles)	752
Number of circuits	1
Wire material	Copper
Rated field current (predicted)	20.7 amps
Peak field winding mag field (predicted) at rated conditions.	0.14 Tesla

Motor Topology

Figure 2-1 presents a cross-sectional view of the stationary and rotating parts of the air core motor. The stationary parts consist of a stationary winding support stainless steel (SS) core tube with attached SS field supports upon which the copper field winding is wound. Four rigid fiberglass tubes were placed at various locations to penetrate the winding, allowing access into the winding space for Hall probe insertion and magnetic field measurement within the winding. A cold inner copper AC flux shield is located just outside the winding and inside the walls of a G-10 liquid nitrogen confinement tank. A layer of foam insulation between the liquid nitrogen confinement tank and a warm outer SS AC flux shield helps to minimize the heat leak into the liquid nitrogen tank.

In order to meet the design goal of two horsepower (1.5 kW) developed power, a very large field winding current density was required [16,200 amp/in^2 (2510 amp/cm^2) in the conductor] so that an air cooled winding would overheat. Thus, during motor operation, the stationary field winding was bathed in a pool of liquid nitrogen which allowed a large field winding current density without overheating the winding. Pretest thermal analysis of the liquid nitrogen cooled field winding indicated that this cooling configuration could be maintained with manageable liquid nitrogen consumption and with a sufficient margin from burnout of the winding.

The rotating parts of the motor in Figure 2-1 comprise a G-10 (epoxy/fiberglass) laminated core with slots for the aluminum armature winding. The G-10 laminated core is surrounded by a steel lamination layer which is confined within an aluminum drum. The aluminum drum, aluminum wire in the armature winding and the G-10 laminated armature winding support structure all serve to reduce the rotating armature weight and keep the first critical speed above operating speed. Figure 2-2 is a photograph of the air core armature showing the G10 laminations inside of the outer laminated steel flux shield. A single steel and G10 lamination is shown in the photograph foreground.

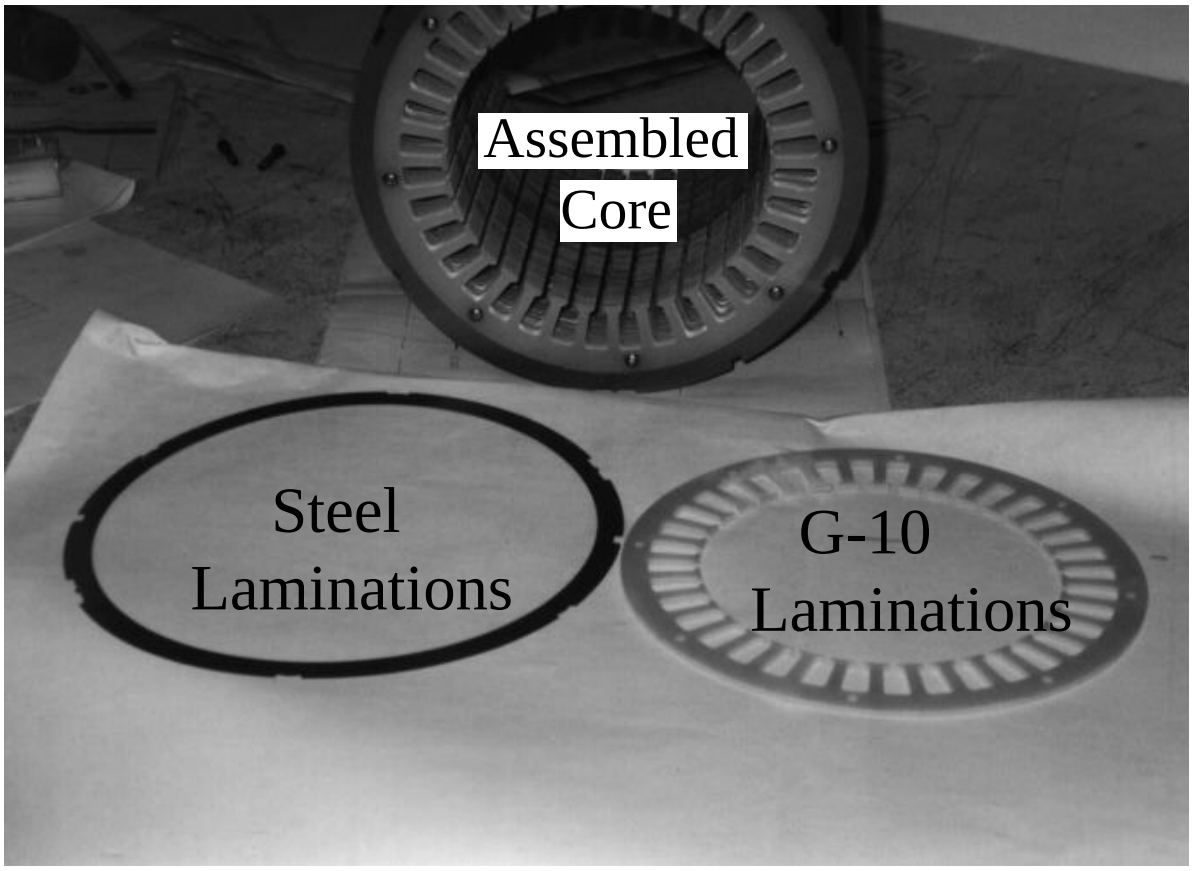

Figure 2-2
Armature core with G-10 and steel laminations in the foreground.

Figure 2-3 presents an exploded view of the air core motor. This motor was constructed by cantilevering the rotating drum, which contains the normal conducting armature winding and core, off of two bearings beneath the drum. The armature winding current is supplied through slip rings located between the two bearings. Due to the close proximity of the upper bearing to the liquid nitrogen confinement tank, the temperature of the bearing was monitored and a heater was located near the bearing to prevent the freezing of the bearing grease. As depicted in Figure 2-3, the motor stood on end with the drive end pointing downward, leaving unobstructed access to the stationary field winding.

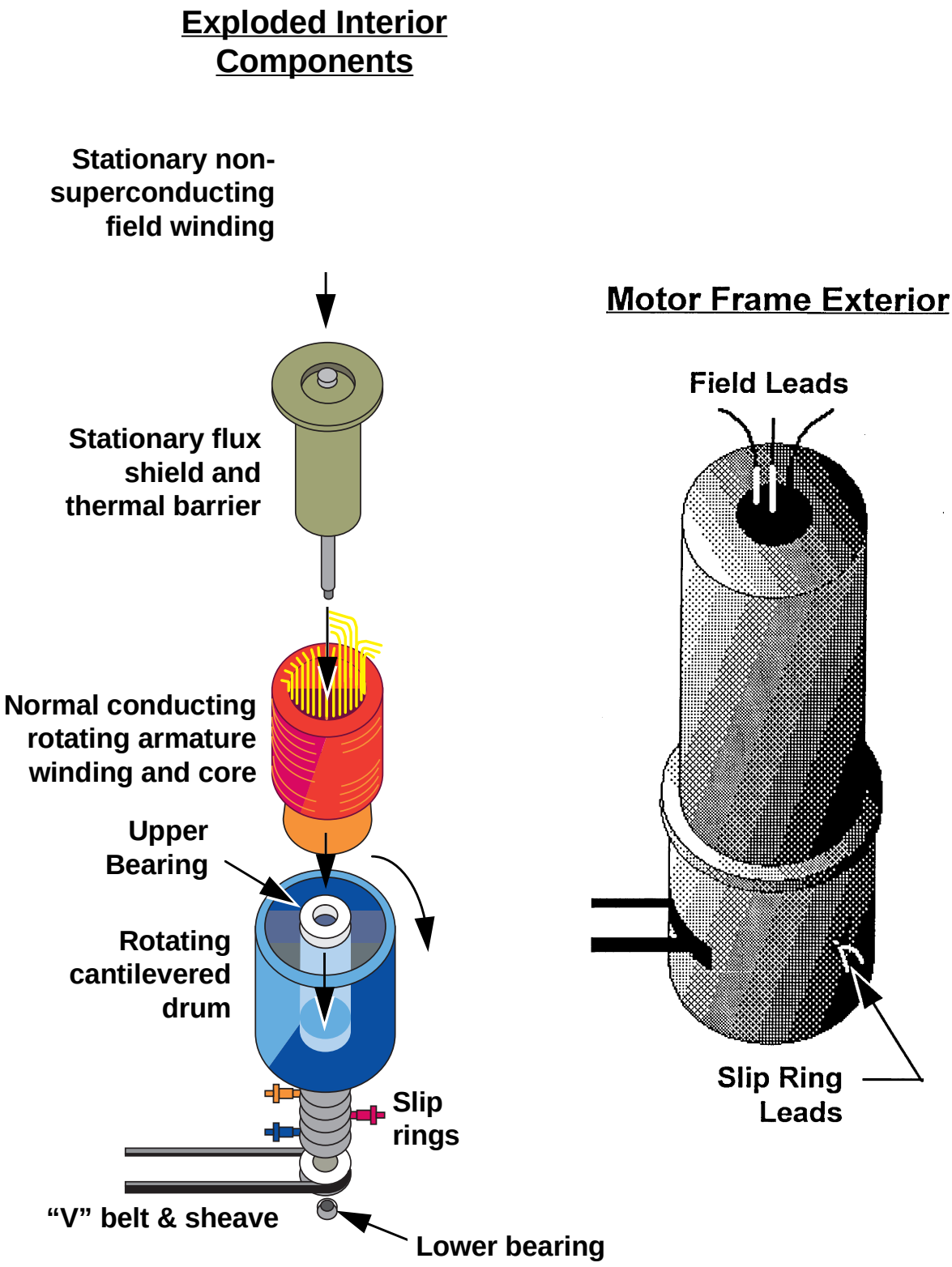

Figure 2-3
Exploded view of the air core motor.

Test Stand Topology

The test stand for the air core motor shared components with the two horsepower (1.5 kW) superconducting motor described in Chapter 3 (see Chapter 1 and Figure 1-3 for a description of the hardware development for these motors). The shared components are shown in Figure 3-4 and include:

- Induction motor (and inverter) which was used as a pilot motor to rotate the armature winding during soft synchronization of the air core motor.
- DC generator and resistive load bank which served for loading the air core motor during tests.
- Clutch/brake used to isolate the induction motor during load tests using the DC generator.
- Emergency air brake and associated belt system to connect and transfer power between the test motor, induction pilot motor, and DC generator.

The field winding was cooled using liquid nitrogen fed from a feedline tube protruding directly into the G-10 epoxy/fiberglass tank surrounding the field winding. The liquid nitrogen was supplied from a standard storage dewar through an insulated flexible feedline and metering flow valve. The stationary field structure was instrumented with seven thermocouples to monitor the liquid nitrogen cooled copper field winding. It was found that the liquid nitrogen level could be detected by monitoring the thermocouple temperature readings for thermocouples attached directly to the copper field winding.

Test Setup and Results

Figure 2-4 shows the test rig motor and instrumentation with the motor operating as a synchronous motor with a liquid nitrogen cooled field winding. Initial tests of the motor were to test out instrumentation and field winding cooling control methods. Cool down from room temperature to 77 K (43 R) could be accomplished in one to two hours. With the field cooled the motor was spun up to 3600 rpm using an inverter driven pilot induction motor that is belt connected to the air core motor. The open circuit voltage of the air core motor was adjusted to match the design value and the motor was soft synchronized from a three phase, sine wave supply. Once synchronized the field current was turned off to run the motor as an induction motor. By proper timing of reapplication of the field winding excitation the motor pulled into synchronism without slipping poles. Attempts to line start the motor were unsuccessful due to the low starting torque with the liquid nitrogen cooled, copper "cage" winding as well as the low flux level in the air core motor.

Liquid nitrogen cooling of the field winding was found to be easily controlled. We anticipated the need to heat the upper bearing, which lies close to the liquid nitrogen tank, in order to prevent lubrication problems. We found, however, that this bearing remained above 30°C (86°F) during rotating tests without the bearing heater on. Overall, the field cooling system and the mechanical aspects of the air core test rig motor performed well during these initial tests so we proceeded with our motor test plan.

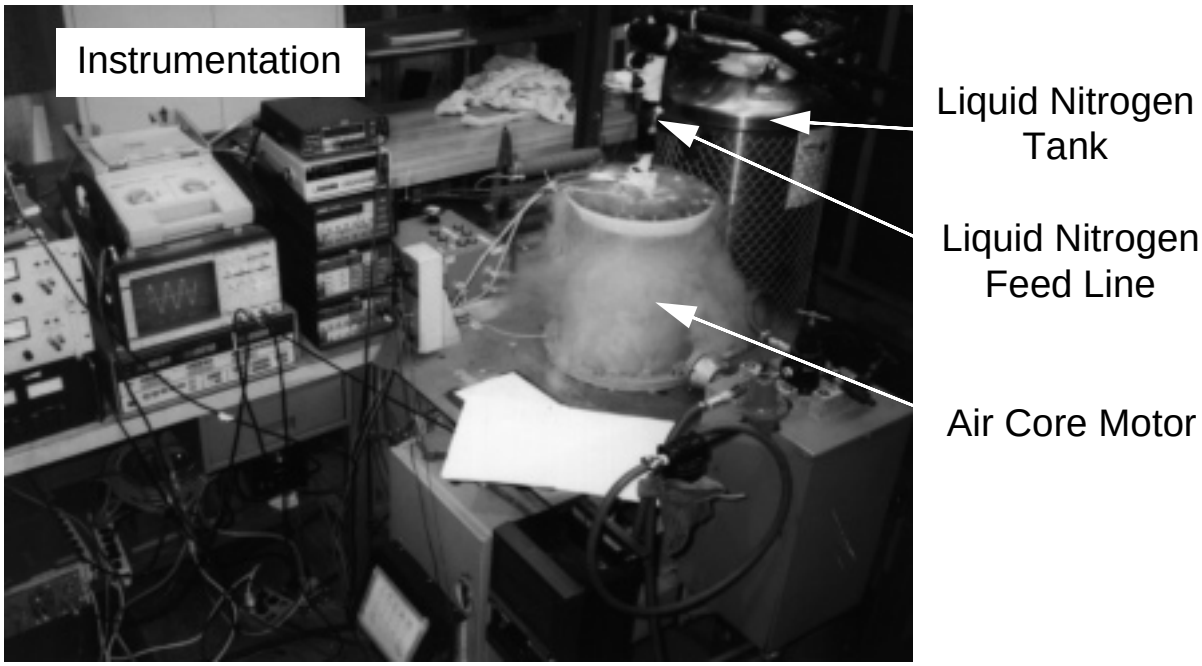

Figure 2-4
Air core motor under test with liquid nitrogen cooling of the nonsuperconducting field winding.

The steady state performance of the motor was characterized by the following per phase, phasor voltage equation:

$$\overline{V_S} = (R_S + jX_S)\overline{I_S} + E_0 \qquad (2.1)$$

where $\overline{V_S}$ is the motor terminal voltage phasor given by $\overline{V_S} = V \angle\delta$ with δ being the torque angle, R_s is the armature resistance per phase, X_s is the synchronous reactance per phase (= $2\pi f L_s$ with f being the armature supply frequency in Hertz and L_s being the synchronous inductance), $\overline{I_S}$ is the motor phase current phasor given by $\overline{I_S} = I \angle\gamma$ with γ being the current angle, and E_0 is the motor open circuit voltage acting in the quadrature axis.

All tests were performed with a simple rotor position sensor providing a one pulse per revolution signal to an oscilloscope. From an open circuit test this pulse can be referenced to the motor quadrature axis. By measuring the phase displacement between the position sensor pulse and the zero crossings of the armature voltage and current, values for δ and γ can be measured for each steady state load point. The stator resistance is directly measured and updated based upon the estimated temperature of the armature winding during operation. Combining this data with the measured rms terminal voltage and current and the motor open circuit voltage, Equation (2.1) can be solved for X_s.

Steady state no load and load performance tests were completed with 60 Hz sine wave armature excitation. From these tests the motor measured synchronous reactance was determined. The air core motor design calculations were based upon two dimensional magnetic field calculations in which the axial length of the coupled windings must be estimated. Test data was used to determine measured values for equivalent axial lengths for key circuit parameters as described in Appendix A. A method to estimate these equivalent lengths was developed based upon motor and winding dimensions and a simple three dimensional magnetic field model for the motor as described in Appendix A. This model development was aided by three dimensional magnetic field measurements in the field region of the air core motor.

Using the calculated equivalent lengths, obtained from actual winding dimensions, a comparison of measured and predicted circuit parameters is given in Table 2-2. As shown, measured and calculated values agree to within 7% for all circuit parameters.

Table 2-2
Air core motor circuit parameters.

Parameter	Calculated Value	Measured Value	Difference
X_S (Ω)	7.91	7.41	7 %
E_0 (volts)	80.7	76.8	5 %
R_S (Ω)	2.76	2.86	- 3 %

The measured and calculated motor power capability curve is shown in Figure 2-5 for rated voltage, sine wave armature excitation. Predicted and measured performance agreed quite well. The maximum difference between measured and calculated performance was at the pull out condition where predicted pull out power was 16% above the measured value. Two horsepower developed power (1490 watts) was easily achieved thus satisfying the design goal. Figure 2-6 contains a plot of the measured and calculated armature current as a function of motor load. Over the range of test data the measured current exceeded the predicted values by about 10% .

Conclusions

The four goals of the nonsuperconducting air core motor demonstration were all met. An air core synchronous motor with output power exceeding two horsepower (1.5 kW) was demonstrated. The motor was based on the existing iron core electromagnetic test rig hardware with modifications to the armature core and field structure. Three dimensional magnetic field data was obtained (see Appendix A) and used to update the motor design procedures. Motor performance tests were completed and results compared to predicted performance based upon a motor model that used a combination of two, two dimensional magnetic field models.

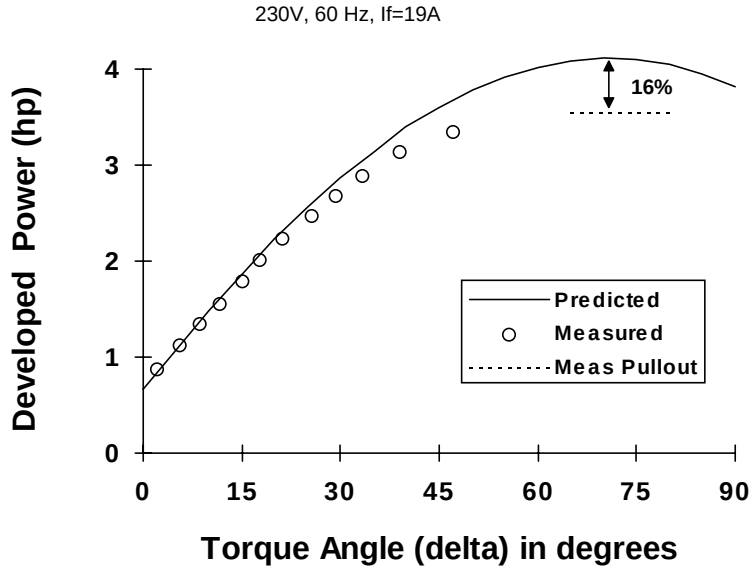

Figure 2-5
Power capability curve for the air core motor with nonsuperconducting field winding.

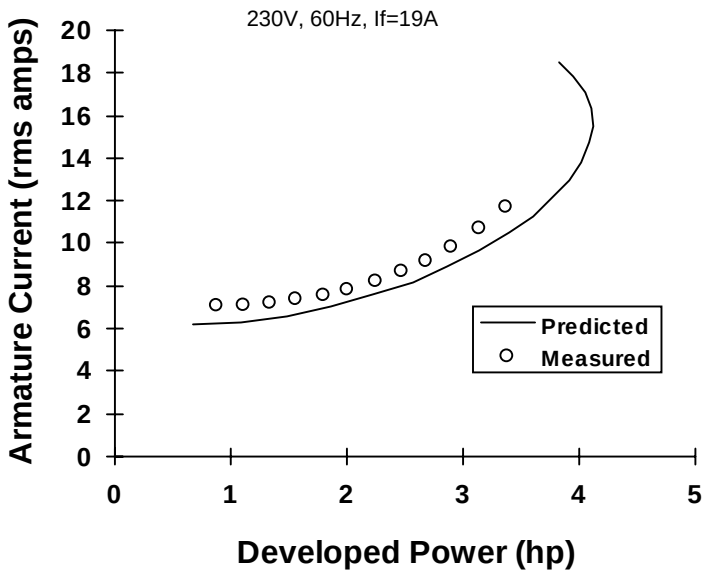

Figure 2-6
Air core motor (with nonsuperconducting field winding) armature current.

Predicted motor power capability was within 16% of measured values which was felt to be quite good for this first air core motor demonstration. This level of accuracy was determined to be acceptable based upon the simple magnetic field model used to obtain the motor parameters. Further research is needed to refine the magnetic model to better model the motor end effects in order to close the gap between predicted and measured performance. This work should include three dimensional finite element magnetic field analysis (3-D FEA) as well as building and testing (including 3-D magnetic field measurements) more air core motors of various geometries and pole numbers. Based on this first air core motor demonstration, the methods currently used will be adequate for general performance calculations of air core motors.

One of the main advantages of the current magnetic field modeling method is its simplicity. This translates into fast design turnaround (compared to direct usage of 3-D FEA in the design process). For HTS motor development, rapid design capability is important since wire and coil performance data is continually evolving as more information about the HTS materials becomes available. To satisfy the goal of rapid design turnaround, further work in this area should concentrate on efficient methods to enhance the magnetic field calculation procedure currently in use in order to obtain better agreement between predicted and measured air core motor performance.

3

TWO HP HTS SYNCHRONOUS MOTOR

Goals

The electromagnetic test rig reported on in the interim report [H] presented an opportunity to easily and quickly demonstrate the first HTS synchronous motor. This demonstration was easily done because it allowed two HTS racetrack coils to be tested in a nonrotating environment. The electromagnetic test rig field pole structure was modified to accept two racetrack HTS coils supplied by American Superconductor Corporation (ASC). The stationary field coils were bathed in a pool of liquid nitrogen. The cooling method was the same as that used for the air core motor described in Chapter 2. The only major modification to the electromagnetic test rig required was the manufacture of a new field pole structure and reinstallation of the iron core. See Figure 1-3 for a description of the evolution of hardware for this HTS motor demonstration.

The iron core was necessary due to the low tolerance of HTS field coils to magnetic fields at the time this motor was constructed. By using an iron core field support structure (compared to a stainless steel support used in the air core motor described in Chapter 2) the air gap flux created by the HTS field coil is carried by the field poles and the magnetic field experienced by the HTS field coil is limited to leakage flux. Consequently, more air gap flux (and a higher motor power capability) can be obtained for a given HTS field winding magnetic field level. The use of a laminated steel armature core in this HTS motor demonstration (compared to the epoxy glass structure for the air core motor described in Chapter 3) results in increased air gap flux per field winding amp. Both of these features result in a higher motor power capability for a given HTS field winding magnetic field level.

The two horsepower (1.5 kW) HTS synchronous motor was built to meet the following goals:

1. Demonstrate the world's first HTS synchronous motor.
2. Measure the magnetic field distribution in the motor and synchronous motor circuit parameters and compare results with predictions.

3. Verify accuracy of iron core synchronous motor electromagnetic design methods.

4. Utilize existing hardware to the extent possible.

The two horsepower (1.5 kW) synchronous motor described in this Chapter represents the first synchronous motor ever demonstrated with an HTS field winding. The motor was comprised of a stationary HTS field winding, with approximately 330 meters (1080 ft) of BSCCO wire in the two racetrack shaped field coils, and a rotating normal conducting aluminum armature winding. The motor possessed an iron core geometry with two salient poles and tests included motor operation with an inverter.

Design

With the exception of the iron field pole structure and the HTS racetrack coils, this motor was virtually the same configuration as the electromagnetic test rig described in [H]. The following paragraphs describe the design aspects of the two horsepower (1.5 kW) HTS synchronous motor. The electrical design is presented first, followed by descriptions of the motor topology, field winding cooling, and finally the test stand topology.

Electrical

A schematic cross section view of the two horsepower (1.5 kW) motor is shown in Figure 3-1. The motor has an iron core armature and field support structure so that the motor is a salient pole, synchronous motor with an HTS field winding. The motor field incorporates all of the electromagnetic features of a large horsepower HTS motor envisioned for commercial applications, including the air gap AC flux shields. Although the armature core and field support structure are magnetic, the copper and stainless steel AC flux shields and thermal insulation create a very large magnetic air gap between the field and the armature winding. Standard one dimensional magnetic field analysis techniques used for conventional motor design could not be applied for this large air gap motor–so electrical design calculations were based upon two dimensional finite element analysis (FEA). A Reliance Electric, internally developed FEA package tailored to electric motor design was used in the design process. Open circuit voltage and the direct and quadrature axis reactance values were determined from the three FEA solutions shown in Figure 3-2. From these solutions the armature winding flux linkages were found and the associated synchronous reactances were calculated.

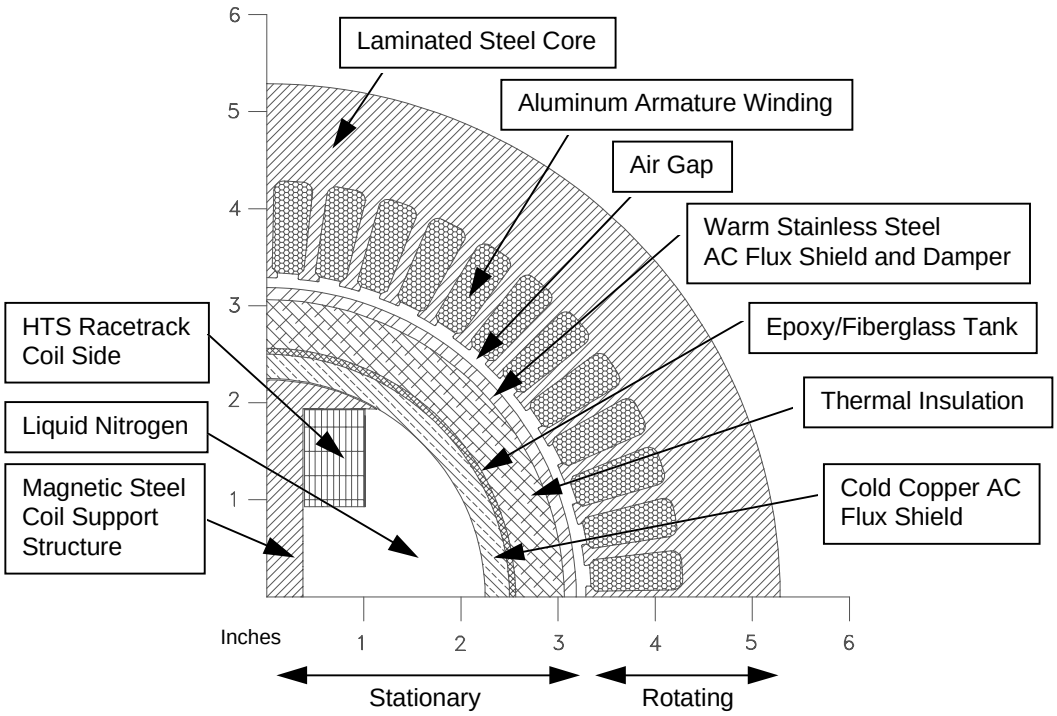

Figure 3-1
Quarter section cross section schematic of the two horsepower (1.5 kW) motor.

Table 3-1
Electrical design parameters for the two horsepower (1.5 kW) HTS motor.

Parameter	Value
Armature OD over steel laminations	10.5 in (26.7 cm)
Armature core length	8.0 in (20 cm)
Total armature end winding extension (per side)	3.75 in (9.53 cm)
Number of stator slots	48
Number of poles	2
Armature Winding	
Line to line voltage	230 V rms
Number of turns per coil	11
Conductor strands	4
Coil throw	1 to 21
Number of circuits	1
Wire material	Aluminum
Field Winding	
Number of turns (all poles)	468
Number of circuits	1
Wire material	BSCCO HTS tape
Total HTS wire length (all poles)	337 m (1100 ft)

The motor electrical design parameters are summarized in Table 3-1. The field winding consisted of two racetrack HTS coils mounted on a specially designed field support structure. Coil voltage taps on the field coils were used to measure the HTS coil voltage drop while the motor was running. Static HTS coil tests were used to estimate the critical current of the racetrack coils. Using this critical current as the motor field winding current the estimated motor developed power capability was found to exceed two horsepower (1.5 kW). Based on this preliminary electromagnetic design the motor field structure mechanical design was completed and the motor was assembled for test.

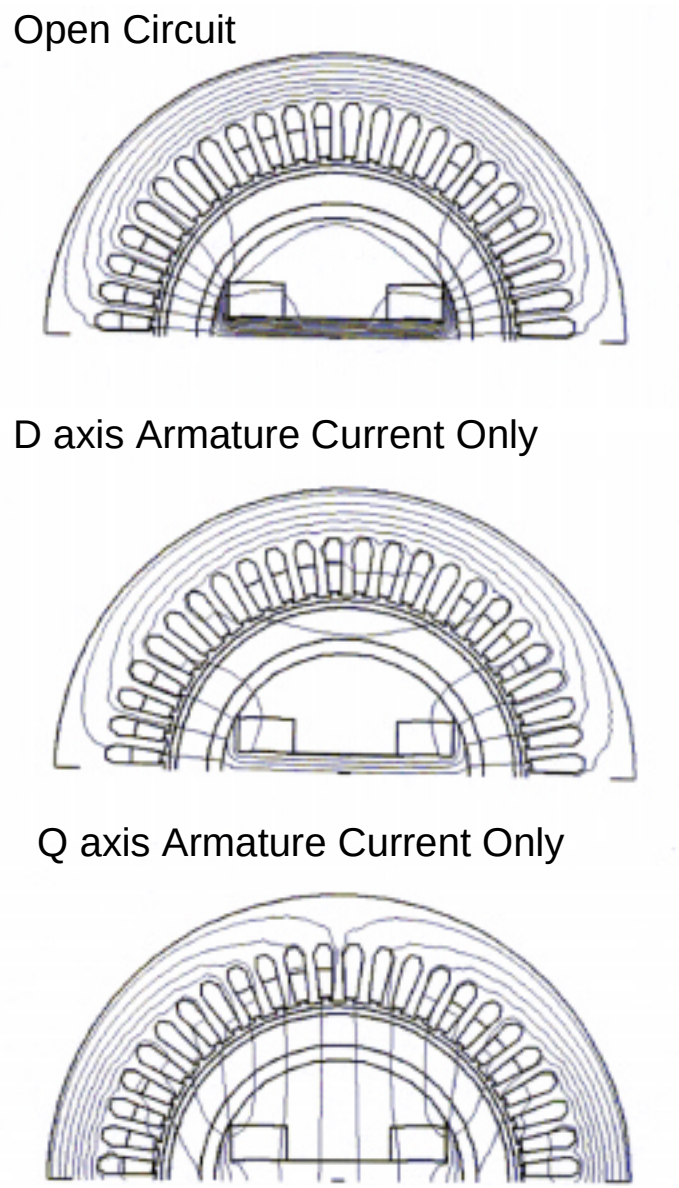

Figure 3-2
Finite element magnetic field distribution equal potential line plots for various coil excitations.

Motor Topology

Figure 3-1 presents a quarter cross-sectional view of the HTS motor showing the relative dimensions of the internal components. The motor itself is approximately 13 inches (33 cm) in diameter and 28 inches (71 cm) in length–including slip rings and drive shaft. As depicted in the figure, the laminated steel core and normal conducting armature winding are part of the rotating structure. The stationary part of the motor

included a G-10 fiberglass epoxy tank, used to confine the liquid nitrogen coolant, which was surrounded by a layer of thermal insulation and a stainless steel outer cylinder. This outer cylinder served as a warm AC flux shield and damper. Inside the G-10 tank, the HTS racetrack shaped coils were mounted in a vertical orientation on a magnetic steel pole structure which was surrounded by a cold copper AC flux shield. An exploded view of the motor is depicted in Figure 2-3 with the copper field winding replaced by the HTS racetrack coils.

Figure 3-3 is a photograph of the two HTS racetrack coils used in the field winding. The total length of HTS BSCCO wire in the coils is approximately 330 meters (1080 ft). The coil dimensions were approximately 14 inch (36 cm) long by 2 inch (5 cm) wide by 1 inch (2.5 cm) thick. The HTS racetrack coils were supplied by American Superconductor Corporation through a Department of Commerce Advanced Technology Program award.

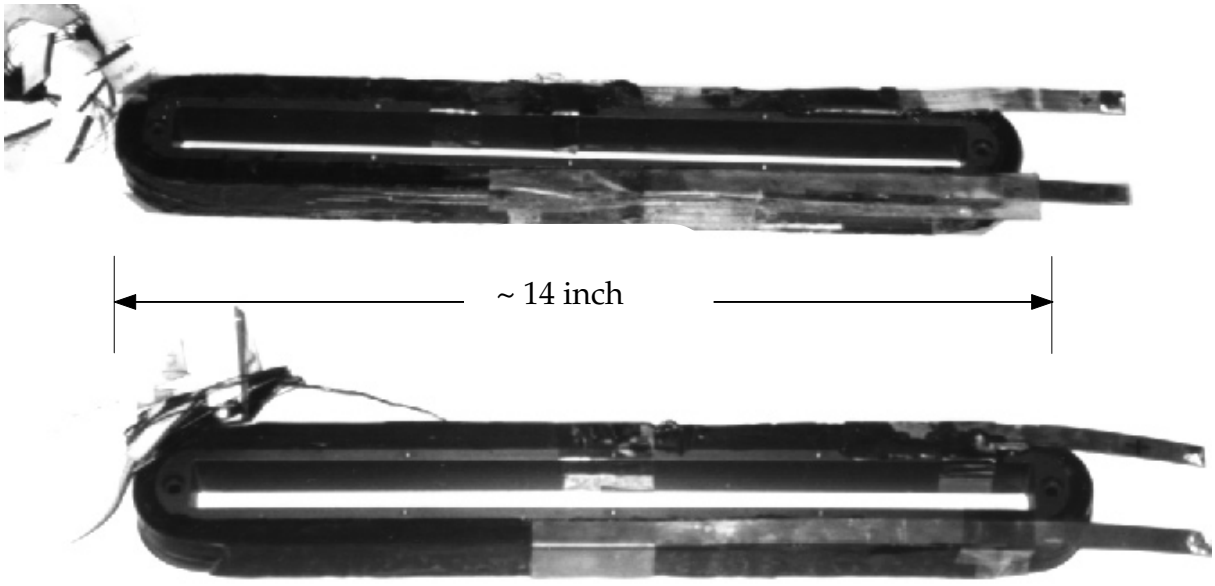

Figure 3-3
HTS racetrack coils used in the 2 hp (1.5 kW) synchronous motor field winding.

Field Winding Cooling

The stationary field winding geometry, as in the air core motor described in Chapter 2, allowed the use of a simple field winding cooling system in which the HTS coils were immersed in a stationary pool of liquid nitrogen. Three thermocouples were mounted on one of the HTS coils, one at each end turn and one at mid span, to monitor coil temperatures and the depth of liquid nitrogen. See Chapter 2 for further details on the cooling system.

Test Stand Topology

Figure 3-4 presents a photograph of the two horsepower (1.5 kW) HTS synchronous motor under test. The test stand components include:

- Two horsepower (1.5 kW) HTS synchronous test motor.
- Induction motor (and inverter) which serves as a pilot motor to rotate the armature winding during soft synchronization of the HTS motor.
- DC generator and resistive load bank which served for loading the test motor.
- Clutch/brake (attached to the drive end of the pilot induction motor) to isolate the pilot motor during load tests using the DC generator.
- Emergency air brake and associated belt system to connect and transfer power between the three motors.

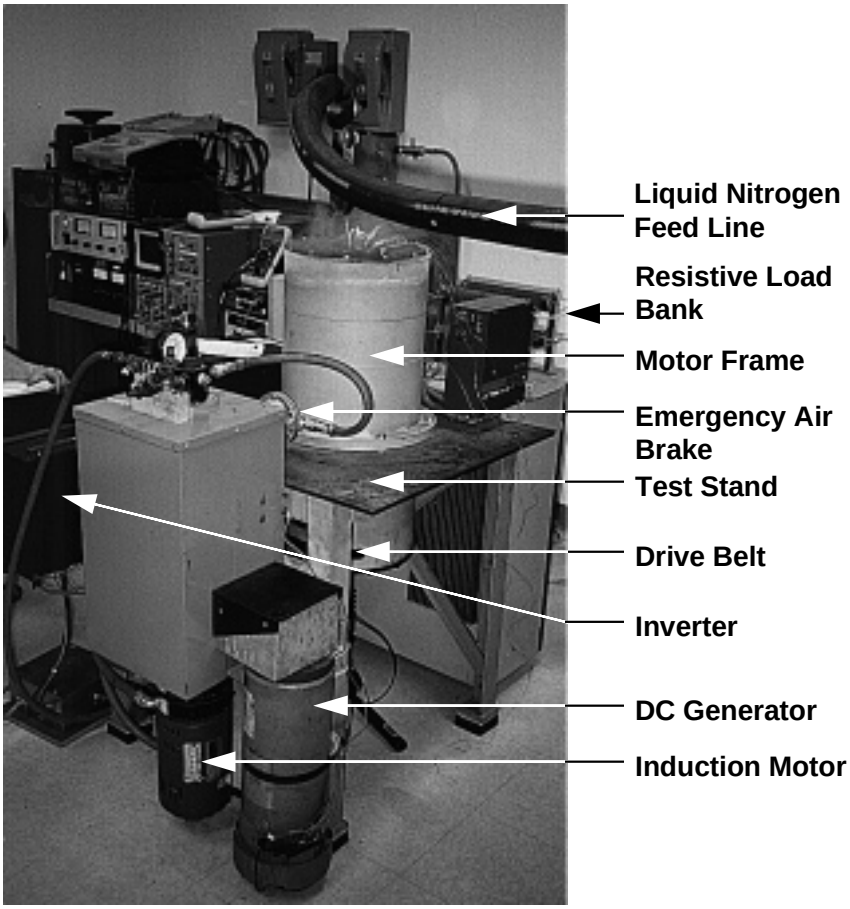

Figure 3-4
Two horsepower (1.5 kW) synchronous motor under test.

Test Results

The steady state, per phase equivalent circuit equations for the two horsepower (1.5 kW) motor are given below:

$$\overline{V_s} = V_q - jV_d \tag{3.1}$$

where $\overline{V_s} = V\angle\delta$ = motor terminal voltage phasor with δ being the torque angle

V_q = Quadrature axis armature voltage = V cos δ.

V_d = Direct axis armature voltage = -V sin δ

$$\overline{I_s} = I_q - jI_d \tag{3.2}$$

$\overline{I_s} = I\angle\gamma$ = motor phase current phasor with γ being the current angle

I_q = Quadrature axis armature current = I cos γ.

I_d = Direct axis armature current = -I sin γ

and

$$V_q = E_o + X_d I_d + R_s I_q \tag{3.3}$$

$$V_d = -X_q I_q + R_s I_d \tag{3.4}$$

with E_o = motor open circuit voltage acting in the quadrature axis.

R_s = armature resistance per phase

X_d and X_q = direct and quadrature axis synchronous reactance.

All motor tests were conducted with a one pulse per revolution position detector on the rotating armature sent out to an oscilloscope. By comparing phase displacement between this position pulse with the zero crossing of the armature voltages and currents at any load point and the zero crossing of the open circuit voltage, phase angles for the current (γ) and voltage (δ) were measured. With this method these angles can be determined to within plus or minus 1 electrical degree. Combining this information with the measured armature voltage and current rms values, and the measured armature resistance, the motor synchronous reactances were found from steady state tests. Table 3-2 presents a comparison of measured and calculated motor parameters. All predicted values were within 6% of measured values.

The motor power capability curves for a number of HTS field winding currents (both predicted and measured) are given in Figure 3-5. Armature currents as a function of motor developed power are shown in Figure 3-6. In both figures, measured and predicted performance agree very well across a wide load range for all field currents.

Table 3-2
Calculated and measured parameters for the two horsepower (1.5 kW) HTS synchronous motor.

Parameter	Measured Value	Calculated Value	% Difference
E_o at I_f = 5 amps	115.5 rms V, $\ell\ell$	109.6 V, $\ell\ell$	- 5 %
X_q at 60 Hz	12.2 Ω	11.5 Ω	- 6 %
X_d at 60 Hz	17.2 Ω	17.5 Ω	+ 2 %
Pull out at 230 V, 60 Hz with I_f=4.0 Amps	2.16 hp (1612 W)	2.12hp (1580 W)	- 2 %
Pull out at 230 V, 60 Hz with I_f=4.5 Amps	2.26 hp (1687 W)	2.27 hp (1690 W)	0 %

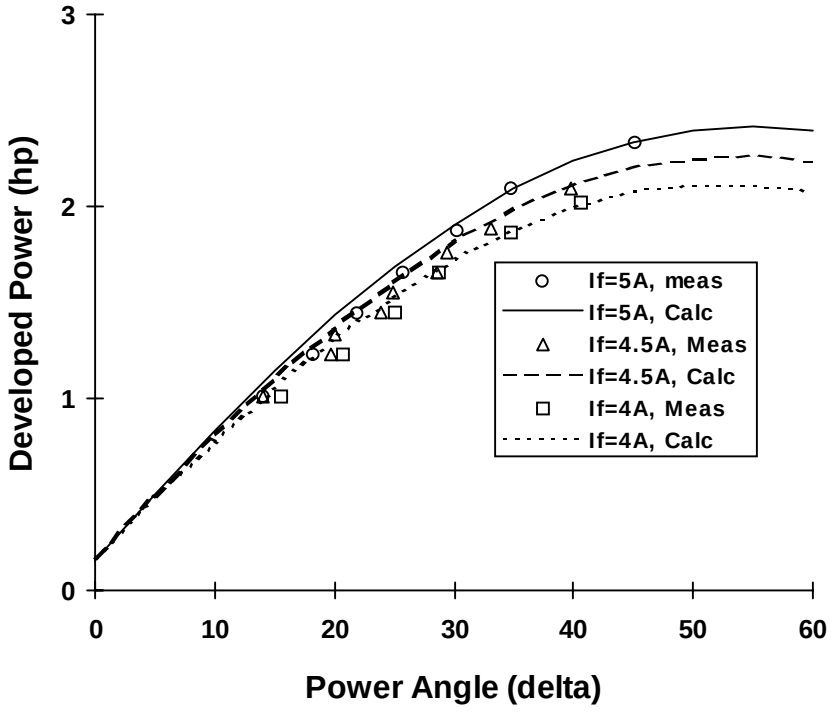

Figure 3-5
Measured and predicted power capability curves for the two horsepower (1.5 kW) HTS synchronous motor at various field currents. All data with 230 Volt, 60 Hz, sine wave armature excitation.

The next set of performance tests of the two horsepower (1.5 kW) motor was with the motor operated from a PWM (Reliance model GP1000) inverter. This represented the first superconducting motor demonstration with inverter power. For 3600 rpm operation the motor was started by setting the inverter output frequency to around 60 Hz and letting the current limit circuitry in the drive control the output frequency ramp rate. (The motor accelerates very slowly due to the high inertia of the outer rotating armature.) This is done with the HTS field current turned off (so the motor starts as an induction motor using the air gap AC flux shields as the starting cage). When the motor speed reaches about 3500 rpm the field current is turned on and the motor synchronizes. The final 3600 rpm operating speed can be reached by fine adjustment of the inverter output frequency. The motor can also be started by synchronizing at a low speed and very slowly increasing the inverter output frequency to reach the desired speed.

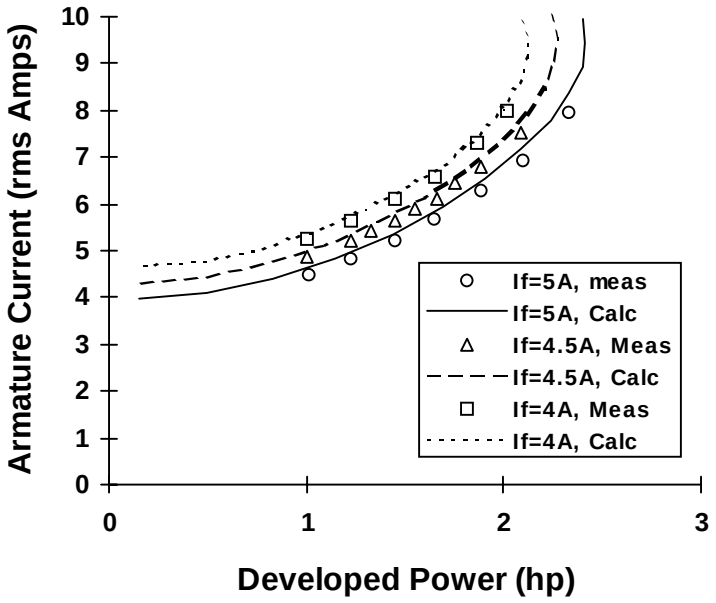

Figure 3-6
Measured and predicted armature currents for the two horsepower (1.5 kW) HTS synchronous motor at various field currents. All data with 230 Volt, 60 Hz, sine wave armature excitation.

The HTS field winding voltage drop was measured for all steady state operating conditions under test. The state of the HTS coils can be determined by monitoring the field voltage drop. Figure 3-7 shows this field voltage as a function of motor load for three different field winding currents. A voltage drop less than 1 μV/cm (2.5 μV/in) in a superconducting wire is commonly used as a measure of superconductivity. As shown, the HTS coil voltage remained below 1μV/cm (2.5 μV/in) for developed power

in excess of two horsepower (1490 watts) for a field current of 4 amps. HTS coil voltage drops, with sine wave and inverter armature excitation, were found to be virtually identical (see Figure 3-7). This indicates that the harmonics generated by the inverter excitation (largely above 2 kHz) had no effect on the HTS coil performance.

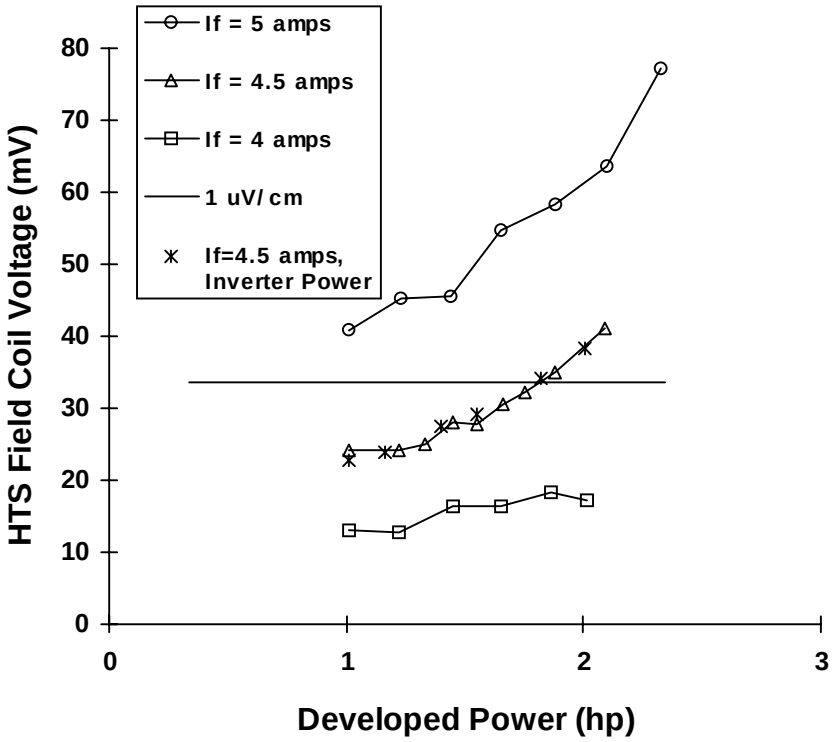

Figure 3-7
HTS winding voltage for various operating conditions of the two horsepower (1.5 kW) HTS motor. All are 60 Hz operation (3600 rpm) with sinusoidal armature voltage except where noted. Inverter power is with a PWM inverter powering the armature.

The HTS coil voltage increases with increasing load, as seen in Figure 3-7, due to the effects of the armature reaction magnetic field. Figure 3-8 has V-I curves for the motor for a number of operating conditions. Here again, the effects of armature reaction fields on the HTS coil performance can be seen. In this demonstration motor the field coil operating current is nearly equal to the HTS wire critical current. This is why a significant change in HTS coil voltage drop occurs due to this armature reaction effect. In a commercial motor the superconducting coil operating current is expected to be in the range of 80% of the coil critical current. At this 80% level the coil voltage drop (and the losses in the motor cold space) will be, for all practical purposes, load independent.

Two dimensional finite element analysis was used to estimate the magnetic field that the HTS conductors experience with the motor under load. For two horsepower

(1.5 kW) output at 230 V and a field current of 4.4 amps, the calculated maximum two dimensional field in the superconducting winding was found to be 1150 Gauss (1000 Gauss parallel to the tape conductor and 570 Gauss perpendicular to the tape conductor). This compares to a calculated maximum two dimensional field in the HTS coils under open circuit conditions, with a field current of 4.4 amps, of 680 Gauss (620 Gauss parallel to the tap conductor and 270 Gauss perpendicular to the tape). The armature reaction effects increase the HTS winding field by 70% at this two horsepower (1.5 kW) load point. This is the cause of the increased HTS winding voltage drop shown above. At 4.4 amps, the current density of the superconducting portion of the HTS wire cross section is 3550 amps/cm^2 (22.9 kA/in^2). This is a very low flux density machine, mainly due to the low values of magnetic field the HTS conductors can withstand at liquid nitrogen temperature.

Hall sensors were located on the HTS field winding in an attempt to measure magnetic field levels in the HTS winding during motor operation and compare them to calculated values. Correlation between measured and calculated magnetic fields was very poor largely due to the high sensitivity of magnetic field level to small changes in position of the Hall sensors. (This phenomenon was confirmed with 2D FEA analysis). Although point verification of magnetic field levels could not be accomplished, the overall accuracy of the FEA design calculations were verified by motor performance and circuit parameter comparisons between calculated and measured values as described above.

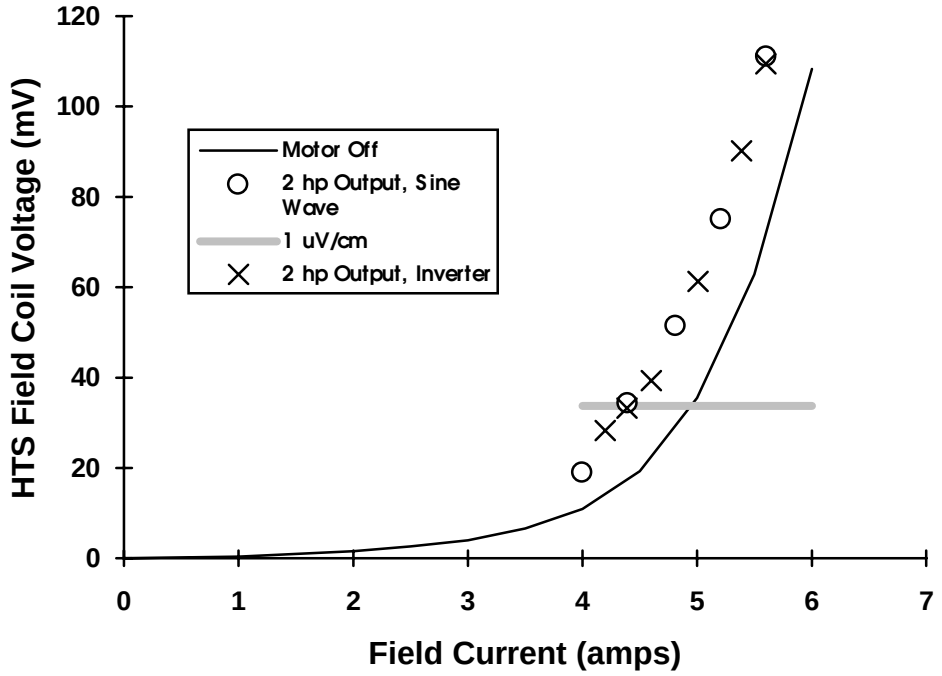

Figure 3-8
HTS winding voltage for various operating conditions of the two horsepower (1.5 kW) HTS motor. All are 60 Hz operation (3600 rpm) with sinusoidal armature voltage except where noted. Inverter power is with a PWM inverter powering the armature.

Conclusions

Overall the two horsepower (1.5 kW) synchronous motor with HTS field winding design, construction and test was a success, and was an important step forward in HTS motor development. This was the first synchronous motor with an HTS field winding built, and the motor developed power was 50 times larger than that obtained from any previous HTS motor prototype demonstrated as part of this project.

The four goals of the HTS synchronous motor demonstration were all met. An HTS synchronous motor with output power exceeding two horsepower (1.5 kW) was demonstrated. The motor was based on the existing iron core electromagnetic test rig hardware with modifications to the stationary field structure. Motor performance tests were completed and results compared to predicted performance based upon design calculations using two dimensional finite element analysis. Motor operation with inverter power also was successful

Motor performance predictions (circuit parameters and power capability) agreed to within 6% of test data. This level of accuracy is adequate for iron core demonstration

motor design and performance prediction. Ultimately, HTS motors will be air core. Further refinements of the iron core design and analysis techniques will not contribute to better air core models since the analysis methodology for the two types of motors are very different. Air core motors are modeled with closed form magnetic field solutions (see Chapter 2) while the iron core motor described here requires two dimensional FEA modeling due to its large magnetic air gap.

4

FIVE HP HTS SYNCHRONOUS MOTOR

Goals

The five horsepower (3.7 kW) synchronous motor was built to meet the following goals:

- Demonstrate a motor which more closely matches the configuration of the final HTS motor product (i.e. synchronous motor with a rotating HTS field winding).
- Demonstrate, evaluate, and verify analyses of liquid nitrogen pool boiling in a rotating environment as a means of cooling the HTS coils and maintaining their operational temperatures.
- Demonstrate the largest horsepower motor possible with HTS coils which represent the state-of-the-art in HTS wire performance.
- Identify design issues which may arise for larger HTS motors.

The rotor for the five horsepower (3.7 kW) motor was built early on in this project for initial testing (separate from the motor armature) and demonstration of the cryogenic cooling system (see Figure 1-4). This rotor, at the time, was referred to as the *rotor/cryostat test rig* [H]. The rotor/cryostat test rig possessed the following features:

- Rotor including a vacuum insulation space to minimize heat leak, liquid nitrogen feed line tube for delivering liquid nitrogen to the cold space of the rotor, cryogenic vacuum seal for access to the cold space, slip ring assembly for cryogenic sensor input/output, and a fractional horsepower motor for rotating the rotor to 1800 rpm.
- Mock HTS racetrack coils machined from G-10 epoxy/glass composite.
- Simulated armature with stationary tube and barrel heaters to mimic armature heating.

The main reasons for construction and test of the rotor/cryostat test rig were for studying pool boiling as a means of cooling HTS coils and gain experience in using cryogenic sensors in the rotating environment of an electric motor–prior to actually

building a motor with rotating HTS coils. Mock coil temperatures and vibration data results from the initial testing of the rotor cryostat did not indicate any insurmountable problems with the pool boiling cooling system.

The HTS racetrack coils, which were to replace the mock racetrack coils in the rotor/cryostat, were manufactured by American Superconductor Corporation. The design of the armature was pursued after measuring the performance of the HTS racetrack coils and updating the electrical design of a motor which was to utilize the rotor/cryostat test rig rotor. The motor constructed was tested to an output power of five horsepower (3.7 kW) and represented the first motor built with rotating HTS coils. The remainder of this chapter describes the HTS motor design and test results.

Design

The following paragraphs describe the design aspects of the five horsepower (3.7 kW) HTS motor. The electrical design is presented first, followed by descriptions of the motor topology, field winding cooling, rotor instrumentation, and finally the test stand topology.

Electrical

Improvements in HTS wire and coil performance (defined here to mean current carrying capability in the coil's self magnetic field at 77 Kelvin) continued throughout the design phase of this motor. Since synchronous motor power capability is directly related to the field winding MMF that is produced, the predicted power rating of this motor increased over time as new information about HTS coil performance became available. Due to the uncertainty in the final level of HTS coil performance, electromagnetic motor performance calculations were based on a range of field MMF values. As described above, one of the goals was to demonstrate the largest horsepower motor possible. Ultimately, the HTS coils supplied exceeded the original MMF per pole specification (for a one horsepower motor) by 70%. By reconnecting the armature winding (to a parallel connection described below) a factor of two increase in armature winding current density was made available. All initial design calculations, described below, were based upon the series winding connection. The parallel connection was tried, at the last minute, to meet the stated goal of obtaining the highest horsepower output possible. The combination of field MMF increase and doubling the armature current density resulted in a motor power capability of five horsepower (3.7 kW).

A quarter section, cross section of the five horsepower (3.7 kW) motor is shown in Figure 4-1. This is an iron core, salient pole, four pole motor with a magnetic steel field support structure and a vacuum insulated cryostat. The stator consists of a laminated core with a standard, lap wound, copper armature winding. The rotor has a warm

(stainless steel) and a cold (copper at liquid nitrogen temperature) AC flux shield that act to keep AC magnetic fields from reaching the racetrack shaped superconducting coils. These flux shields also act as the damper winding to damp rotor oscillations during motor transients. The motor uses four racetrack HTS coils for the field winding. The coils are protected from armature reaction fields by the steel pole shoes that extend beyond the coil sides at the outer radius of the coils.

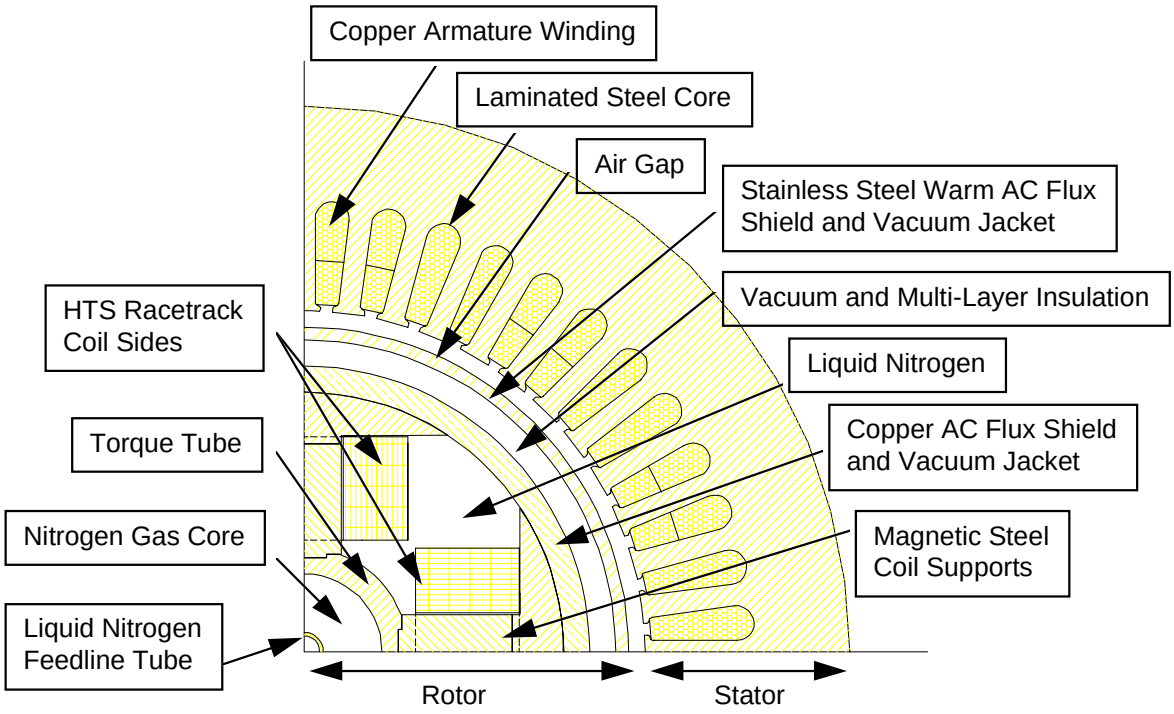

Figure 4-1
Quarter section cross section of the five horsepower (3.7 kW) synchronous motor with HTS field coils.

Two dimensional finite element analysis (FEA) techniques (as described in Chapter 3) were used to determine the steady state circuit parameters. The original design goal for the motor was a one horsepower (0.7 kW) rating at 1800 rpm. This was believed possible, at that time, given the state of the HTS wire technology. This 1 hp (0.7 kW) rating required an HTS field winding with 630 amp-turns per pole. With this field excitation level the motor was predicted to have a 160% overload capability [i. e. maximum power capability of 1.6 hp (1.2 kW)]. Detailed HTS coil specifications were determined for a variety of coil performance levels. Magnetic field specifications for the HTS conductors were based upon the two dimensional FEA as well as measured magnetic fields (in the end winding region) made with equivalent copper field coils. Table 4-1 contains motor performance estimates as a function of HTS field coil performance values.

Table 4-1
HTS coil specifications as a function of motor power capability at 1800 rpm. All data is for series armature winding connection.

Motor Peak HP (kW)	HTS Field Winding MMF per Pole (Amp-turns)	HTS Field Winding Peak Magnetic Field (Gauss)
1.6 (1.2)	630	400
2.6 (1.9)	1080	640
3.9 (2.9)	1680	960
5.2 (3.9)	2240	1280
6.5 (4.8)	3120	1770

The original design concept required four coils per pole (each being a layer in the racetrack) stacked together to produce the 630 amp-turns. One coil layer was purchased from American Superconductor Corporation and performance tested. With this design concept much of the field winding area would be occupied by coil support plates and filler material so that it would be difficult to obtain the 630 amp-turn goal. The next coil purchased from American Superconductor was a single coil that filled the entire winding space for each pole. Three more coils were supplied by American Superconductor Corporation as part of a Department of Commerce Advanced Technology Program award to complete the field winding. Each coil had 234 turns and 168 meters (551 ft) of wire for a total field winding wire length for the motor of 673 meters (2210 ft).

HTS coil performance is a strong function of magnetic field magnitude *and direction* throughout the coil. Static tests on these coils in a specially designed magnetic test fixture, shown in Figure 4-2, were done before installing the coils in the rotor. This fixture mimics the magnetic field distribution in the motor rotor for the field coil self field. FEA field calculations showed that the armature reaction fields, over and above this self field, contribute less than 10% to the maximum flux density experienced by the field coils. Based upon this small effect, HTS coil performance in the motor was predicted by the self field test alone. Coil tests were done in a liquid nitrogen tank by measuring the coil V-I curve to determine the coil critical current. Four racetrack coils were separately tested in the test fixture. At each current, the measured coil voltages for the four coils were added together in order to predict the field winding voltage expected in the motor. Figure 4-3 has a plot of this predicted field winding voltage as a function of field coil MMF per pole. A voltage drop of less than 1 μV/cm (2.5 μV/in) in a superconducting wire is commonly used as a measure of superconductivity. This voltage level is plotted in the figure and used to determine the predicted critical MMF per pole for the motor.

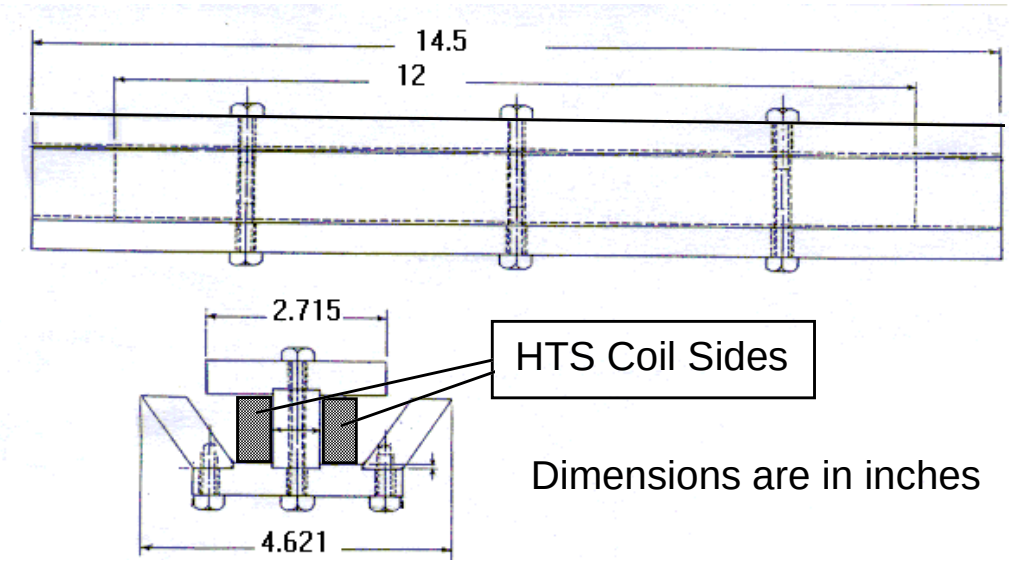

The magnetic field experienced by the HTS coils is entirely its self field. The magnetic steel component shapes (top plate, bottom plate and angled sides) are designed to produce a magnetic field distribution in the HTS coils that is similar to what will be experienced in the motor.

Figure 4-2
Full pole test fixture for racetrack HTS coils. All components are magnetic steel (except for HTS coil sides shown).

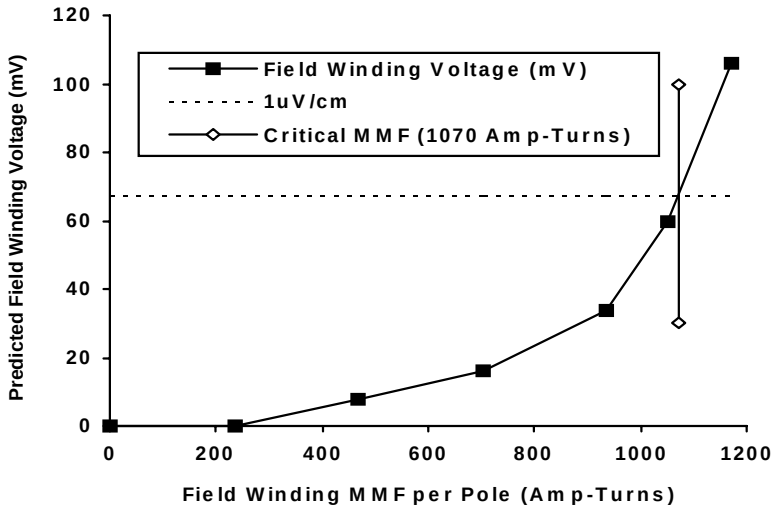

Field winding voltage curve obtained from adding measured voltages of four coils tested at each test MMF.

Figure 4-3
Field winding voltage drop prediction obtained from racetrack coil tests in the test fixture of Figure 4-2.

Results of the full pole coil tests indicated a field MMF per pole of 1070 amp-turns would be achievable in the rotor. This exceeded the original design specifications of 630 amp-turns by 70%, indicating the HTS wire performance improvements that occurred from the time the motor was originally designed to when the coils were actually manufactured and delivered. At 1070 amp-turns per pole the peak power capability for the motor was expected to be 2.6 hp (1.9 kW) (see Table 4-1) for the series armature winding connection. The electromagnetic design of the motor was then revisited, with the parallel armature winding connection option evaluated, to develop an armature winding design that would take full advantage of this field MMF level.

The original motor design for one horsepower output had armature winding copper that was very lightly loaded. This was done to keep the motor power factor high (above 0.8) so that inverter testing could be done with a conventional induction motor inverter without exceeding the inverter current rating. The one horsepower design was intended to have two circuits per phase, in series, to get the 230 volt rated voltage. Once the HTS coil performance was established (from data of Figure 4-3), a parallel circuit connection was evaluated in order to demonstrate the highest horsepower motor possible (one of the design goals for this motor). The parallel circuit connection would be only tested with sine wave power, removing the restrictions placed in total armature current by an inverter. By putting the two circuits in parallel and applying the same voltage the motor air gap magnetic field is increased by a factor of two (at the expense of increased armature magnetizing current and a lower power factor) and the motor power capability is increased. Steady state electrical performance predictions indicated that the armature winding copper could withstand the extra current with this parallel circuit connection so two dimensional FEA was used to find out if the additional armature currents would increase the magnetic field experienced by the HTS coils.

A comparison of predicted motor performance for the two armature winding connections is given in Table 4-2. As shown, even with nearly double armature conductor currents and air gap flux density, the HTS coils see only a 14% increase in magnetic field. The field pole shoes act to shield the HTS coils from the armature reaction fields so that, for this iron core motor design, the majority of HTS winding magnetic field is due to its self field. Figure 4-4 contains flux plots for the two armature winding connections at full load showing this effect. The increased power capability for the parallel winding connection is at the expense of a significant decrease in motor efficiency as shown in the table.

Table 4-2
Comparison of HTS motor performance with two different armature winding connections.

(230 Volt, 60 Hz armature excitation and 1200 amp-turns per pole field excitation)

Parameter	Windings in Series	Windings in Parallel
Rated motor Power	2.3 hp (1720 watts)	4.8 hp (3580 watts)
Armature copper current density	1230 amps/in^2 (190 amps/cm^2)	2390 amps/in^2 (370 amps/cm^2)
Power factor at rated power	0.84 lag	0.48 lag
Maximum B field in HTS winding	700 Gauss	800 Gauss
Peak fundamental component radial B field at the stator bore at full load	770 Gauss	1400 Gauss
Efficiency (excluding cooling power)	92%	86%
Relative power density (hp/volume)	1.0	1.7

The motor was wound with two circuits and tests with both connections were planned. Electromagnetic design parameters are given in Table 4-3. Rated voltage performance curves for the two winding connections are shown in Figure 4-5 for a 1200 amp-turn per pole field winding. Peak output power was expected to exceed five horsepower (3.7 kW) with the parallel winding armature connection.

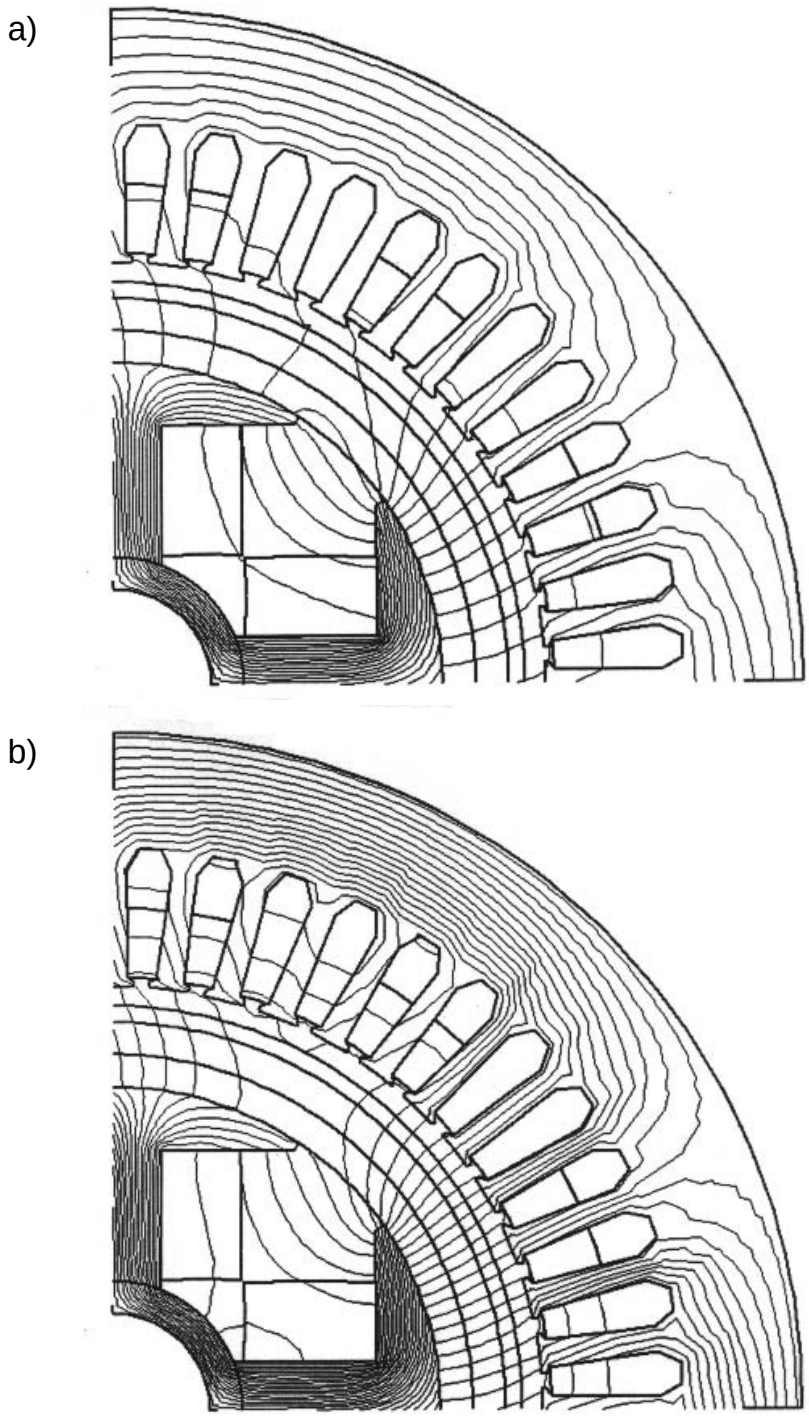

Figure 4-4
Rated load equal magnetic potential line plots for the two armature winding connections. Both plots are for 1200 amp-turn per pole HTS field winding MMF and 230 Volt terminal voltage at 60 Hz. Difference in potential between lines is 400 Gauss-cm. a) Series connection, 2.5 hp (1.9 kW) developed, b) Parallel connection, 5.1 hp (3.8 kW) developed.

Table 4-3
Electrical design parameters for the five horsepower (3.7 kW) HTS motor.

Parameter	Value
Armature OD over steel laminations	10.5 in (26.7 cm)
Armature core length	12.0 in (30.5 cm)
Number of stator slots	48
Number of poles	4
Armature Winding	
Line to line voltage	230 V rms
Number of turns per coil	15
Conductor strands	3
Coil throw	1 to 11
Number of circuits	1 for series connection 2 for parallel connection
Wire material	Copper
Field Winding	
Number of turns (all poles)	936
Number of circuits	1
Wire material	BSCCO HTS tape
Total HTS wire length (all poles)	673 m (2210 ft)

Motor Topology

The with an HTS field winding was first demonstrated near the end of 1993. The five horsepower (3.7 kW) HTS motor, shown in Figure 4-6, was the second synchronous motor built and the first motor to use rotating HTS field coils. As in the two horsepower HTS motor (Chapter 3), this is an iron core motor, however it has a more conventional motor geometry (i.e. a rotating field winding and a stationary armature winding) and four salient field poles. The field winding consists of four racetrack shaped HTS coils with a total BSCCO wire length of approximately 670 meters (2200 ft). Two of the four HTS racetrack shaped coils are shown in Figure 3-3.

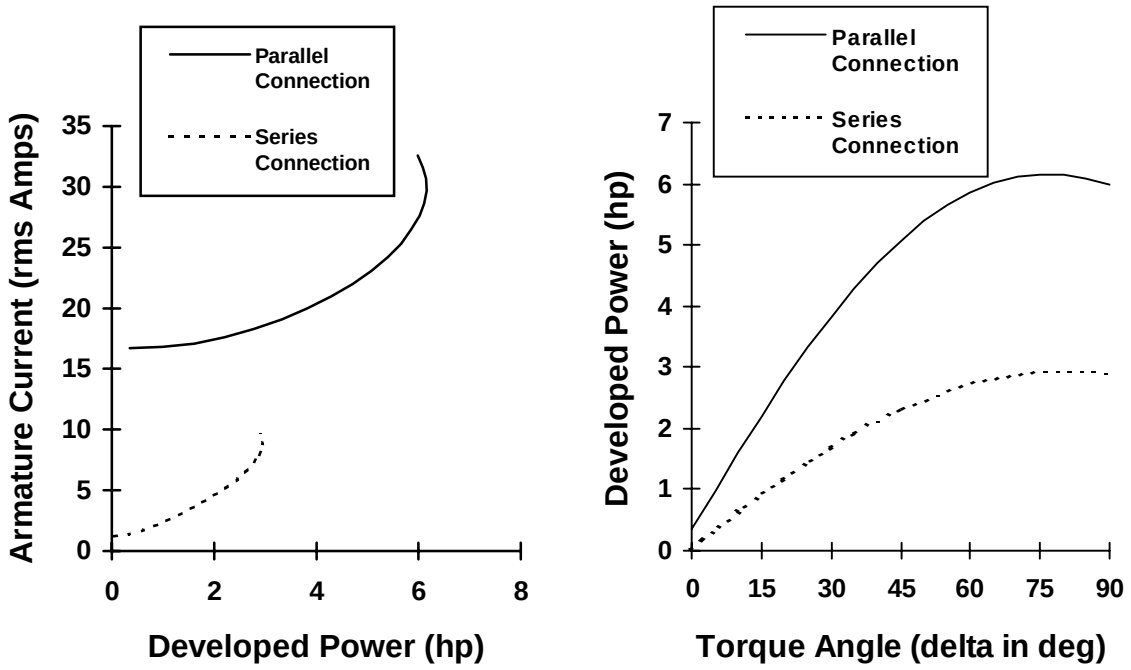

Figure 4-5
Predicted performance of the HTS motor with 1200 amp-turn field winding at 230 volts, 60 Hz armature excitation (measured performance data are presented in Figures 4-14 and 4-17).

Figure 4-7 presents a cross-sectional view of the five horsepower (3.7 kW) HTS motor rotor which is approximately six inches in diameter. This figure clearly shows the pole structure of the rotor. The four HTS racetrack shaped coils are mounted on the four poles of the rotor and each pole is attached to a central core tube. The pole structure is surrounded by a cold copper AC flux shield inner wall, a vacuum insulation space containing multilayer insulation, and a stainless steel outer shell which serves as a warm AC flux shield and damper.

The rotor is assembled from two major components—a drive end section and a nondrive end section. This construction allows quick disassembly and access to the cold space. Figure 4-8 depicts the rotor in its partially disassembled and fully assembled states. The drive end section of the rotor consists of a hollow drive shaft connected to the central core tube on which the poles and HTS coils are mounted. Flanges for the connections of the inner and outer walls of the vacuum space, a bearing mounting collar, a slip ring assembly, and a drive sheave are all parts of the drive end section. The coil current and instrumentation leads are passed from the slip ring assembly through the hollow drive shaft and directly into the cold/coil space of the rotor. This section is the rigid torque transferring component of the rotor and allows disassembly without disconnecting coil and instrumentation leads.

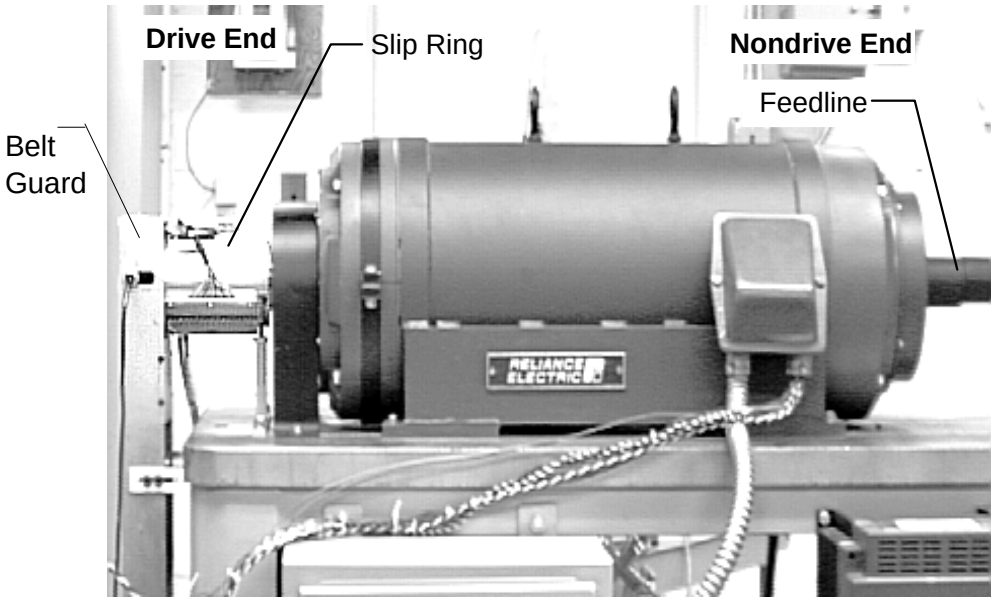

Figure 4-6
Four pole synchronous HTS motor.

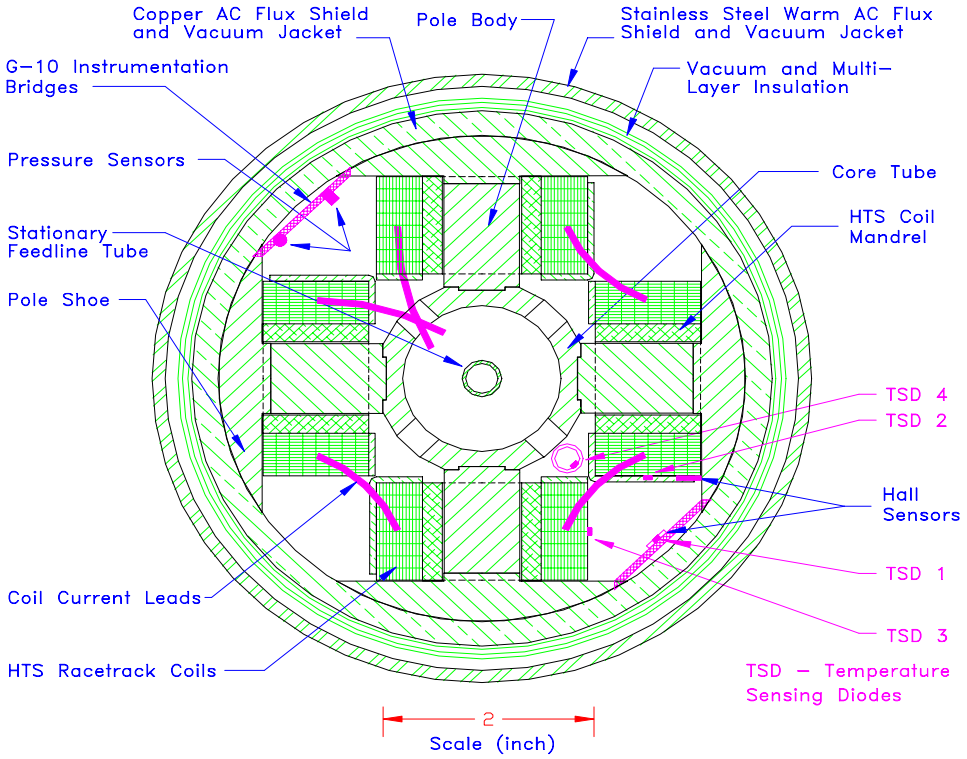

Figure 4-7
Cross-section of the four pole HTS synchronous motor rotor showing cryogenic sensor locations.

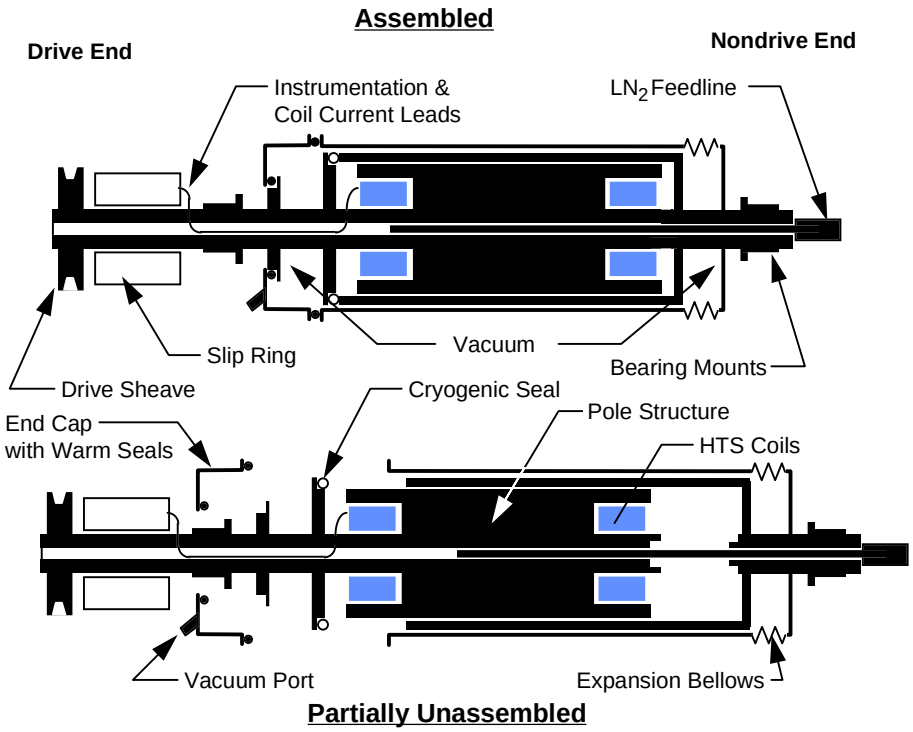

Figure 4-8
Assembly of the four pole HTS synchronous motor rotor.

The nondrive end section of the rotor consists of a short hollow shaft extension on which the inner and outer vacuum space walls and a bearing mounting collar are attached. The outer vacuum shell includes bellows which accommodate the differential thermal contraction between the inner and outer vacuum shells. Upon assembly of the drive and nondrive end sections, a cryogenic seal between the cold space of the rotor and the vacuum space is made using an indium foil coated stainless steel metal o-ring (tubular). Once the cryogenic seal is secured and checked, the vacuum space is sealed by attaching the end cap. The end cap includes two warm o-ring seals, and the vacuum is pumped through a valve located on the end cap. The assembled length of the rotor from bearing to bearing was slightly over 2 feet (61 cm).

The cryogenic seal for this rotor was a modification which was performed after initial testing of the rotor with mock HTS coils. The original design was an all welded construction which did not allow easy access to the cold space of the rotor. During initial testing of the rotor, cryogenic sensor and vacuum leakage problems prompted the modifications to the demountable cryogenic seal design; however, vacuum leakage problems were not alleviated with the rotor modification. The exact cause or causes of the vacuum leak/s was never isolated. There were three areas of concern with regard to vacuum leaks: 1) the cryogenic seal was extremely difficult to assemble without tearing the indium foil coating, 2) the 'warm' o-ring on the end cap of the rotor experienced very low temperatures due to the shaft extension through the vacuum

space, which essentially cold strapped the o-ring to the cold space of the rotor, and 3) the copper to stainless steel brazed butt joints on the inner vacuum jacket wall. Low vacuum pressures were held for sufficient time, however to allow good test results to be obtained.

Optimization of the motor efficiency was not a design goal since, due to the performance level of state-of-the-art HTS wire, the motor would be significantly larger than a conventional five horsepower (3.7 kW) motor–which translates to higher friction losses and windage losses which cannot be compared. In addition, to accurately determine the motor efficiency, the cooling system requirements should be charged against the efficiency of the motor. Since neither the cooling system or the rotor were designed for optimal cooling efficiency, a calculation or estimate of the total motor efficiency was not considered to be useful or necessary information. Friction and windage losses for the motor, however, were experimentally determined and are presented in the results section.

Field Winding Cooling

One of the goals for this motor was to demonstrate and test a rotating pool boiling method of maintaining the HTS coils at their operational temperature. Liquid nitrogen flows from a supply tank, through a subcooler and metering flow control valve to a stationary feed line tube which protrudes into the cold space along the centerline of rotation (see Figure 4-8 and 4-9). Both the liquid nitrogen feed and boil-off nitrogen gas are passed through the hollow shaft at the nondrive end of the rotor. The boil-off nitrogen gas is passed through the motor stator/frame upon leaving the rotor. This aids in cooling the stator winding, and provides a dry atmosphere inside the frame to minimize frost build-up inside the frame and on the rotor.

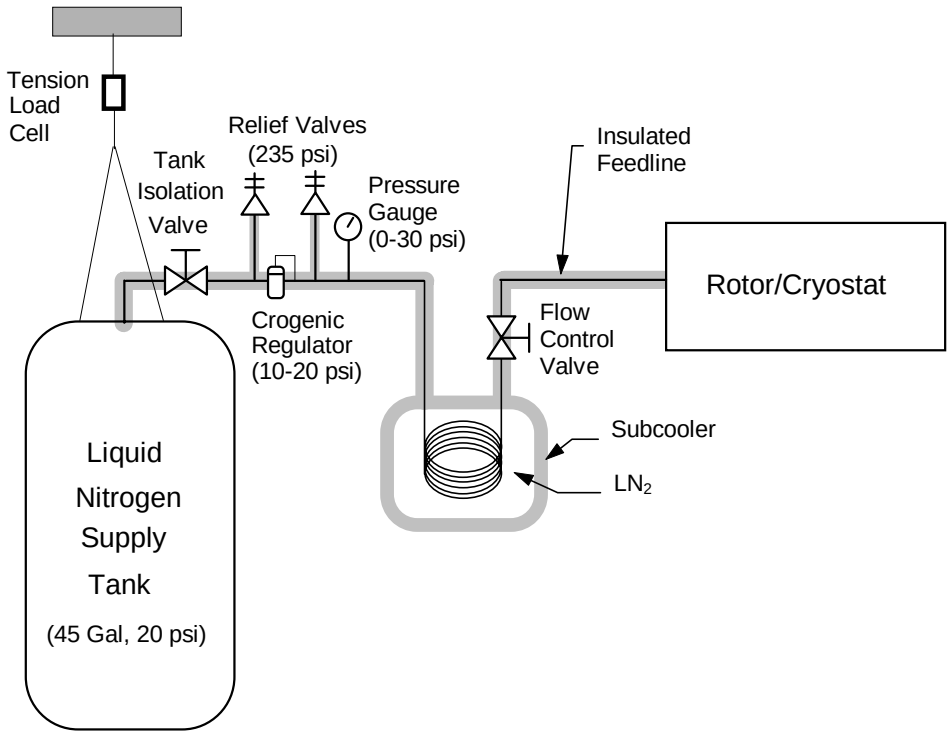

Figure 4-9
Configuration of the once through liquid nitrogen rotor cooling supply system.

Once inside the rotor, the liquid nitrogen migrates toward the copper inner wall, due to the centrifugal forces of rotation, forming a central gas core. The liquid fills the cold space of the rotor from the copper inner wall toward the central core tube. Tests on the motor were performed with different pool depths and included the complete immersion of the HTS coils in liquid. Prior to testing, analysis indicated that the heat leak into the cold space of the rotor would be approximately 107 W. Experimental data indicated that the heat leak into the cold space of the rotor was in the range of 103 to 115 W, agreeing well with the calculated estimate.

Rotor Instrumentation

The field winding of the motor is made up of four racetrack coils connected in series. The connections between the coils were made with normal conducting (copper) bus bar and wire inside the rotor cryostat. The state of the superconducting coils was determined by measuring the voltage drop of each coil at voltage taps located near the coil terminals and adding these voltages together to get a total HTS field winding voltage. This method eliminated the voltage drop in the copper connections between coils. Coil voltages were measured using a passive RC filter in order to obtain the DC coil voltage drop. The filter allowed stable voltage readings for all motor operating

conditions; including the electromagnetically noisy PWM inverter armature power tests.

The coil space of the rotor was instrumented with cryogenic temperature sensing diodes, pressure sensors, Hall sensors, and a liquid level sensor (refer to Figure 4-7). A liquid level sensor (not shown in Figure 4-7), which diametrically spanned the cold space of the rotor, was used for some tests but was abandoned after it was found unreliable. The two cryogenic pressure sensors, located on a G-10 bridge between two pole shoes and in the axial center of the rotor, were found to be more reliable in determining the liquid nitrogen level inside the rotor. The pressure sensors were supplied by Lake Shore Cryotonics–one was a commercially available product and the other, at that time, was a prototype which was not commercially available. The prototype sensor was extremely reliable and less susceptive to temperature changes than the commercial version.

Four cryogenic temperature sensing diodes (TSDs) were used to determine the radial temperature distribution inside the cold space–no attempt was made to determine the axial temperature distribution. The TSDs were ineffective during motor tests using PWM inverter armature power. Inverter operation was electromagnetically noisy and this noise was rectified by the TSDs causing erroneous readings. The solution to this problem is believed to be the shielding or use of twisted pairs for the TSD leads which passed from the slip ring assembly to the cold space of the rotor, however this was not attempted because it required a complete disassembly of the rotor.

Two cryogenic Hall sensors were mounted inside the rotor to measure the internal magnetic field. One Hall sensor was mounted on a coil side near the pole shoe to measure the field perpendicular to the plane of the HTS tape conductor. The second Hall sensor was mounted on the same G-10 bridge as TSD 1 to measure the radial field between two HTS coils.

Extensive data acquisition software was developed for Lab Windows to monitor the rotor sensors and various external sensors (e.g. the rotor speed, bearing and motor frame temperatures, and liquid nitrogen consumption). The data acquisition software possessed a cycle time of approximately one minute for collecting, displaying, and saving data from all sensors.

Test Stand Topology

Figure 4-10 shows a rear view of the 5 hp (3.7 kW) HTS motor and test stand. A 7.5 hp (5.6 kW) DC motor (with regenerative drive) was used as the spin up pilot motor and load motor. The motor was located on a test shelf below the HTS motor. A belt connection between the two motors was used to transfer energy. A Reliance AC

inverter was used for inverter operation tests of the HTS motor. Both motors and drives were mounted on the test stand.

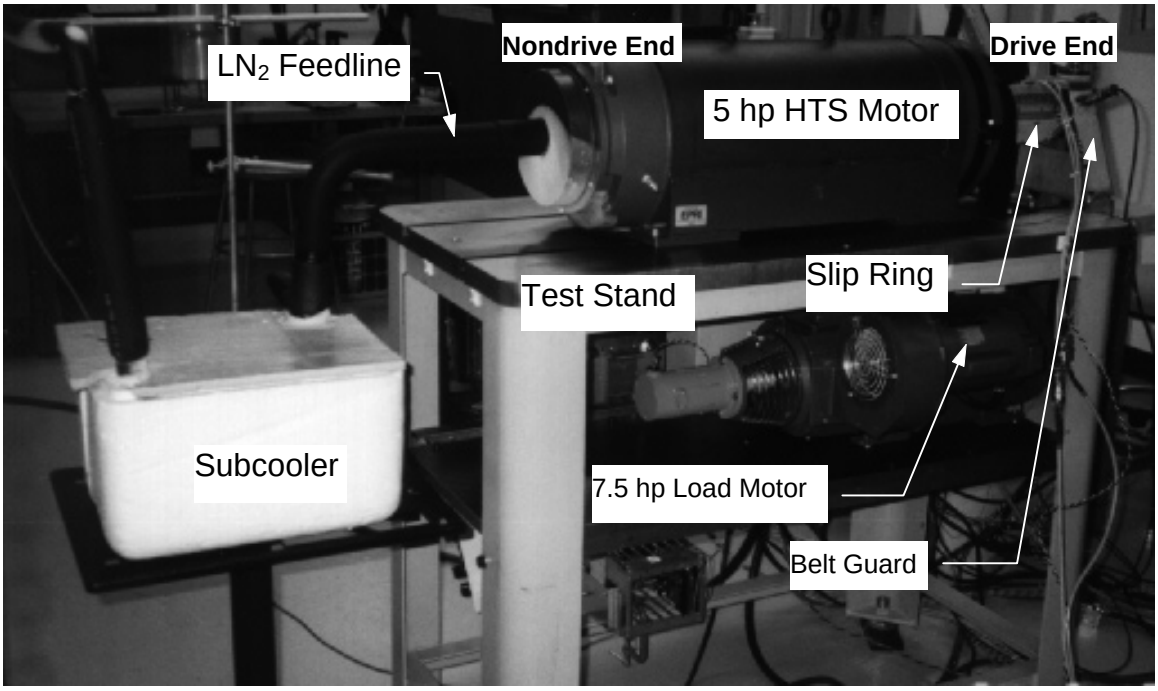

Figure 4-10
Rear view of four pole synchronous HTS motor and test stand.

Test Results

The first rotating tests with the HTS coils excited were to determine the effects of rotation on the coil performance. Mechanical stress as well as liquid nitrogen pool temperature (due to pressure increase in the rotating pool) were expected to increase with rotation speed. Both of these phenomenon can cause increased HTS coil voltage. HTS field winding V-I curves are presented in Figure 4-11 for a variety of motor speeds. Also shown is the V-I curve obtained from static test data taken with the coils in the full pole racetrack coil test fixture (see Figure 4-2 and Figure 4-3). Static and rotating test data are nearly identical. HTS coil voltage was found to be independent of motor speed (under open circuit conditions) indicating that the HTS coils are not affected by rotation. This also suggests that the liquid nitrogen pool temperature is not significantly affected by rotation. The HTS field winding voltage drop remains below 1 μV/cm (2.5 μV/in) for field currents up to 4.5 amps. The 1 μV/cm (2.5 μV/in) criteria is often used to indicate the onset of superconductivity. A field current of 4.5 amps results in 1050 amp-turns per pole or 88% of the target value used for performance predictions of Figure 4-5.

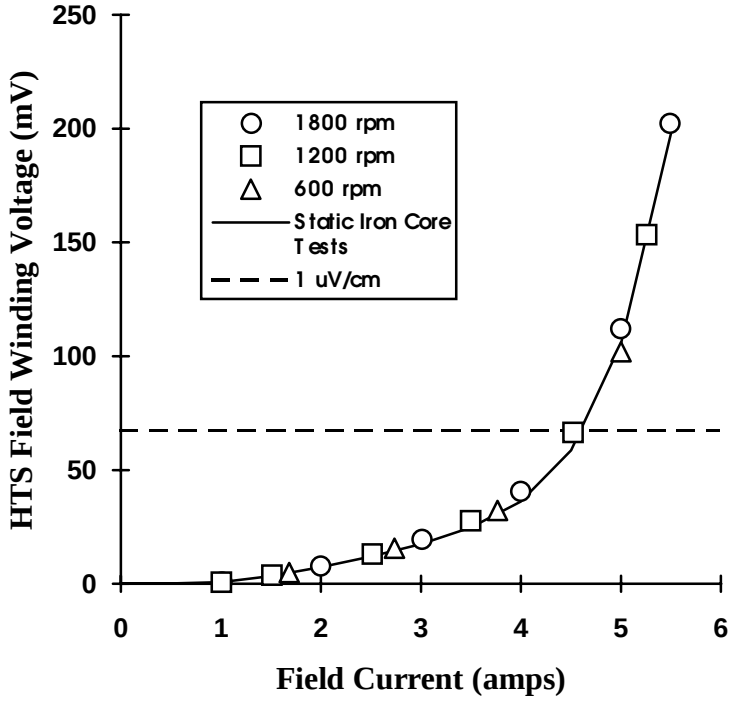

Figure 4-11
HTS field winding V-I curves for static and rotating tests.

Field Winding Cooling Test Results

Cooling tests were performed in which cryogenic temperatures and rotational velocities were recorded while operating at a specific liquid nitrogen level (HTS coils immersed). Figure 4-12 presents the experimental data for the cryogenic temperature sensing diodes (TSDs) versus rotational speed of the rotor. The temperatures presented in the figure represent the differential temperature from the saturation temperature of liquid nitrogen at ambient conditions (77.4K or 43 R). This data was obtained by noting when the liquid level reached the outer diameter of the core tube and then recording the temperature data. The point at which the liquid level reaches the core tube can be determined by monitoring the pressure sensors–a sharp increase in pressure occurs when the liquid level rises through the core tube. The locations of the TSDs are depicted in Figure 4-7.

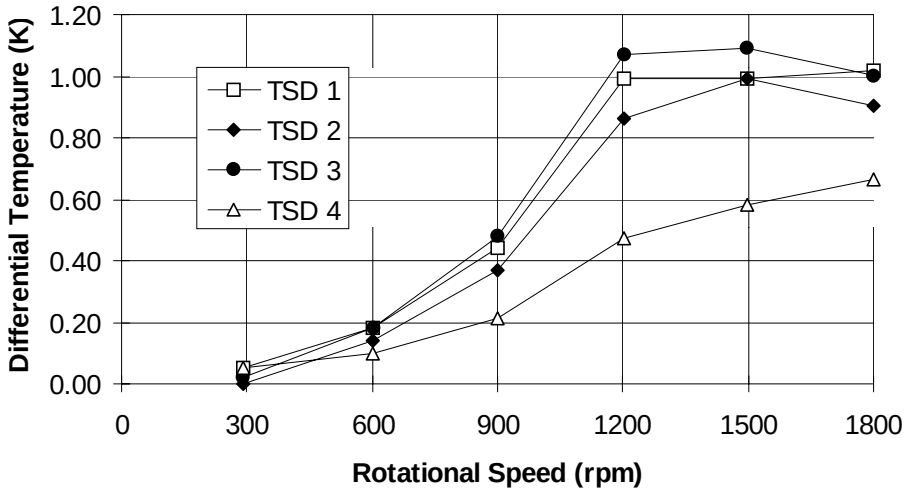

Figure 4-12
Experimental differential temperature versus rotational speed with complete immersion of the HTS coils. Diode locations: 1) near cold copper flux shield inner wall, 2) middle of HTS coil side, 3) middle of HTS coil side opposite TSD 2 and, 4) just outside core tube.

Figure 4-12 shows a general increase in temperatures, with an increase in rotational speed, up to approximately 1200 rpm. Above 1200 rpm, the diodes mounted on the HTS coils (TSD 2 and TSD 3) indicate a peaking of the temperatures with temperatures decreasing above 1500 rpm. This figure shows that the maximum coil space temperature is approximately 1 K above the saturation temperature of liquid nitrogen at atmospheric pressure.

In the pool boiling configuration of this the rotor, the limits on the cold space temperatures can be easily determined. The lower temperature limit is determined by the saturation temperature at the nitrogen liquid/gas interface, and since the gas core region of the rotor is very near atmospheric pressure, the lower temperature limit is near 77.4 K (43 R). The upper temperature limit is determined by the saturation temperature at the copper flux shield inner wall which is a function of the rotational speed of the rotor. The difference between the lower and upper temperature limits is presented as a function of rotational speed in Figure 4-13. The trend in temperatures below 1200 rpm shown in Figure 4-12 closely matches the trend in the temperature difference presented in Figure 4-13. Above 1200 rpm the temperatures in Figure 4-12 stop following the trend of Figure 4-13 and appear to begin to decrease. This phenomenon is significant because the coil performance is highly dependent on their temperature and it shows that the coils may not ever experience the wall saturation temperature difference at 1800 rpm of 4 K (2.2 R), or 14 K (7.8 R) at 3600 rpm. In larger

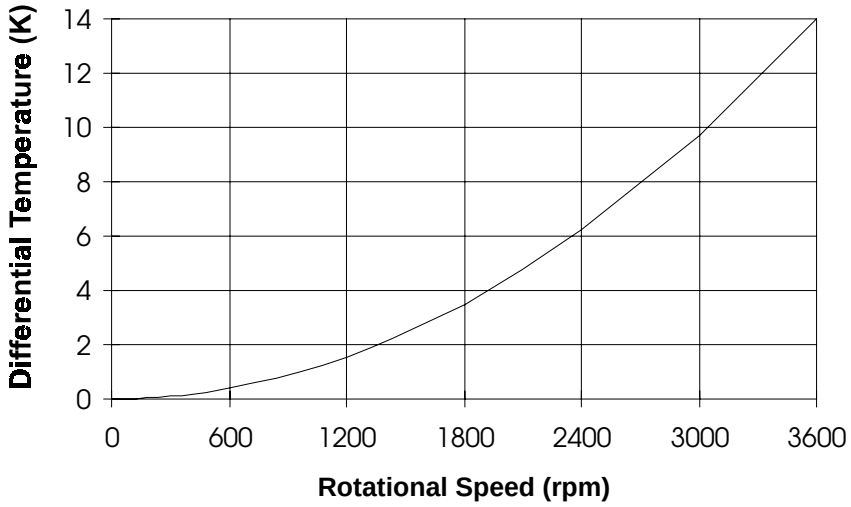

Figure 4-13
Differential saturation temperature variation between the nitrogen liquid/gas interface and the cold copper flux shield inner wall as a function of rotational speed.

HTS rotor designs, depending on the rotational speed and rotor diameter, the wall saturation temperature difference may be significantly larger than 14 K (7.8 R).

One explanation for the peaking of the temperatures near 1200 rpm is that convection cells in the liquid nitrogen begin to dominate in the pool and tend to moderate the temperatures. This explanation can be supported by considering the behavior of free convection within a horizontal cavity heated from below–this analysis is presented in Appendix B and is further supported by data taken at rotational speeds between 1800 rpm and 3000 rpm (see Appendix B).

In addition to the tests presented above, which were performed with the HTS coils fully immersed in liquid nitrogen, a number of motor demonstrations and tests were performed with the HTS coils only partially immersed. Tests performed with only a very thin layer of liquid nitrogen in the rotor near the copper flux shield wall, such that the HTS coils were predominately immersed in saturated nitrogen gas, had no noticeable affect on the HTS motor performance.

Synchronous Test Results

First operational tests of the four pole, rotating field HTS motor were with the series armature connection and sine wave armature excitation. Figure 4-14 presents power capability and armature current curves for the motor with rated voltage and speed test points. With this connection the motor produced more than 2.5 horsepower

(1860 watts). Motor power output exceeded the predicted values for large torque angles while measured armature current was below predicted values over the entire load range.

The motor performance testing was repeated with a PWM inverter supplying the armature power. A comparison of HTS field winding voltage drop with sine wave and PWM armature excitation is presented in Figure 4-15. There was no significant difference in HTS coil voltage between sine wave and inverter armature excitation indicating no adverse effects of the inverter generated time harmonic currents. The HTS coil voltage remained below 1 μV/cm (2.5 μV/in) for output power in excess of 2 horsepower (1490 watts). Figure 4-16 presents V-I curves at one load point for inverter and sine wave excitation. Again, the inverter had no influence on the HTS coil performance over a wide field current range. Inverter operation is important since future commercial high horsepower motors will be inverter driven for pump and fan applications.

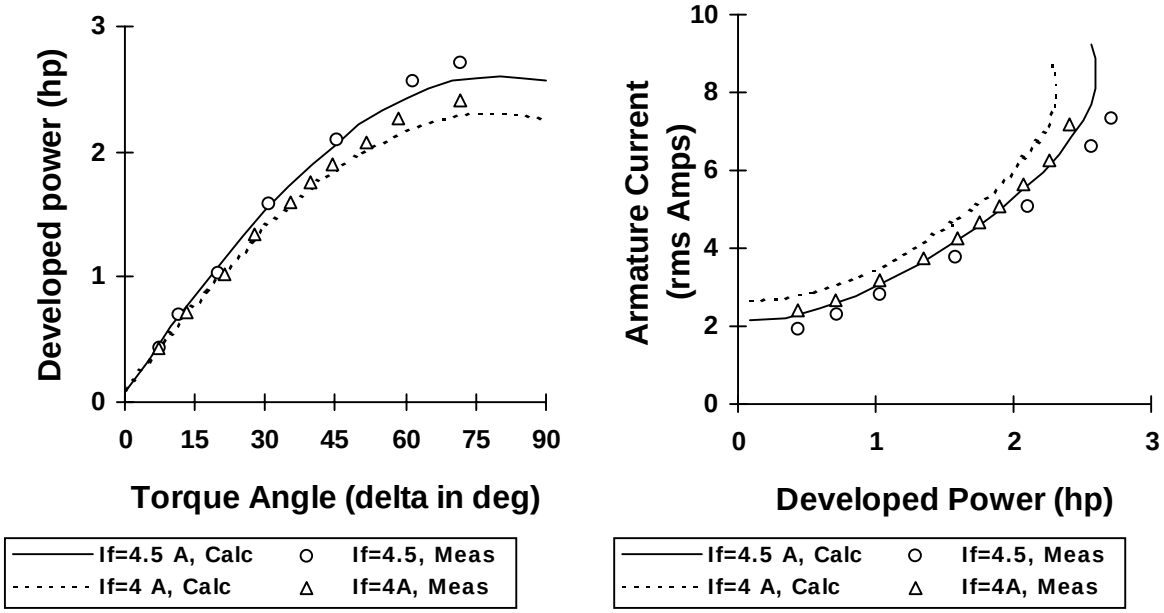

Figure 4-14
Measured and calculated motor performance curves for 230 volt, 60 Hz, sine wave armature excitation and series armature connection at two field currents.

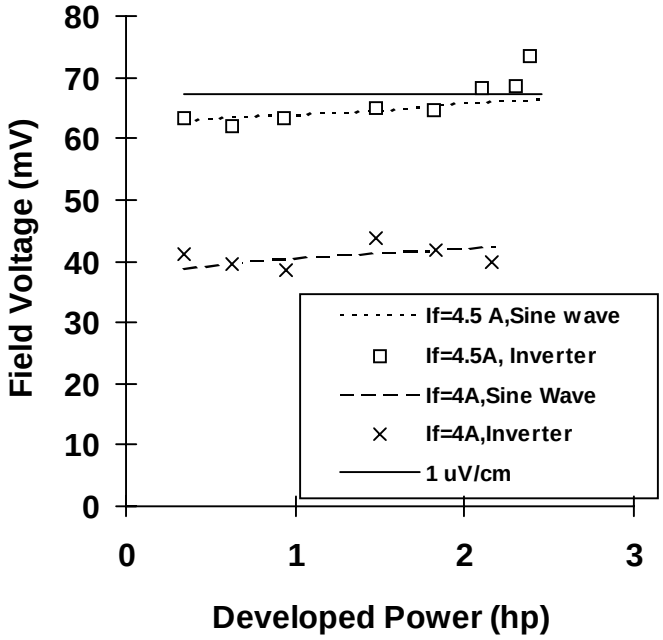

Figure 4-15
Measured HTS field winding voltage for the five horsepower (3.7 kW) motor with sine wave and inverter armature excitation. All data is with the series armature winding connection at rated voltage and speed (1800 rpm).

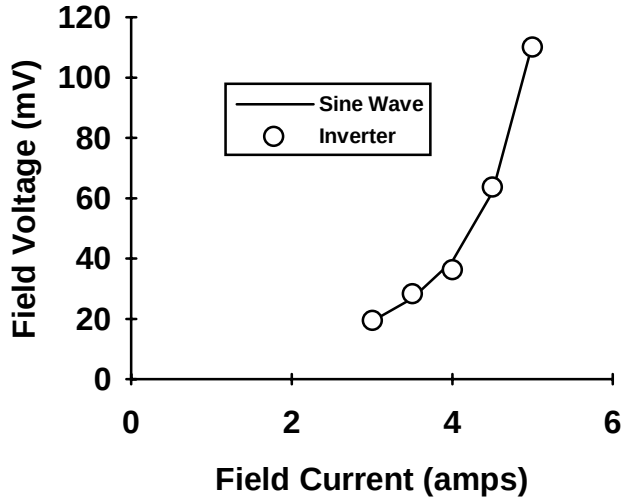

Figure 4-16
Measured HTS field winding voltage with sine wave and PWM inverter armature excitation for 1120 watts (1.5 horsepower) output at rated voltage and speed. All data is with the series armature winding connection.

Armature inverter power has the potential of creating additional losses in the rotor cold space due to time harmonic fields. As shown above, the losses in the coils are not affected by the inverter excitation but currents induced in the cold copper flux shield or the rotor support structure are a possibility. Two test runs were conducted with the same steady state operating conditions (field current of 4.5 amps, rated voltage armature excitation at 60 Hz and 2 horsepower (1490 watts) output) while the rate of liquid nitrogen consumption for rotor cooling was monitored over time for a period of one hour. One test used sine wave armature excitation while the other used the PWM inverter. During these tests the liquid nitrogen pool depth in the rotor was kept at a constant value. Results showed less than a 1% difference in the rate of liquid nitrogen consumption (well within the accuracy of the test method) indicating no increased losses in the rotor due to PWM armature excitation.

The synchronous motor parameters for the five horsepower (3.7 kW) motor were determined from load performance test data using the method described in Chapter 3. Table 4-4 lists measured and predicted values for the motor electrical circuit parameters for the series armature connection. A surprising test result was to find X_d smaller than X_q. This pattern was observed in several test runs with series and parallel armature winding connections. No plausible explanation for this phenomena could be determined. Overall, predicted motor performance was found to agree quite well with measured performance, as shown in Figure 4-14.

Motor performance testing with the armature windings connected in parallel with the same 230 volt rated voltage resulted in higher motor power capability as predicted. Figure 4-17 presents measured and predicted motor performance for this connection while Figure 4-18 presents measured HTS winding voltage as a function of motor load. The motor had more power capability and lower armature currents than was predicted. Measured HTS coil voltage was found to be less than 1μV/cm (2.5 μV/in) for up to five horsepower (3.7 kW) output with a field current of 4 amps.

Table 4-4
Calculated and measured parameters for the five horsepower (3.7 kW) HTS synchronous motor for the series armature winding connection.

Parameter	Measured Value	Calculated Value	% Difference
E_o at I_f = 4 amps	156 rms V, $\ell\ell$	146 rms V, $\ell\ell$	- 6 %
X_q at 60 Hz	21.0 Ω	17.4 Ω	- 17 %
X_d at 60 Hz	17.3 Ω	18.6 Ω	8 %

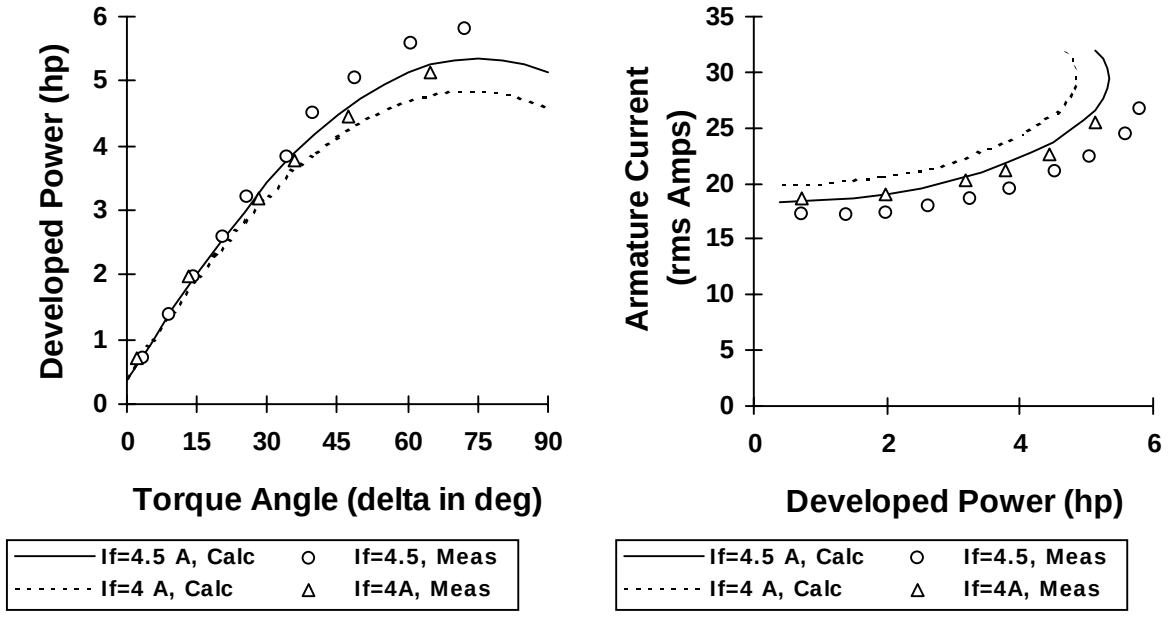

Figure 4-17
Measured and calculated motor performance curves for 230 volt, sine wave armature excitation and parallel armature connection at two field currents.

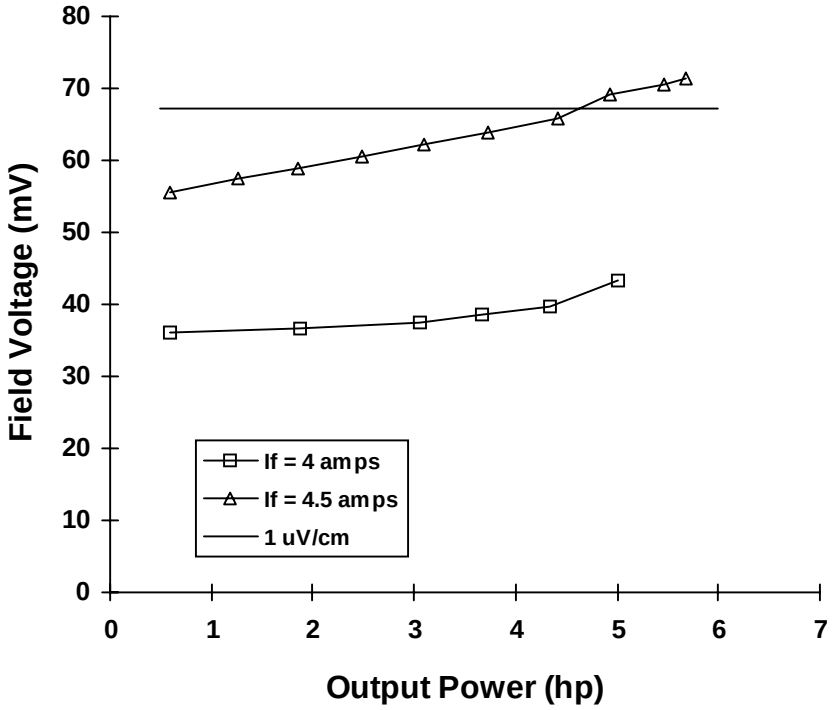

Figure 4-18
Measured HTS field winding voltage for 230 Volt, 60 Hz, sine wave armature excitation with the parallel armature winding connection.

Friction & Windage Test Results

Coast-down tests and no load tests, with the motor operating as an induction motor, were performed to estimate the motor friction and windage loss. Table 4-5 presents a summary of the test results which agree well. The tests were performed when the HTS motor was both at room temperature (warm) and operational temperature (cold). In addition, the tests were performed with the DC pilot motor both coupled through the drive-belt connection and uncoupled. From the table, the friction and windage of the uncoupled HTS motor is near 100 W (0.13 hp) in the warm condition and in the range of 68 to 77 W (0.09 to 0.10 hp) in the cold condition. The reason for decreased friction and windage in the cold condition is unclear. A test was performed to determine if the unloading of the bearings due to thermal contraction of the rotor shaft was the cause. This test did not indicate that this was the case. Another plausible explanation is that the drag coefficient on the rotor decreases with very cold nitrogen gas inside the motor frame; however, the windage losses would be a smaller percentage of the total friction and windage loss than the friction loss.

Table 4-6 presents a summary of no load motor friction and windage tests performed with the motor operating in synchronism at different field currents. From these test

results, the friction and windage power appeared to be approximately two percent of the total HTS motor output power capability.

Table 4-5
Summary of induction motor and coast-down tests for friction and windage.

Condition	Friction & Windage Loss	
	Induction Motor Tests	Coast-down Tests
Warm/coupled	360 W (0.483 hp)	354 W (0.475 hp)
Warm/uncoupled	100 W (0.134 hp)	97 W (0.130 hp)
Cold/coupled	336 W (0.451 hp)	288 W (0.386 hp)
Cold/uncoupled	68 W (0.09 hp)	77 W (0.10 hp)

Table 4-6
Summary of no load tests for friction and windage (all tests with motor cold/uncoupled and synchronized with high voltage connection).

Condition	Friction and Windage	Average Nondrive-End Bearing Temp	Average Drive-End Bearing Temp
If = 4.5 amps	68 W (0.091 hp)	27 °C (81 °F)	24 °C (75 °F)
If = 4.0 amps	72 W (0.097 hp)	27 °C (81 °F)	24 °C (75 °F)
If = 3.5 amps	69 W (0.093 hp)	26 °C (79 °F)	25 °C (77 °F)

Conclusions

The five horsepower (3.7 kW) motor demonstration met its design goals and represents a major milestone in HTS motor development. This was the first motor operating with rotating HTS coils. The motor components are similar to the components to be found in commercial HTS motors. Racetrack HTS coils performed flawlessly and remained superconducting for a motor output power to five horsepower (3.7 kW). Throughout all testing of the racetrack coils more than 40 thermal cycles from room temperature to liquid nitrogen temperature occurred. No degradation of HTS coil performance was observed throughout these thermal cycles indicating American Superconductor's wire and coil technology is able to produce reliable coils for motor applications. Coil

performance during rotating tests was identical to that measured under static conditions.

Test results indicated that, at least on the scale of the rotor tested, rotating pool boiling cooling is a viable option for maintaining the HTS coils at their operating temperature. For full immersion of the HTS coils in liquid nitrogen, the pool temperatures were moderated to less than 1 K above the saturation temperature of liquid nitrogen at atmospheric pressure due to convection currents in the pool. Tests performed with only a very thin layer of liquid nitrogen in the rotor near the copper flux shield wall, such that the HTS coils were predominately immersed in saturated nitrogen gas, had no noticeable affect on the HTS motor performance compared to full coil immersion in liquid nitrogen.

Reconfiguration of the armature wiring allowed the demonstration of the largest horsepower motor possible with HTS coils which represent the state-of-the-art in HTS wire performance. Five horsepower (3.7 kW) output was obtained.

The accuracy of predicted motor performance, based on two dimensional magnetic finite element analysis methods, was found to be adequate for this demonstration motor. The goals of this motor demonstration *did not* include verification of the accuracy of the electromagnetic motor model since commercial HTS motors are intended to be air core (see Chapter 2) and this five horsepower (3.7 kW) motor was a salient pole, iron core motor. Air core magnetic modeling techniques can be based on closed form solutions to the magnetic field equations so that finite element methods are not required. Further improvements in FEA design techniques for iron core motors were, therefore, not pursued in this project.

5

CONCLUSIONS

Progress in demonstration motor fabrication and testing from the beginning of the EPRI/Reliance Electric HTS motor project is summarized in Figure 5-1. Output power increases have paralleled HTS wire development progress. Early motors were small table-top DC motors with solenoid HTS field coils and output powers from zero to 35 watts (0 to 0.05 hp). These motors utilized tens of meters of HTS wire. This report describes the design and testing of two synchronous motors with HTS field windings that were recently demonstrated, the largest of these having a rotating HTS field winding and an output power of 5 horsepower (3.7 kW) while operating in the superconducting state. The synchronous motors had robust, reliable superconducting coils with hundreds of meters of HTS wire. These motors were tested with PWM inverter power to investigate the effects of the time harmonic currents on the HTS field winding performance. These types of tests are important since the first commercial HTS motors are expected to be coupled with an adjustable speed inverter for pump and fan duty. Test results showed no degradation in HTS coil performance due to inverter time harmonics.

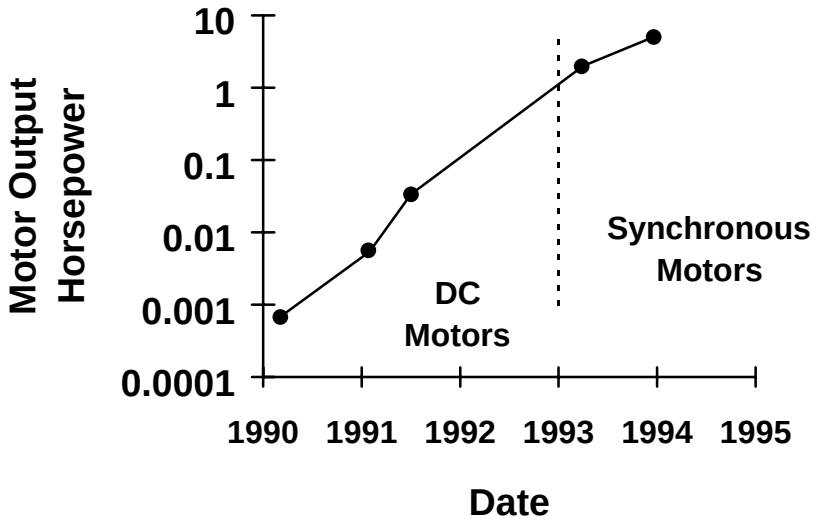

Figure 5-1
Motor demonstrations as part of the Reliance/EPRI HTS motor research project.

Over the time period of motor demonstrations indicated in Figure 5-1, HTS wire and coil technology progressed from fragile extruded solenoid coils with a few meters of wire to long length, robust, racetrack coils made from react and wind HTS wire that performs reliably after dozens of thermal cycles. Much of this improvement in wire technology has taken place at American Superconductor Corporation. The success of this project lends credence to the plan to develop application technology in parallel with HTS wire development research. This strategy will ultimately result in the earliest possible introduction of commercially viable HTS motors.

In parallel with the HTS motor demonstrations, Reliance Electric designed, built and tested an air core, nonsuperconducting synchronous motor to validate internally developed motor design techniques for commercial air core HTS motors of the future. Test results for this motor were described in this report and showed reasonable correlation with predictions (steady state circuit parameters to within 7% and peak power capability prediction to within 16%). Improvements in air core motor modeling are needed to increase the accuracy of performance predictions for commercial air core motor designs. Suggested improvements are described in Chapter 2.

This report ends the current work with liquid nitrogen cooled HTS coils applied to the development of commercial electric motors. The results reported herein, along with previous work described in [H], has laid the groundwork for continued development of HTS motors. The future prospects of HTS motor development with liquid nitrogen cooled HTS coils is mainly bounded by the performance limitations of high temperature superconducting coils at 77 Kelvin (43 R). The decreased loss and size reduction required for an economically viable HTS motor requires superconducting coils that can operate in high magnetic fields. Magnetic fields in the range of five Tesla will be required. The intrinsic properties of state of the art HTS wire imply that high field HTS wire will not be available in the foreseeable future at liquid nitrogen temperatures. At an operating temperature of 20 to 40 Kelvin (11 to 22 R), however, short sample HTS wire available today does have the required performance in a high magnetic field. Work continues to apply HTS technology, at this temperature range, to commercially viable electric motors.

6

REFERENCES

[1] S. A. Nasar, Ed., *Handbook of Electric Machines*, New York, McGraw-Hill, 1987, Chapter 10.

[2] Dykhuizen, R. C., "Stability of Rotating Flows with Radial Heat Transfer," Accepted for publication in *Cryogenics*, 1995.

[3] Incropera and DeWitt, "Fundamentals of Heat Transfer", John Wiley & Sons, NY, 1981.

[4] Marto and Gray, "Effects of High Acceleration and Heat Fluxes on Nucleate Boiling of Water in an Axisymmetric Rotating Boiler," NASA-TN-D-6307.

[5] Dykhuizen, R. C., Baca, R. G. and T. C. Bickel, "Flow and Heat Transfer Model for a Rotating Cryogenic Motor," Sandia National Labs Report number SAND 93-1588, August 1993, available from Sandia National Labs, Albuquerque, New Mexico 87185

[6] W. H. Hayt, Jr. *Engineering Electromagnetic*, Fourth Edition, McGraw Hill, Inc., New York, 1981, pp 244-245.

Publications which were a result of this contract:

[A] Jordan, H. "Feasibility Study of Electric Motors Constructed with High Temperature Superconducting Materials," *Electric Machines and Power Systems*, Vol 16, 1989, pp 15-23.

[B] Edmonds, J. S., H. E. Jordan, J. D. Edick and R. F. Schiferl, "Application of High Temperature Superconducting Materials to Electric Motors," International Conference on Electrical Machines, August, 1990, Cambridge Massachusetts, Conference Record, pp. 1-6.

[C] Schiferl, Rich, "High Temperature Superconductivity Applied to Electric Motors," Ninth Annual Conference on Properties and Applications of Magnetic Materials, Illinois Institute of Technology, May, 1990.

[D] Jordan, H. E., “Development Program for High Temperature Superconducting Motors,” TcSUH Workshop on Materials, Bulk Processing and Applications, Texas Center for Superconductivity, Houston, Texas, Feb 27-28, 1992.

[E] Schiferl, R. and Stein, J., "High-Tc Superconducting Electric Motors," American Power Conference, April 13-15, 1992, Chicago, IL, Conference Record, pp. 1256 - 1260.

[F] Edmonds, J. S., Sharma, D. K., Jordan, H. E., Edick, J. D. and Schiferl, R. F., “Application of High Temperature Superconductivity to Electric Motor Design,” *IEEE Transactions on Energy Conversion*, Vol. 7, No. 2, June 1992, pp. 322 - 329.

[G] Dykhuizen, R. C. , T. C. Bickel, R. G. Baca, S. N. Kempka, R. D. Skocypec, J. D. Edick, R. F. Schiferl and H. E. Jordan, “Steady-state Cooling of a High-Temperature Superconducting Motor,” American Society of Mechanical Engineers Conference, 1992.

[J] Jordan, H. E. , Edick, J. D. and Schiferl, R. F., “Electric Motors Using Superconducting Materials Applied to Power Generating Station Equipment,” *EPRI TR-101127*, Interim Report for Projects 3149-01, 7911-02, September 1992.

[I] Edick, J. D., Schiferl, R. F. and Jordan, H. E., "High Temperature Superconductivity Applied to Electric Motors," *IEEE Transactions on Applied Superconductivity*, Vol. 2. No. 4, December 1992, pp. 189 - 194.

[J] Joshi, C. and Schiferl, R. F., "Design and Fabrication of High Temperature Superconducting Field Coils for a Demonstration DC Motor," *IEEE Transactions on Applied Superconductivity*, Vol. 3. No. 1, March 1993, pp. 373 - 375.

[K] Schiferl, R. F., D. I. Driscoll and J. Stein, “Current Status of High Temperature Superconducting Motor Development,” American Power Conference, April 1994, Chicago, IL, Conference Record, pp. 1351 - 1355.

[L] Joshi, C. H., R. F. Schiferl and D. I. Driscoll, “Progress in the Application of High Temperature Superconductors to Electric Motors,” Technical Innovation Symposium 1994, September 7 - 9, Pittsburgh, PA.

[M] Joshi, C. H., C. B. Prum, R. F. Schiferl and D. I. Driscoll, “Demonstration of Two Synchronous Motors Using High Temperature Superconducting Field Coils,” presented at the Applied Superconductivity Conference, Boston, MA, October 16-21, 1994.

Appendix A

AIR CORE MOTOR EQUIVALENT LENGTH CALCULATION

Overview

Air core motors have no magnetic material inside of the outer laminated frame and flux shield (see Chapter 1). Since most of the magnetic field path is not iron in these motors, the solution to the magnetic field equations can be done assuming linear magnetic material throughout the entire motor volume. At the axial center of the motor (z = 0) a two dimensional, closed form solution to the magnetic field equations will result in a very good estimate of the magnetic field distribution (see below). The field equations for this motor cross section used in the Reliance Electric motor modeling are given in [1]. Moving out from the motor axial center a correct model of the magnetic field distribution requires three dimensional field mapping. Three dimensional, magnetic field, finite element analysis (3-D FEA) modeling can be used to obtain the magnetic field distribution. Unfortunately, in 1992, when this work was done, or even today, 3-D FEA requires large computer resources and computer time so a simpler approach must be looked for.

Motor performance predictions such as armature current, torque angle and losses at a given load, requires accurate prediction of the armature synchronous inductance (L_S) and the linkage between the armature and field winding (i. e. the back emf (E_o) at a given speed and field current). The approach taken here to obtain an estimate of L_S and E_o is to use the two dimensional closed form magnetic field solution to obtain the magnetic field in a motor cross section through the motor shaft and to incorporate end effects by the proper choice of an equivalent length for the motor. In essence, it is assumed that the two dimensional solution is constant across the equivalent length (no end effects) and the field goes to zero beyond the equivalent length. Separate equivalent lengths were used for L_S and E_o. Ultimately, these lengths need to be calculated based upon the motor geometry. Test data, from the air core motor described in Chapter 2, along with combinations of two dimensional magnetic field solutions was used to develop a method of predicting these equivalent lengths. This process is described as follows:

1. Measure the motor Ls and Eo through steady state motor tests.

2. Adjust the equivalent lengths for the Ls and Eo calculation in the design program so that the correct Ls and Eo is predicted. These adjusted equivalent lengths will be called the measured equivalent lengths below.

3. Measure the three dimensional magnetic field solution in the air core motor field region with the armature excited and the field structure removed.

4. From measured data, devise a method to predict the three dimensional magnetic field solution from winding and core geometry and compare prediction to measurement.

5. Take calculated three dimensional magnetic field data derived in 4) and calculate equivalent lengths for the motor.

This Appendix describes the results of these five steps for the two horsepower air core motor described in Chapter 2.

Measured Motor Parameters and Magnetic Fields

Steady state motor performance tests were conducted on the air core motor and the following parameters and equivalent lengths were found:

Parameter	Measured Value	Measured equivalent length (inches)
Synchronous Inductance (L_s)	19.7 mH	12.7
Back EMF at 60 Hz (E_o)	4.04 volts/field amp	8.92

After testing was completed the motor field assembly was removed and the magnetic field distribution inside of the armature due to armature currents was measured. For these tests the armature was powered by a DC current source with the phase A lead connected to one terminal and the phase B and C lead connected to the other terminal. This connection mimics the phase currents at one instant of time when the motor is running. Radial (Br), circumferential (Bc) and axial (Bz) magnetic fields were measured as a function of axial distance from the center of the rotor (z), radius (r) and circumferential angle (θ). Measured data was plotted in three dimensions to determine trends that could be used to find approximate three dimensional magnetic field solutions. Based on this exercise the following data trends were discovered:

1. Measured Br and Bc vs r and θ at z = 0 agree very well with calculated values from the closed form, two dimensional field solution described in [1].

2. Br vs θ is sinusoidal at all z's.

3. Br vs θ does not show a significant phase shift with respect to θ for all z's. In essence, peak Br occurred at the A phase winding magnetic axis for all z's.

4. Bz vs θ is sinusoidal with respect to θ for all z's. Peak Bz occurred at the A phase winding magnetic axis for all z's.

5. Peak Br decreases with increasing z. At smaller radii this decrease is more pronounced than at larger radii.

These observations, coupled with the fact that winding flux linkage and inductance is most easily calculated by integrating Br over θ and z at the winding radius, resulted in the following conclusions :

A) Calculated values of L_S and E_o require accurate estimates of Br at the armature and field winding radius, respectively.

B) Accurate estimates of Br at the armature and field winding radius require a method to calculate Br and Bz vs radius at only one θ, the angle that corresponds to the armature winding magnetic axis. This angle will be called θmag below.

A simple method to predict Br and Bz vs radius at θmag was developed as described below.

Br and Bz Calculation

Measured and calculated radial magnetic field at z = 0 for three radii inside of the armature bore are given in Figure A-1. The 2-D calculated values were obtained from the closed form solution equations from [1]. Measured and calculated values agree to within 3%. It is safe to say that the two dimensional model is adequate at z = 0.

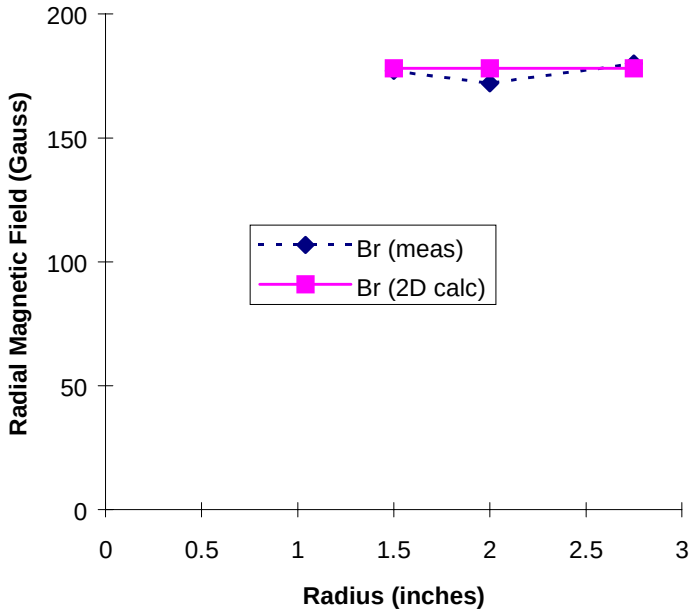

Figure A-1
Radial magnetic field at the a phase winding axis (θmag) at z = 0.

Figure A-2 shows a plot of measured Br vs z at the same three radii normalized to Br at z = 0. Br drops off with increasing z, as expected for an air core winding. This drop is more rapid at lower radii. An accurate prediction of L_s and E_o can be made if a method is found to predict the curves in Figure A-2 from winding and motor dimension data. The method used was based on two separate two dimensional magnetic field calculations, one for the axial directed conductors of the armature (in the armature slots), and one for an equivalent circumferential current due to the end winding.

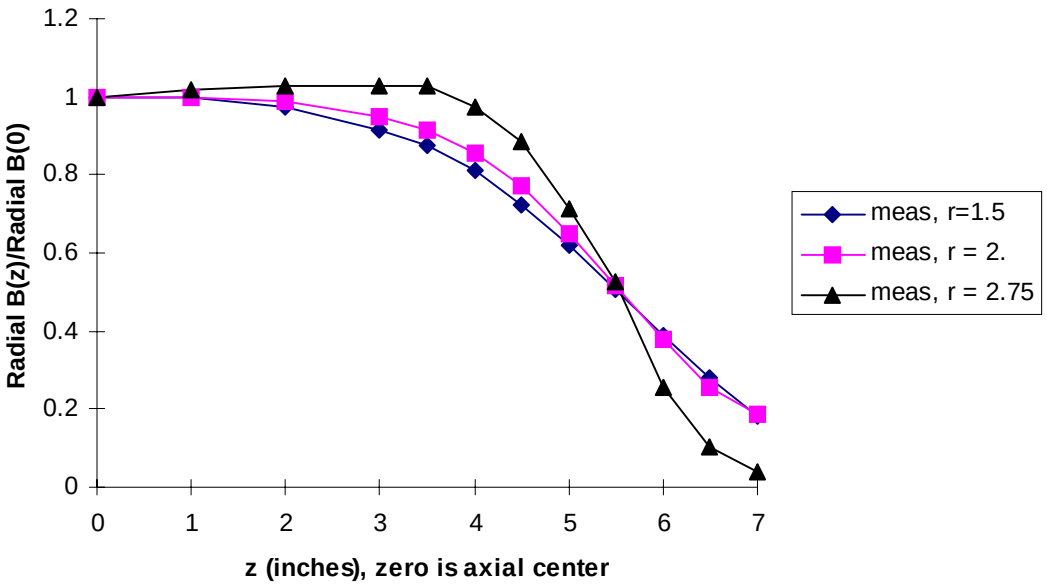

Figure A-2
Measured radial magnetic field at θmag at three radii.

The radial magnetic field due to the axial conductors in the armature winding (Brm(r,z)) was calculated from the 2-D solution at z = 0 of Figure A-1 (Brm(r,0)) times a correction factor (K[(r-ra)/h,d/h] that is derived from the known two dimensional field distribution about a finite length conductor [6], where ra is the radius to the center of the armature winding (middle of armature slot) and h is half the length of the straight section of the axial conductors. (The straight section being the core stack length plus the two straight end extensions beyond the core that make up the start of the end winding). A plot of this correction factor is given in Figure A-3.

The magnetic field due to the end winding is calculated only at the magnetic axis of the coil (at θmag). It is found by concentrating the circumferential current in the end winding at this angle (Isum) at a single conductor located at radius ra and z = h+lslant/2, where lslant is the axial length of the slanted portion of the end winding extension (h is as in the previous paragraph). The effects of the laminated frame and flux shield are taken into account by an image conductor as shown in Figure A-4. At the field calculation point the magnetic flux density magnitude due to conductors 1 and 2 are simply

$$B_1 = \frac{\mu_o \, Isum}{2\pi(r1)}, \qquad B_2 = \frac{\mu_o \, Isum}{2\pi(r2)}$$ and their directions are circumferentially around the conductors as shown in the Figure. The combined effects of these two fields yields the magnetic field vector due to end winding currents. The total magnetic field at any point in the θmag plane is found by adding together the end winding fields and the main winding fields.

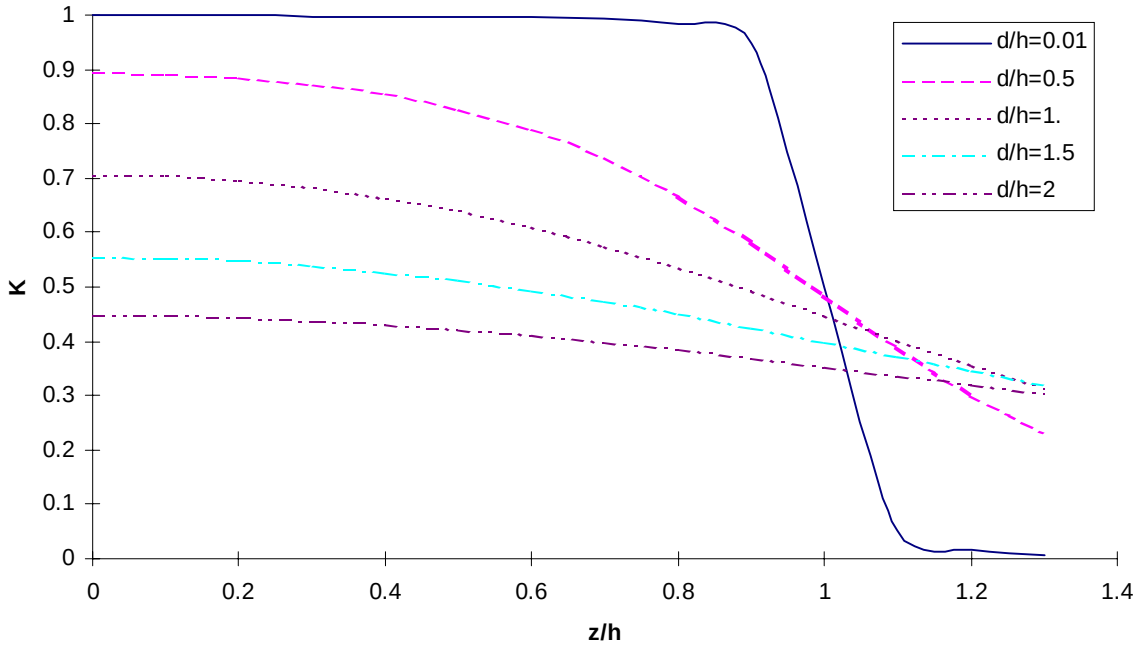

Figure A-3
Correction factor for two dimensional field calculations at a distance from a conductor. For a finite length conductor of length 2h carrying current I, the circumferential magnetic field around this conductor at a distance from the conductor d and distance from the center of the conductor z is simply:

$$Bc = \frac{I}{2\pi d} * K(\frac{d}{h}, \frac{z}{h}) \ .$$

Comparison of Measured and Calculated Trends

Figure A-5 shows a plot of calculated, normalized flux density due to the armature winding currents using the method described above at three different radii. These curves show the same trends as the measured curves in Figure A-2. Figure A-6 has measured and calculated curves at each radius. The agreement between these curves is not exact but the trends in measured and calculated curves match. The results are certainly a better approximation than assuming the 2-D magnetic field at z=0 is constant throughout the active length of the motor.

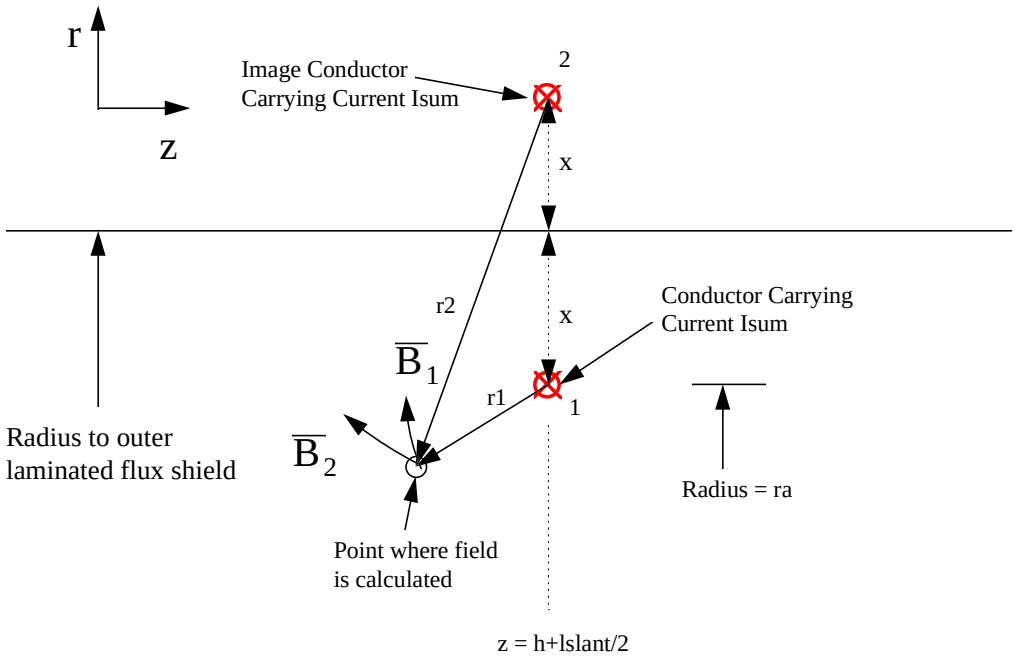

Figure A-4
Conductor locations for calculating r and z directed magnetic flux density in the plane located at θmag.

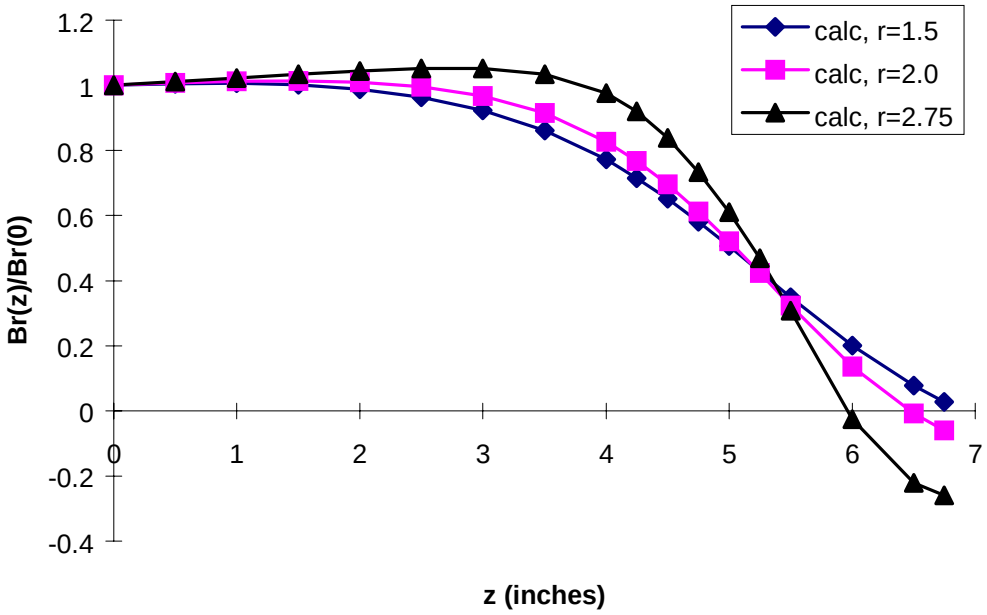

Figure A-5
Calculated radial magnetic field at θmag for the air core motor due to armature currents.

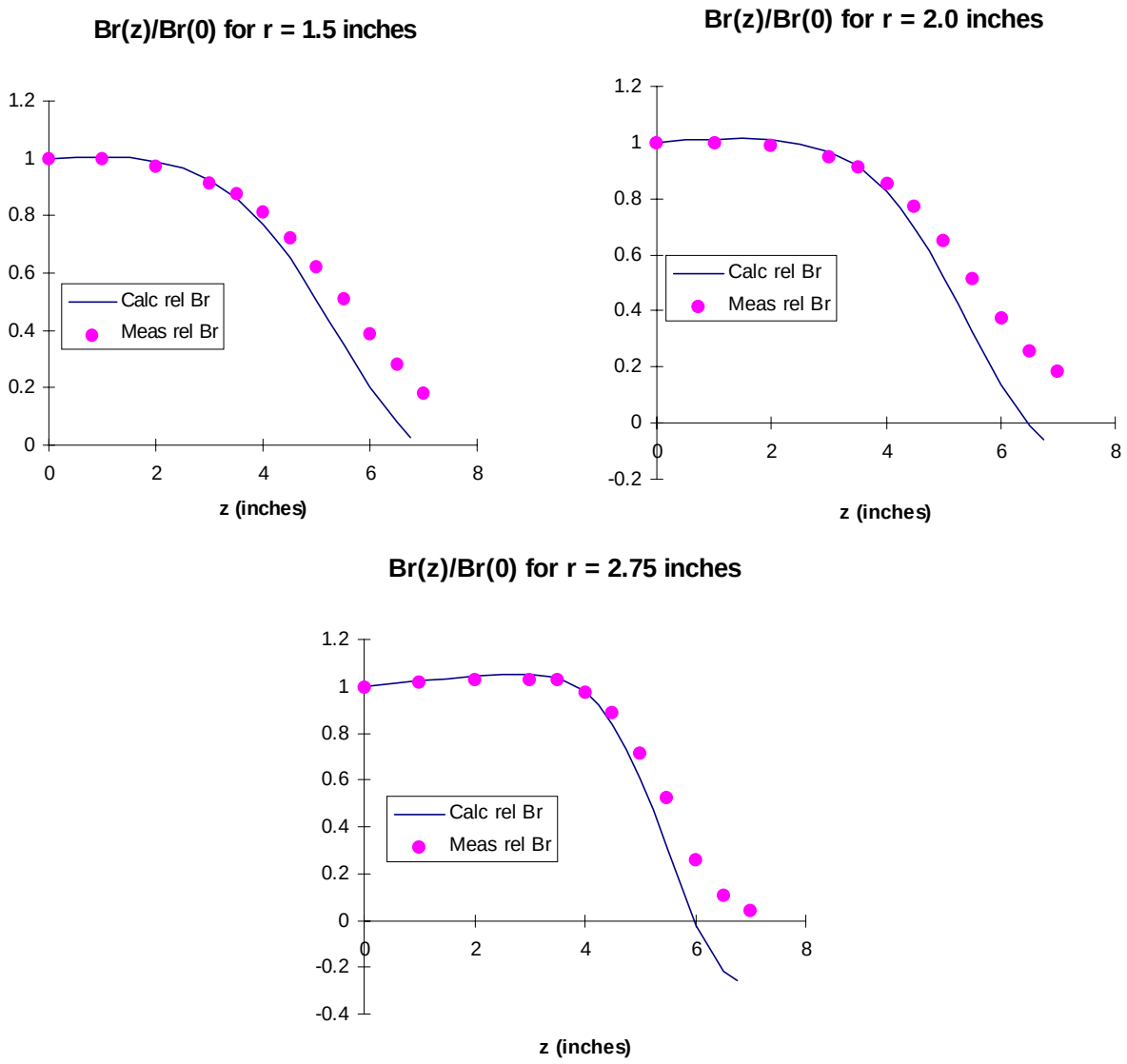

Figure A-6
Comparison of calculated and measured radial magnetic fields due to armature currents at θmag at three different radii.

Equivalent Length Calculations

Equivalent lengths for calculating L_s and E_o are found as follows.

1. Calculate Br(ra,z) at θmag. Call this Br(ra,z,θmag).

2. Integrate over the active region of the coil to obtain a number that is proportional to the flux linking the armature coil, i. e.

$$\text{Fluxa} = \int_{0}^{h+\text{lslant}/2} \text{Br}(\text{ra}, z, \theta\text{mag})dz$$

3. Calculate the equivalent length for L_S as $\frac{\text{Fluxa}}{\text{Br}(\text{ra},0,\theta\text{mag})}$, where Br(ra,0,θmag) is the calculated flux density at z = 0 using the combination of main and end winding flux density, as described above.

4. Repeat process for E_o at the mid radius of the field winding (rfmid) to get Fluxo where

$$\text{Fluxo} = \int_{0}^{hr+\text{lfend}/2} \text{Br}(\text{rfmid}, z, \theta\text{mag})dz$$

   where lfend is the axial length of the field winding end winding.

5. Calculate the equivalent length for E_o as $\frac{\text{Fluxo}}{\text{Br}(\text{rfmid},0,\theta\text{mag})}$, where Br(rfmid,0,θmag) is the calculated flux density at z = 0 using the combination of main and end winding flux density as described above.

Using this method the following calculated equivalent lengths were determined:

Equivalent Length for Parameter	Calculated Value	Measured Value	Difference
Synchronous Inductance (L_S)	13.6 in (34.5 cm)	12.7 in (32.3 cm)	7 %
Back EMF at 60 Hz, E_o	9.38 in (23.8 cm)	8.92 in (22.7 cm)	5%

As shown they agree with measured values to within 7%.

Discussion

The method described can be used to estimate the equivalent lengths to use in calculating air core motor circuit parameters. Using this method predicted circuit parameters for the air core motor were found to be within 7%. Further work is needed to refine the method to obtain better correlation between test and measured data.

Appendix B

FIVE HORSEPOWER MOTOR DRAWINGS

The axial cross-section of the five horsepower (3.7 kW) HTS motor rotor is presented in Figure B-1 on page B-3. Figure B-2 on page B-5 presents a radial quarter cross-section of the five horsepower (3.7 kW) HTS motor rotor and stator. An assembly view of the five horsepower (3.7 kW) HTS motor is presented in Figure B-3 on page B-7. Dimensions in all figures are in inches.

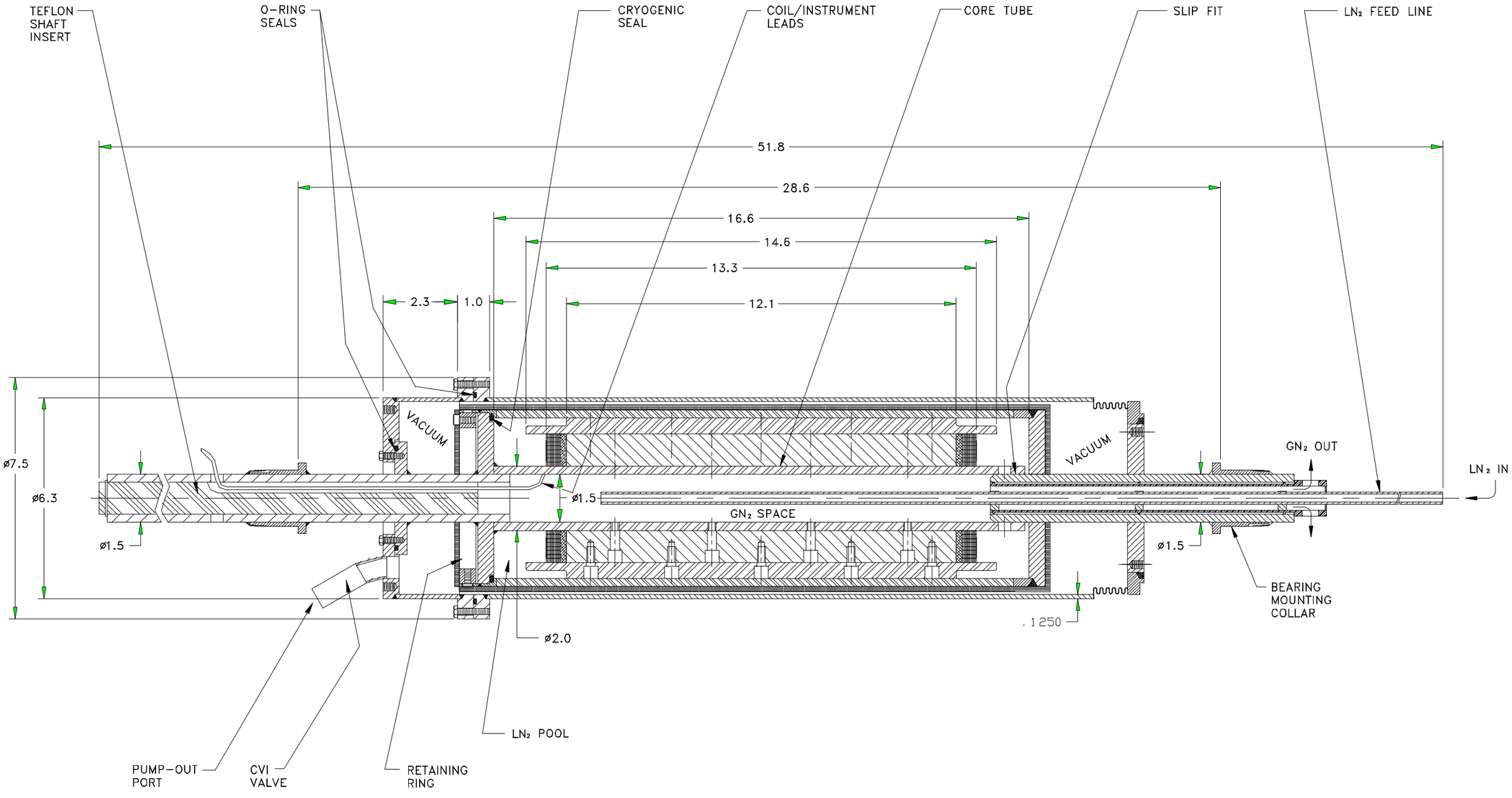

Figure B-1
Axial cross-section of the five horsepower (3.7 kW) HTS motor rotor.

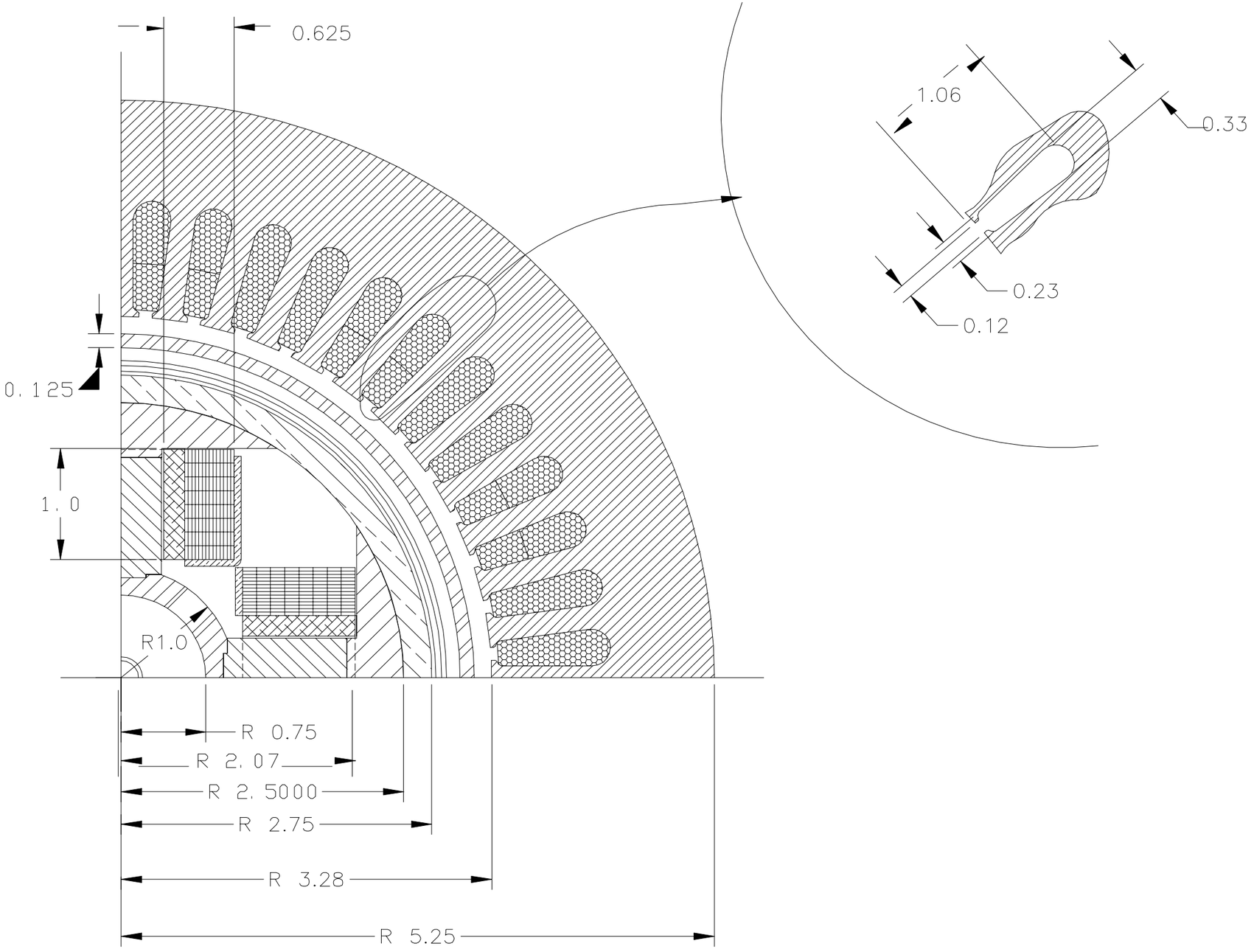

Figure B-2
Radial quarter cross-section of the five horsepower (3.7 kW) HTS motor rotor and stator.

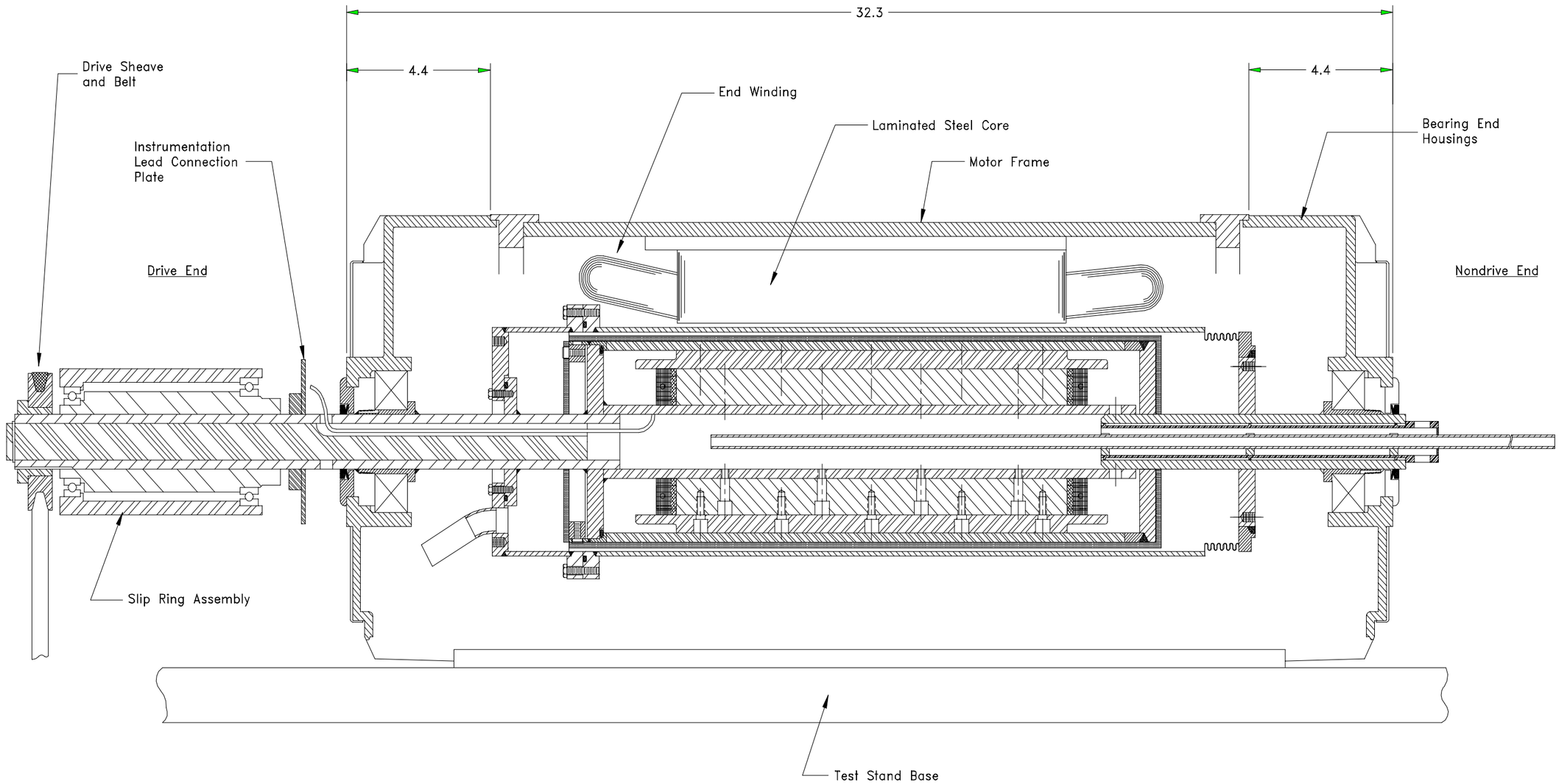

Figure B-3
Assembly view of the five horsepower (3.7 kW) HTS motor.

Appendix C

FIVE HORSEPOWER MOTOR ROTOR COOLING TEST RESULTS

One explanation for the peaking of the temperatures near 20 Hz in Figure 4-11 is that convection cells in the liquid nitrogen begin to dominate in the pool and tend to moderate the temperatures. This explanation can be supported by considering the behavior of free convection within a horizontal cavity heated from below. A free convection correlation which models the thermal behavior of this configuration was proposed by Globe and Dropkin [11] is given by

$$Nu = 0.069\, Ra^{1/3}\, Pr^{0.074}, \tag{C.1}$$

where Nu is the Nusselt number (ratio of convection to conduction heat transfer) given by

$$Nu = \frac{hL}{k} = \frac{qL}{k\Delta T} \tag{C.2}$$

In Equation (C.2), h is the convection coefficient, L is the distance between the cavity walls (pool depth in the rotor), k is the thermal conductivity of liquid nitrogen, q is the heat flux, and ΔT is the temperature difference across the cavity (radially across the pool depth). In Equation (C.1), Pr is the Prandtl number (ratio of the molecular momentum and thermal diffusivities) and Ra is the Rayleigh number (ratio of buoyancy forces to viscous forces) given by

$$\mathrm{Ra} = \frac{\rho a \beta \Delta T L^3}{\nu \alpha} \tag{C.3}$$

where here ρ is the fluid density, a is the system acceleration ($r\omega^2$ for the rotor), β is the volumetric expansion coefficient, ν is the viscosity, and α is the thermal diffusivity. Using Equations (C.1) through (C.3) and appropriate experimental conditions, an equation can be obtained which describes the temperature difference across the pool as a function of rotational speed (ω). This result is shown by the dashed line in Figure C-1. Convection in the pool increases as the rotational speed increases, thereby decreasing the temperature difference radially across the pool. In Figure C-1 this mechanism

would dominate above 1000 rpm and, as occurred in the experimental data, would limit the temperature rise in the pool to approximately 1 K. Below 1000 rpm, temperatures will be driven by the saturation differential temperature curve shown as a solid line in Figure C-1. The results presented in Figure C-1 support the trend in the experimental data presented in Figure 4-11.

It is encouraging that the simplified analysis presented above indicates a maximum temperature rise in the pool which closely matches the experimental results, however experimental data above 30 Hz was desired to further confirm this trend. In an effort to confirm this same trend at higher rotational speeds, the DC pilot motor drive was reconfigured to allow speeds on the HTS rotor above 30 Hz. Figure C-2 presents the experimental differential temperature data for rotational speeds of the rotor up to 50 Hz. This data was similar to the previously obtained data and indicated that the temperatures also moderate in the 30 to 50 Hz range–as the analytical analysis indicated it would. New data was obtained in the 5 to 30 Hz range as a check of previous data.

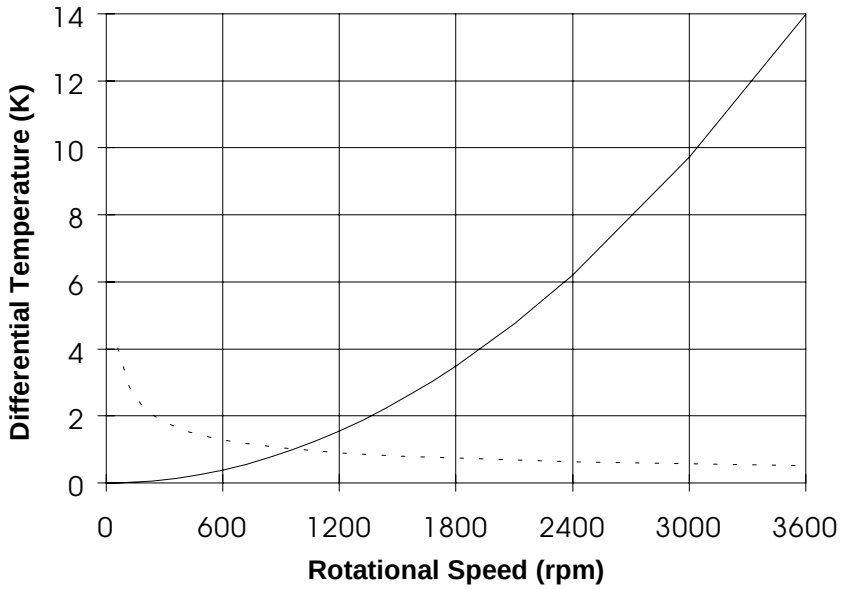

Figure C-1
Differential temperature variations versus rotational speed. Solid line represents the saturation temperature variation at the cold copper flux shield inner wall. Dashed line represents the temperature difference between parallel plates predicted by a standard correlation using experimental conditions.

Pressure sensor data, from the experimental tests used to monitor the liquid nitrogen temperature as a function of rotational speed, was used to compute an average effective void fraction in the liquid nitrogen pool. The relation that predicts the change in pressure through the liquid nitrogen pool is given by

$$\Delta P = \frac{1}{2}\rho\omega^2\left(r_o^2 - r_i^2\right) , \tag{C.4}$$

where here ρ is the effective fluid density, ω is the rotational speed, r_o is the radial location of the sensing element on the pressure sensor, and r_i is the radial location of the liquid/gas interface. For the data obtained, all quantities in Equation (C.4) were measured with the exception of the effective fluid density. The average two-phase density ($\rho_{2\phi}$) as a function of the vapor void fraction (α) is defined as

$$\rho_{2\phi} = \alpha\rho_v + (1-\alpha)\rho_l , \tag{C.5}$$

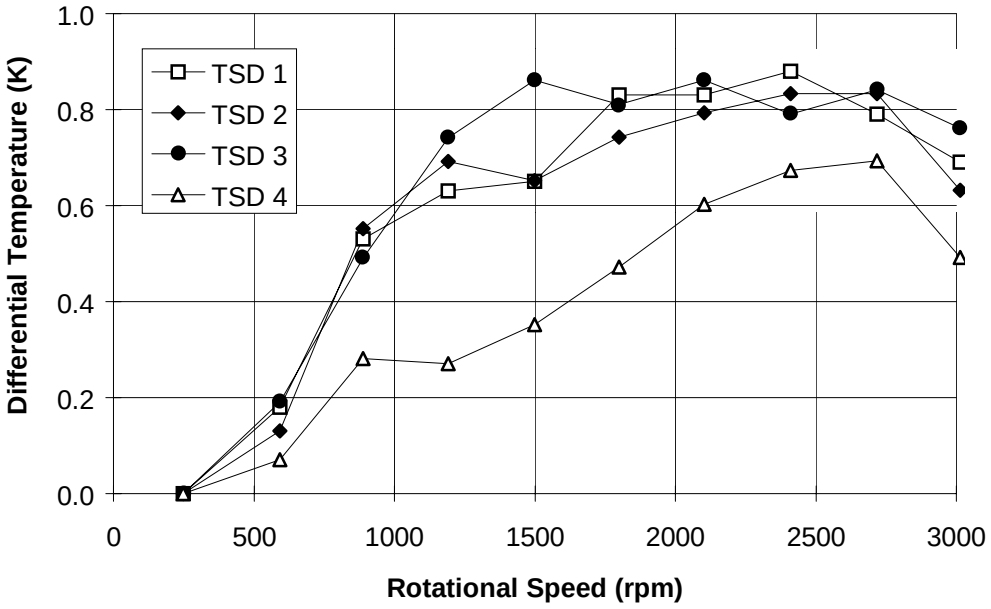

Figure C-2
Differential temperature data as a function of rotational speed with complete immersion of the HTS coils. Diode locations: 1) near cold copper flux shield inner wall, 2) middle of HTS coil side, 3) middle of HTS coil side opposite TSD 2 and, 4) just outside core tube.

where ρ_v is the vapor density and ρ_l is the liquid density. Combining Equations (C.4) and (C.5), the average effective void fraction is given by

$$\alpha = \frac{\rho_l - \dfrac{2\Delta P}{\omega^2\left(r_o^2 - r_i^2\right)}}{\rho_l - \rho_v} \ . \qquad \text{(C.6)}$$

Figure C-3 presents the average effective void fraction (α) as a function of rotational speed for two different sets of experimental data (data presented in Figures 4-11 and C-2). A large void fraction is present at lower rotational speeds due to boiling throughout the depth of the pool. At higher rotational speeds the void fraction is small due to the increase in saturation temperature near the outer wall where the boiling is suppressed–in this case boiling only occurs at the inner surface (liquid/gas interface) of the liquid nitrogen. The results presented in Figure C-3 are supported by the work of Marto and Gray [4].

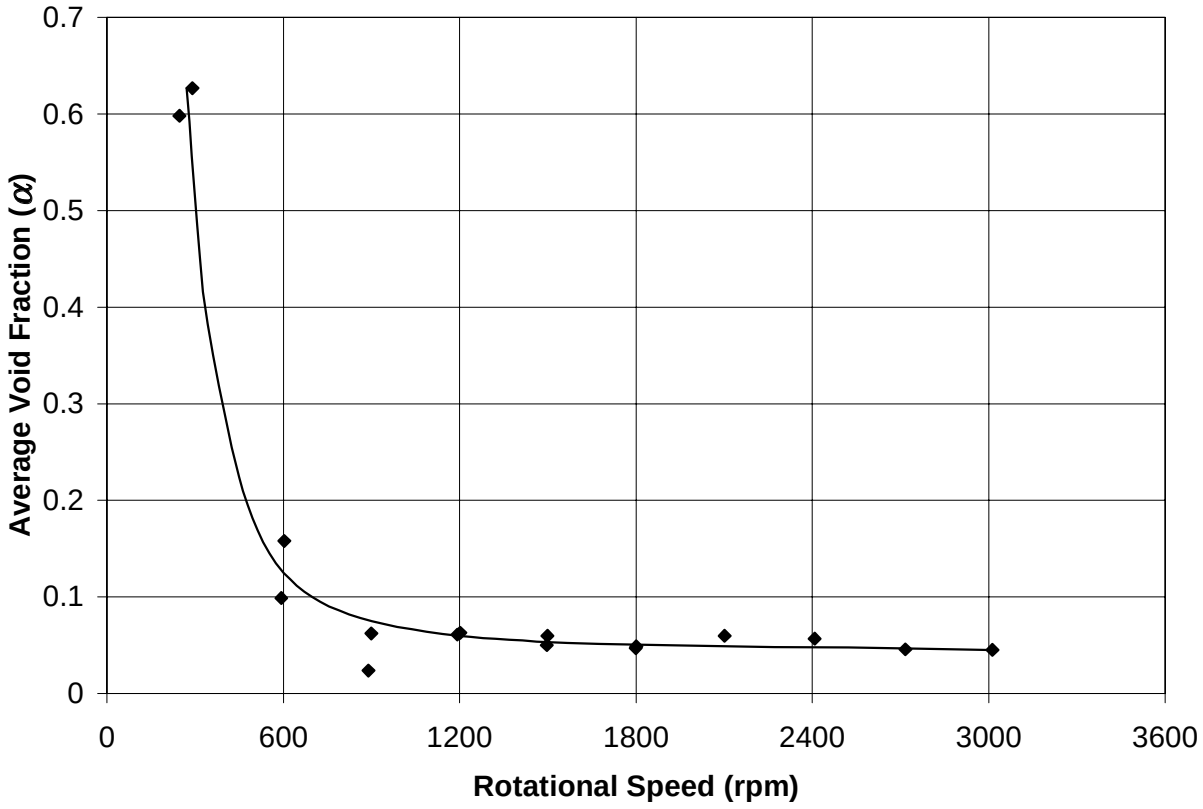

Figure C-3
Average effective void fraction (α) as a function of rotational speed with complete immersion of the HTS coils.